

# The post-Caledonian history of the Røldal Shear Zone (SW Norway): an apatite fission track study

Master of Science Thesis

by

Camilla Hermansen



Department of Earth Science

University of Bergen

2015



## Abstract

The post-Caledonian tectonic history and landscape evolution of southwestern Norway is not very well understood and therefore the subject of an ongoing debate. The lack of onshore post-Devonian sediments makes the study of vertical movements in the upper few kilometers of the crust a challenge. At the present time, the only means for constraining upper crustal movements directly are thermochronological analyses. Apatite fission track analysis was applied with an aim to shed light on the post-Caledonian history of the Røldal Shear Zone area. The Røldal Shear Zone is a major shear zone running parallel to the Hardangerfjord Shear Zone located north of the study area. The Røldal Shear Zone is, however, much less studied. The apatite fission track analyses yielded Permian to early Cretaceous ages with the majority of Jurassic ages. The ages are generally decreasing from the coast towards the inland, and are clearly offset across the Røldal Shear Zone. Inverse thermal history modeling was applied to four samples from the coast, representing the hangingwall and footwall, and the inland, respectively. The modeling suggested rapid Permo-Triassic cooling for the coastal samples, but slower and more constant cooling until the Cenozoic for the inland sample when it accelerated. This is suggested to reflect a rift related rift flank uplift in the coastal area, whereas the inland sample was much less affected by this uplift. The modeling for the coastal samples also suggested the samples to have been at (or close to) the surface in the Jurassic and was subsequently re-buried in the Cretaceous. This is not the case for the inland sample which reached the surface in the Cenozoic. The cooling rate accelerated dramatically in the Neogene. This is suggested to be a result of increased erosion rates due to the shift to a colder global climate. It is suggested that the evolution of the landscape of southwestern Norway is a result of sustained elevated topography shaped by rift-related uplift, extensional faulting and erosion since the Caledonian Orogeny.



## Acknowledgement

There are a number of people who have helped and supported me during my time as a master student at the University of Bergen. I am most grateful to each and every one of you!

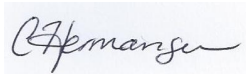
First of all I would like to extend my sincere gratitude to my supervisors, Dr. Anna Katharina Ksienzyk and Prof. Joachim Jacobs, for excellent guidance and support during my master project. Anna, I thank you for teaching me the method, commenting on my work, great advice and helping me whenever I was in need of it. Joachim, I thank you for great advice, fruitful discussions and help with organization. I am very grateful to Tobias Woznitza who provided me with additional samples, and for proof-reading parts of my work. I would also like to thank Tereza Konopaskova and Irina Maria Dumitru for teaching and helping me with the mineral separation and grain mount preparation. You made the long hours of lab work fly by! I also thank Yuval Ronen for etching my mica detectors.

I would like to extend a special thanks to my good friends Christian Rønnevik, Thomas Berg Kristensen, Hallgeir Sirevaag, Julia Linn Nævdal, Karen Johannessen, Mona Karin Boge and Emilie Randeberg for your constant encouragement, cheerfulness, help and friendship. You guys are the best! Christian is especially thanked for helping me with the software whenever I had problems and for proof-reading some of my work. Without you, I would still be working on the front page! Karen has also read and commented on some of my work which I am very grateful for. I would also like to thank all my other friends for being the nicest and most amazing friends I could ever ask for.

I thank the people in the thermochronology group at the University of Bergen for a great time with fun stories and good cakes on our weekly meetings.

I would also like to thank my parents, Borghild and Brynjulf Hermansen, for always supporting me, for showing interest in what I do, and for helping me in so many different ways during my time at the university. I thank my crazy, supernice siblings and their families for always making me laugh and for keeping me sane when I was caught between a rock and a hard place.

I thank my boyfriend, Rune Uldum Flyvholm, for assisting me during field work in the blizzard in January of 2014 (!) and the following mineral separation. I also thank you for encouraging me to always do my best, and for always being there for me.



Camilla Hermansen



# Contents

---

<b>1</b>	<b>INTRODUCTION</b>	<b>1</b>
1.1	Research objectives . . . . .	1
1.2	Study area . . . . .	1
1.3	Sampling . . . . .	2
<b>2</b>	<b>REGIONAL GEOLOGICAL SETTING</b>	<b>3</b>
2.1	The Precambrian . . . . .	3
2.2	The Caledonian Orogeny . . . . .	3
2.3	Post orogenic extension . . . . .	4
2.4	Post-Caledonian tectonic history and landscape evolution of southern Norway	6
2.4.1	Tectonic history . . . . .	6
2.4.2	Landscape evolution . . . . .	8
2.5	Previous low-temperature thermochronological work in southwestern Norway	8
<b>3</b>	<b>METHODOLOGICAL BACKGROUND</b>	<b>11</b>
3.1	Fission track background . . . . .	11
3.1.1	Track formation mechanisms . . . . .	11
3.1.2	Track revelation . . . . .	14
3.2	Factors affecting the appearance and preservation of fission tracks . . . . .	14
3.2.1	Partial annealing . . . . .	14
3.2.2	Chemical composition . . . . .	14
3.2.3	$D_{par}$ . . . . .	15
3.2.4	Crystallography . . . . .	15
3.3	Age determination . . . . .	15
3.3.1	The external detector method . . . . .	15
3.3.2	Age equation . . . . .	17
3.4	Track lengths . . . . .	18
3.4.1	Track classification . . . . .	18
3.4.2	Initial track lengths . . . . .	19
3.4.3	Track length distributions . . . . .	19
<b>4</b>	<b>SAMPLE PREPARATION AND ANALYTICAL PROCEDURE</b>	<b>21</b>
4.1	Sample preparation . . . . .	21
4.1.1	Mineral separation . . . . .	21
4.1.2	Grain mount preparation . . . . .	22
4.1.3	Etching and irradiation . . . . .	22
4.1.4	Post irradiation procedure . . . . .	23
4.2	Analytical procedure . . . . .	24
4.2.1	Equipment . . . . .	24
4.2.2	Counting of dosimeter glasses and $\rho_d$ estimation . . . . .	24
4.2.3	Zeta calibration . . . . .	25
4.2.4	Counting technique . . . . .	25
4.2.5	Calculation of fission track ages . . . . .	25
4.2.6	Track length and $D_{par}$ measurements . . . . .	26
4.2.7	Thermal history modeling . . . . .	26

<b>5</b>	<b>RESULTS</b>	<b>29</b>
5.1	Sample quality . . . . .	29
5.2	Calculations and calibrations . . . . .	31
5.2.1	Counting of dosimeter glasses and estimation of $\rho_d$ . . . . .	31
5.2.2	Zeta calibration . . . . .	31
5.3	AFT analysis . . . . .	32
5.4	Inverse thermal history modeling . . . . .	37
<b>6</b>	<b>INTERPRETATION AND DISCUSSION</b>	<b>47</b>
6.1	Assessment of data quality . . . . .	47
6.1.1	Zeta calibration . . . . .	47
6.1.2	AFT ages . . . . .	47
6.1.3	The failure of the $\chi^2$ test . . . . .	47
6.1.4	Mean track lengths and $D_{par}$ . . . . .	48
6.1.5	Inverse thermal history modeling . . . . .	49
6.2	Discussion of the results . . . . .	49
6.2.1	Interpretation of the AFT ages . . . . .	49
6.2.2	Interpretation of inverse thermal history models . . . . .	51
6.3	Comparison to previous studies . . . . .	52
6.4	Proposed exhumation history for the Røldal Shear Zone area . . . . .	53
<b>7</b>	<b>SUMMARY AND OUTLOOK</b>	<b>55</b>
	References	<b>57</b>
	Appendix A	
	Appendix B	



# 1 INTRODUCTION

---

The post-Caledonian tectonic history and landscape evolution of southwestern Norway is a matter of controversy, as the lack of onshore post-Devonian sediments make uplift events, fault activity and erosion rates hard to constrain. From this debate two end-member models have been subject of discussion - namely the well established and perhaps most accepted model fronted by Gabrielsen et al. (2010a) which states that the topography is the result of Mesozoic peneplanation and Cenozoic uplift (this model will be referred to as the peneplanation-uplift model hereafter), and the ICE (isostasy-climate-erosion) hypothesis by Nielsen et al. (2009) which states that the topography to be the remnant of the  $\sim 410$  Ma Caledonian orogen. To help further the understanding of the evolution, low-temperature thermochronological analyses have been conducted in order to study vertical movements in the upper crust. However, the amount of data available is still not sufficient to decide on either of the two models (Ksienzyk, 2012). In addition, Ksienzyk et al. (2014) have pointed out that any model offering a valid tectonomorphological history of southwestern Norway needs to take active fault tectonics into account, which both models fail to do.

This study aims to enlighten the post-Caledonian history of the Røldal Shear Zone area by means of apatite fission track analyses. It is a part of the Earth System Modelling (ESM) project at the University of Bergen. ESM comprises three interrelated research branches; geodynamics and topography, source-to-sink, and paleoclimate modelling and geological consequences. Its goal is to study how the different systems interact and influence one another. The project contributes to a VISTA postdoc project by A.K. Ksienzyk, which studies the post-Caledonian history of the Norwegian margin along a transect from the Utsira High to the Hardangervidda Plateau.

## 1.1 Research objectives

The Hardangerfjord Shear Zone (HSZ) is a well-studied major crustal lineament that formed as a post-Caledonian extensional detachment in the Devonian (Fossen and Hurich, 2005). Further south, the significantly less studied Røldal Shear Zone (RSZ) runs parallel to the HSZ. This master project aims to study uplift and erosion histories on both sides of the RSZ by means of apatite fission track analysis. The project aims to shed light on the following research questions:

1. How do the age distributions on either side of the Røldal Shear Zone compare to one another?
2. Do the cooling histories vary in the coastal areas compared to the inland?
3. Do the data contribute to illuminate the exhumation history of the area, and if so, what do they tell us?
4. Has the area experienced tectonic activity since the Caledonian Orogeny?
5. How do the results fit the models attempting to explain the landscape evolution of SW Norway?

## 1.2 Study area

The study area is located north and south of the Boknafjord (and adjacent fjords) and inland towards the town of Sauda in the county of Rogaland (Figure 1.1). The landscape

is relatively flat and has a low relief and elevation in the coastal areas. Towards the inland the elevation gradually increases along with the relief. The area is strongly shaped by fjords and valleys, some of which are identified as major shear zones and faults. The area is dominated by Proterozoic basement and the Caledonian thrust nappes of the Lower and Middle Allochthon. Gneisses and plutonic rocks constitute the majority of the lithologies, with elements of phyllites from the decollément zone between the basement and overlying allochthons. It is plain to see that the rocks in the study area are cut by faults and shear zones trending SSW-NNE and N-S. The largest of the shear zones are the Røldal Shear Zone and Stavanger Shear Zone.

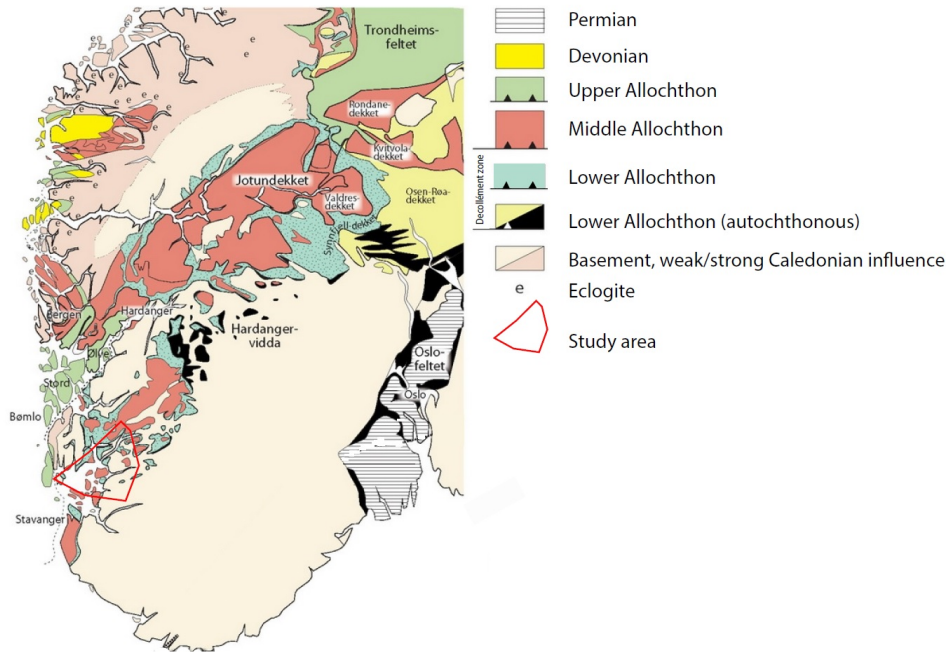


**Figure 1.1:** Simplified geological map of the study area. Modified from Bryhni et al. (2006).

### 1.3 Sampling

The sampling was conducted in January of 2014 where 10 samples were collected (sample numbers starting with CH-). The sample sites were chosen so that the samples are evenly spaced throughout the area. Also, on the northern side of the Røldal Shear Zone, each block separated by the N-S trending faults were sampled. In addition, 15 samples were provided by Tobias Woznitza (sample numbers starting with NTW-). Sampling has been carried out on both sides of the Boknafjord along the roads from the coast and further inland towards the town of Sauda.

## 2 REGIONAL GEOLOGICAL SETTING

---

During the course of Earth's history Norway has been part of several terrains and supercontinents. In the Archean and Paleoproterozoic Era, it was part of the Fennoscandian Shield (Torsvik and Cocks, 2005). In the Mesoproterozoic Era, the latter became part of the supercontinent Rodinia (Torsvik, 2003). At the end of the Precambrian, Norway became a part of Baltica (Cocks and Torsvik, 2002), then Laurussia and finally Eurasia where she is located today (Torsvik and Cocks, 2005). This chapter will focus mainly on the geological history of southern Norway following the Caledonian Orogeny. Note that when speaking of Norway, only the mainland is considered.

### 2.1 The Precambrian

In the Precambrian, Norway's basement was formed as a result of several orogenic events, namely the Lopian (2.9-2.6 Ga) Orogeny, Svecofennian (2.0-1.75 Ga) Orogeny and the Gothian (1.75-1.5 Ga) Orogeny. During these orogenies vast amounts of continental crust were formed, which later got reworked during the Sveconorwegian-Grenvillian (1.25-0.8 Ga) and Caledonian (0.6-0.4 Ga) orogenies (Gaal and Gorbatshev, 1987). These crustal rocks are a part of Fennoscandia, which in Neoproterozoic times was incorporated into the eastern margin of the supercontinent Rodinia (Torsvik, 2003). The dispersion of Rodinia had already started at 750 Ma, not long after its formation, and Norway became part of a new continent called Baltica. Baltica was at first situated on the eastern side of Laurentia, but in late Proterozoic times they separated resulting in the formation of the Iapetus Ocean.

### 2.2 The Caledonian Orogeny

The Caledonian orogen was formed during four or five tectonic events in the Paleozoic Era. The orogenesis was initiated during the Cambrian when the Ægir Sea separating Baltica and Siberia began a phase of subduction. Accompanied by the counter-clockwise rotation of Baltica, this subsequently led to the closing of the Iapetus Ocean as Baltica moved towards Laurentia (Torsvik and Rehnström, 2001). The closure formed a new continent called Laurussia by early-mid Devonian times. It was composed of the landmasses of Baltica, Laurentia, Avalonia and some smaller intervening terrains (Torsvik and Cocks, 2004). The Caledonides in Norway were formed by the oblique collision between Laurentia and Baltica. Several lines of evidence indicate that Baltica was partly subducted beneath Laurentia: (1) the presence of ultra-high pressure eclogite facies parageneses in the Western Gneiss Region on the west coast of Norway; (2) evidence of magmatism on Greenland during the Devonian; (3) the gradually decreasing metamorphism of the bedrock towards the southeast in Norway; (4) the presence of oceanic terrains in the Caledonian thrust nappes in Norway which are not found on Greenland (Dietler et al., 1985b; Dobrzhinetskaya et al., 1995; Gee et al., 2008; Griffin and Brueckner, 1980). The rocks within the Caledonian orogen comprise three tectonic units: (1) The Baltic Shield (basement formed in the Precambrian); (2) a decollement zone; and (3) nappes created during the collision (Fossen, 1992). The nappes are stacked on top of each other and have been assigned to four groups based on their origin: Lower, Middle, Upper and Uppermost allochthons, respectively. The allochthons rest on a decollement zone of Cambro-Silurian metasediments which served as a transport belt during the transport (Figure 2.1a). For the thrust nappes to be transported such a long way, the presence of water filled sediments was essential, because the trapped water created an overpressure and thus reduced the friction between the overriding nappes and the basement (Bryhni

et al., 2006). The Lower Allochthon constitutes remnants of sediments deposited on the continental margin. The Middle Allochthon has been transported a little further and also represents rocks from the continental margin, as well as remnants of microcontinents that may have existed in the time before the collision. The Upper Allochthon includes remnants of the oceanic crust and island arcs that formed in the Iapetus Ocean (Bryhni et al., 2006). Finally, the Uppermost Allochthon comprises the ophiolites of which a Laurentian origin has been suggested (Roberts et al., 2007).

### 2.3 Post orogenic extension

The mountain chain started collapsing in Early Devonian times due to decreasing compressive forces, and the extensional tectonics that followed. Some studies (e.g. Norton, 1986; Andersen and Jamtveit, 1990; Andersen, 1998) have explained the orogenic collapse by back-sliding of the nappes due to crustal thickening. However, Fossen (1992) pointed out that if that were the case the extension would remain SE in the foreland and NW in the hinterland. This would require a lot of space in the central parts of the orogen, which can only be possible by extensional plate movements. The extension has been described by Fossen in several publications (e.g. Fossen, 1992; Fossen, 2000; Fossen, 2010) to have occurred in three stages or modes (Figure 2.1):

**Mode I extension** - The first phase of the collapse was initiated by the reactivation of the decollement zone. During the orogenesis, the decollement zone was a basal thrust. However, as the compressive forces ceased and the orogen collapsed it functioned as a low-angle detachment. The decollement zone and the under- and overlying rocks are exposed by erosion over a large area in southern Norway. Fossen (1992) found both top-to-the-ESE shearing, indicating a contractional regime and top-to-the-WNW shearing indicating an extensional regime. Structures supporting this were: folds, S-C fabrics and asymmetric boudins to mention a few. The translation of the orogenic wedge relative to the basement is estimated to be up to 30 km towards the hinterland (coast).

**Mode II extension** - The backsliding from Mode I was quickly followed by the formation of west and northwest dipping extensional shear zones (Figure 2.2) such as the Hardangerfjord Shear Zone, the Røldal Shear Zone, the Nordfjord-Sogn Detachment Zone and the Bergen Arc Shear Zone. The formation of big shear zones is thought to have happened due to a lowering of the northwesterly dip of the detachment as a response to it being exhumed in the hinterland, making backsliding difficult (Fossen, 2000). The result was crustal collapse, and the shear zones actually cut into the basement leading to extension of the Baltic crust (Fossen, 1992). One of the major structures is the Hardangerfjord Shear Zone (HSZ). It is more than 600 km long and ca. 5 km wide, extending from the inner parts of Hardangerfjorden where it continues as the Lærdal-Gjende Fault System, and into the North Sea where it possibly continues into Scotland as the Highland Boundary Fault (Fossen, 2010).

**Mode III extension** - The formation of ductile shear zones was followed by brittle faulting as the extension continued under decreasing temperatures. This is denoted as Mode III extension. The faults trend NE-SW and exhibit semiductile structures which indicate formation near the brittle-ductile transition (Fossen, 2000). The Lærdal-Gjende Fault System (LGFS) is the largest fault system of Mode III origin, and is interpreted by Fossen and Hurich (2005) to be a high-level brittle equivalent of the Hardangerfjord Shear Zone, formed during a late phase of the development of this structure. It follows the trend of the HSZ, but should be considered as a separate zone and not a part of the HSZ itself.

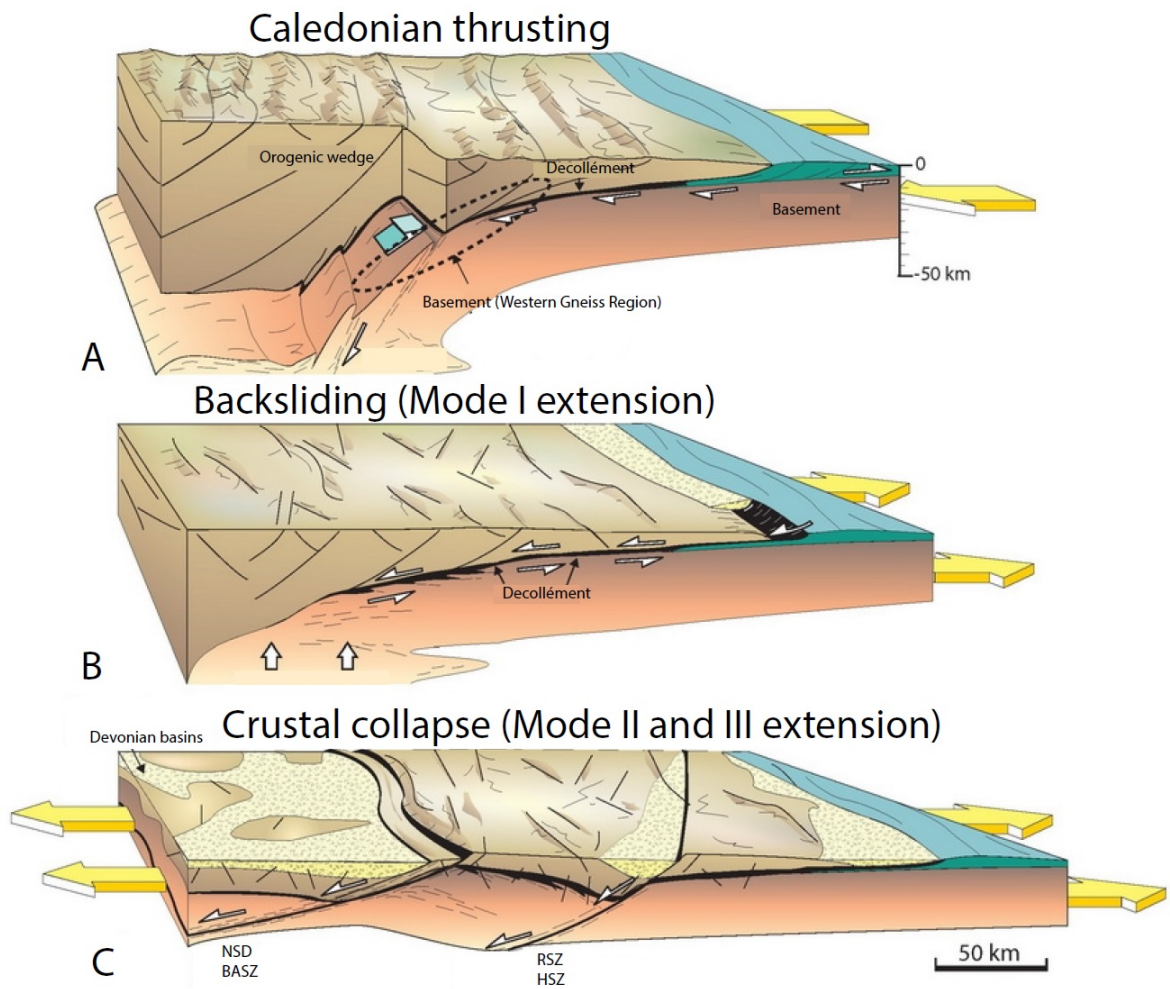


**Figure 2.1:** Formation (A) and disintegration of the Caledonian Orogen (B and C). See text for further explanation. Modified from Bryhni et al. (2006).

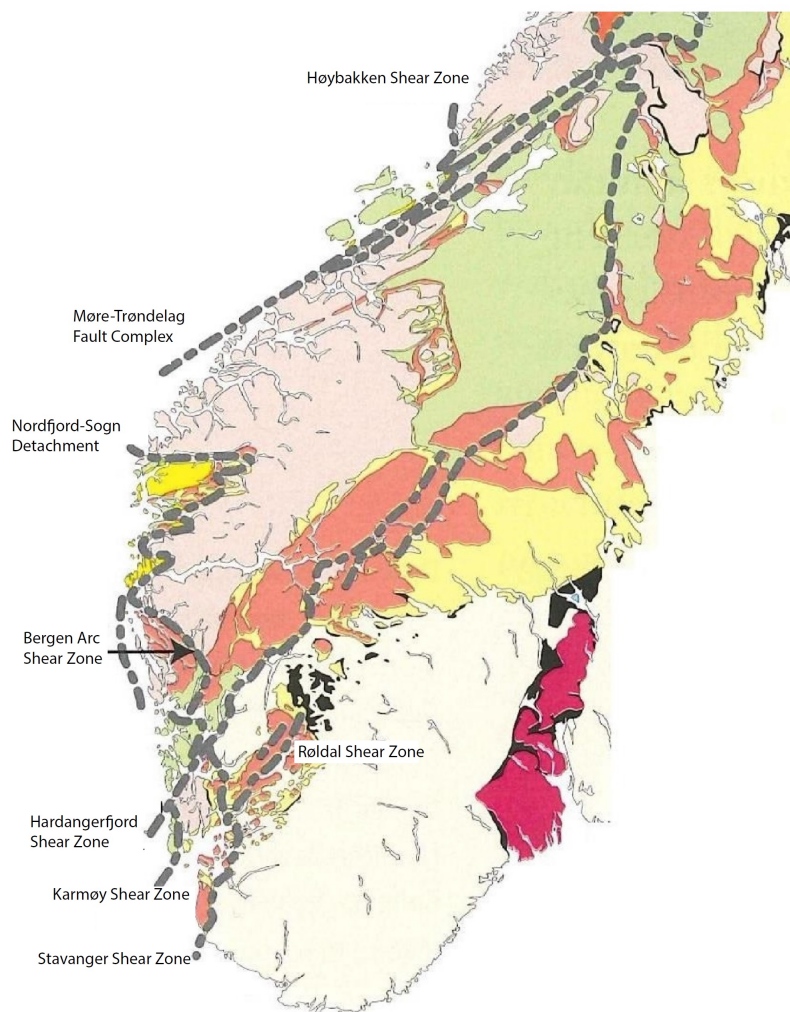


**Figure 2.2:** Overview of major shear zones in southern Norway. Modified from Bryhni et al. (2006).

## 2.4 Post-Caledonian tectonic history and landscape evolution of southern Norway

### 2.4.1 Tectonic history

As a result of the extension and formation of shear zones, clastic sedimentary basins such as the Solund Basin, Hornelen Basin and Kvamshesten Basin were formed in SW-Norway in the Devonian. Underneath these basins, the Nordfjord-Sogn Detachment Zone (NSDZ) is located which is the largest of the shear zones and extends for 120 km from the Hornelen Basin to the outer Sognefjord area where it meets the Bergen Arc Shear Zone (BAZS) (Fossen, 2010). A period of tectonic quiescence and hence thermal stability followed the extensional collapse. According to Gabrielsen et al. (2010a), the tectonic component of the topographic evolution of the Caledonides had ceased by the late Devonian to early Cretaceous. The topography was therefore likely controlled by surface-processes, which is supported by the lack of onshore post-Devonian sediments in southern Norway (Fossen and Dunlap, 1998).

During the Permian-Triassic all the continents coalesced to form the supercontinent Pangea. It was, however, a short-lived affair and the continents broke apart once more along mountain belts where the lithosphere was weakened (Ryan and Dewey, 1997).

Later, extension and rifting commenced in the North Atlantic Ocean and the North Sea, by reactivation of structures formed during the orogenic collapse. To the east rifting started in the Oslo Graben. The structural grain of the rifting both in the Oslo region and the North Atlantic was N-S, which is indicative of an E-W extensional regime (Færseth et al., 1996). Coast parallel dolerite dykes related to the Permian extension crop out in Sunnfjord, Sotra and Sunnhordland. They show ages of  $\sim 260$  Ma and have mostly been formed in connection to N-S trending brittle faults related to the extension. Another set of dykes have been dated to ca. 220 Ma, and are related to Late Triassic extension on the Hordaplattform (Fossen and Dunlap, 1999). Based on K/Ar illite data from fault gouges Ksienzyk (2012) suggested that there has been fault activity in the Carboniferous-Permian to latest Permian. Also, fault reactivation in the Late Triassic to Early Jurassic seems to coincide with the formation of dykes at ca. 220 Ma.

In the Middle-Late Jurassic another phase of rifting commenced in northwestern Europe, leading to the development of the Viking Graben, Central Graben and Moray Firth Basin (e.g. Doré et al., 1999). Considerable rift shoulder uplift was also happening as a result of the extension. This is indicated by propagation of clastic sedimentary units originating from the Norwegian mainland (Gabrielsen et al., 2010a). Also, thermochronological data have shown that faults onshore were reactivated during the uplift (e.g. Andersen et al., 1999; Fossen et al., 1997; Ksienzyk, 2012).

In the Cretaceous, the spreading of the Atlantic Ocean propagated northwards, due to the ongoing disintegration of Pangea. The rifting was followed by Atlantic sea-floor spreading in the Early Eocene (Doré et al., 1999). The sea level was much higher in the Cretaceous, perhaps as much as 350 meters higher than today (Bryhni et al., 2006). Two pronounced episodes of uplift have been suggested in Palaeogene and Neogene times, respectively. The first episode has been linked to the formation and passage of the Icelandic plume (e.g. Nadin et al., 1997a), or other tectonic events such as plume activity which is related to continental break-up (White and McKenzie, 1989). The second episode has been linked to flank uplift created by isostatic movements, distribution and erosion of glaciers and tectonic uplift (Gabrielsen et al., 2010a and references therein). Thermochronological data do not indicate a lot of uplift in the late Jurassic and there are no signs of igneous activity in southern Norway in the Jurassic. It is therefore suggested by Fossen and Dunlap (1999) that the rifting has had little influence onshore.

The rifting of the North Atlantic margins ceased as Atlantic sea-floor spreading was initiated in the early Eocene (Doré et al., 1999). Combined with the far-field stresses from the Laramide event of the Alpine Orogeny, inversion of structures created by extension started in the North Sea (Vågnes et al., 1998).

The lack of onshore post-Devonian sediments makes the study of the post-Caledonian tectonic history and landscape evolution a challenge. However, apatite fission track and (U-Th)/He data from southwestern Norway show reactivation of many faults throughout the Mesozoic (e.g. Redfield et al., 2004; Leighton, 2007; Ksienzyk et al., 2014). One major structure that may have been reactivated is the Hardangerfjord Shear Zone, a crustal scale structure of Devonian origin (Kohlmann et al. 2013).

After the glaciations in late Pliocene and Pleistocene times, the area has been undergoing glacioisostatic uplift of a dome-like character. The uplift is ongoing to this day at a rate of ca. 1-4 mm/yr (Fjeldskaar et al., 2000).

### 2.4.2 Landscape evolution

The landscape of southern Norway is one of great diversity ranging from deep fjords and steep valleys to high plateaus and mountain peaks. Even though the landscape has been studied and described for more than a century, starting with the pioneering work of Reusch (1901) who described the undulating surfaces at higher elevations, the evolution of the landscape features still remains an enigma. Two end-member models have emerged over the years, namely the “peneplanation-uplift model” and the “ICE (isostasy-climate-erosion)-hypothesis”. The peneplanation-uplift model is the older and perhaps most accepted one, but is currently being challenged by the more recent ICE-hypothesis.

The peneplanation-uplift model is based on the cyclic model of landscape evolution put forward by Davis (1889). In the Davisian model so-called peneplains (or erosional surfaces) are formed close to sea level as a result of a decrease in surface gradients. An uplift event would place the peneplain at a higher elevation, creating a plateau that rivers would cut into and form valleys. During time this elevated landscape would once again be eroded to sea level, and the cycle would be complete. The peneplanation-uplift model suggests that the elevated topography is the result of complete orogenic collapse, followed by peneplanation and uplift events during Palaeogene and Neogene times (Lidmar-Bergström et al., 2000; Gabrielsen et al., 2010a).

In the ICE-hypothesis, the high elevations are created because the orogenic collapse and extension in Devonian times did not obliterate the entire orogen. The hypotheses therefore suggest that an orogenic root has been preserved in southern Norway and has sustained an elevated topography which has been eroded to today’s level (Nielsen et al., 2009). Another important aspect is the observation that the rift-geometry of passive continental margins to a great extent pre-determines the topography. During extension, rift-flanks are being uplifted on a kilometric scale, and despite erosion they continue to exist for millions of years after the rifting has ceased. Why these escarpments are being preserved or rejuvenated is not understood, but they are linked to crustal thinning gradients established during rifting (Osmundsen and Redfield, 2011 and references therein).

### 2.5 Previous low-temperature thermochronological work in southwestern Norway

Andriessen and Bos (1986) carried out the pioneering low-temperature thermochronological study in southwestern Norway. They studied the Eidfjord area in the innermost part of the Hardangerfjord by means of apatite and zircon fission track analysis. The apatite fission track analysis yielded ages from 110 Ma at sea level to 166 Ma at higher altitudes (1620 m). Hence, the ages increased with elevation. The zircon fission track analysis yielded three ages from 294 Ma to 317 Ma from samples taken at sea level, 700 m and 1620 m, but here, however, they found no correlation between age and elevation. They interpreted this as a result of rapid uplift through the partial retention zone in late Carboniferous times. These results were interpreted in combination with the results of Priem et al. (1976) who reported biotite Rb-Sr and K-Ar ages of  $\sim 385$  Ma and  $\sim 420$  Ma, respectively. They concluded that the area had experienced rapid uplift directly following the Caledonian Orogeny associated with 13 km of erosion and then slower uplift since the late Carboniferous with 8 km erosion since this time.

In 1995, Rohrman et al. presented a more extensive apatite fission track study where they produced two N-W and NW-SE trending profiles and three elevation profiles (one



of which was in the Eidfjord area previously studied by Andriessen and Bos, 1986). The result of the study showed an increase in cooling ages from the inland towards the coast, and from sea level towards the peaks in the inner parts of Norway. The youngest ages (early Cretaceous) were found at low elevations in the innermost part of the fjords, and the oldest ages (middle to late Triassic) were found at the south coast, respectively. Jurassic ages were obtained at the highest elevations along the western coast. For the vertical profiles, the ages increase with elevation and range from early Jurassic to early Cretaceous (predominantly Jurassic ages). Rohrman et al. (1995) concluded, based on the AFT data and thermal history modeling, that there must have been two pronounced episodes of rapid exhumation: (1) A phase that started in the east in the late Triassic and migrated westwards yielding late Jurassic ages. A phase of slower cooling rates is inferring peneplanation of southwestern Norway in Cretaceous/Paleocene times; (2) A phase of Neogene uplift causing the AFT isochrones to be warped in a domal style thus resulting in stronger exhumation in the inner parts than at the coast. This led to the conclusion that southern Norway had behaved as a single coherent block since the Permian, and so was unaffected by faulting in the Mesozoic and Cenozoic.

The conclusion drawn by Rohrman et al. (1995) was later challenged by Redfield et al. (2004, 2005a) who in their AFT-study of two horizontal transects perpendicular to the strike of the Møre Trøndelag Fault Complex, found that the AFT ages were offset across known faults and lineaments. The age offset was as high as 97 Ma for samples collected relatively close to one another. The sampling was conducted away from the fault zones in order to avoid thermally induced overprint of AFT ages and lengths. The study resulted in the identification of four distinct crustal blocks with increasing ages towards the coast. In addition, they found that the AFT ages of the hangingwall of the Hitra-Snåsa Fault close to the coast was significantly older (280 Ma) than the AFT ages from the footwall of the innermost Bæverdalen Lineament (93 Ma). This led to the conclusion of post-Permian fault activity, and that the tectonic history of southern Norway could be explained by a flexed lithosphere with an uplifted core of the Fennoscandian craton with a down-faulted thinning margin of the Norwegian Sea. This was later developed into the crustal taper hypothesis (Osmundsen and Redfield, 2011; Redfield and Osmundsen, 2013)

A few years later, Leighton (2007) also found large age offsets across major fault zones in southern Norway, indicating fault activity in the Mesozoic (and possibly the Cenozoic). This is in accordance with what Redfield et al. (2004, 2005a) found. AFT ages range from Permian to early Cretaceous (280 to 110 Ma). Leighton (2007) suggested rapid cooling (1-5 °C/Ma) in the Permian/Triassic followed by slow cooling (<1 °C/Ma) in the Jurassic throughout Paleogene times. In the Neogene, cooling rates increased once more. Thermal histories from adjacent structural blocks were quite different, supporting a more dynamic tectonic evolution of southern Norway than that suggested by Rohrman et al. (1995).

A more recent study was carried out in the Bergen area by Ksienzyk (2012) and Ksienzyk et al. (2014). Apatite fission track analyses as well as apatite and zircon (U-Th)/He analyses yielded late Permian to Jurassic, Triassic to Cretaceous and Carboniferous to Triassic ages, respectively. The study found that also in this area, the ages are offset across faults leading to the conclusion that the faults must have been reactivated in the Mesozoic. Thermal history modeling suggests a high cooling rate of 2-3 °C/Ma in the Permian to early Jurassic. In the Cretaceous, samples that had stayed close to the surface since the Jurassic were buried by sediments and heated to 30-50 °C. Samples from the inland did not reach the surface until the Cenozoic and thus experienced a

slower cooling rate of  $<1$  °C/Ma. It is suggested that the tectonomorphologic evolution of southwestern Norway is one of high complexity, and is strongly affected by rift- and post rift tectonics in the North Sea and the rifting in the North Atlantic. It is further suggested that the topographic relief was repeatedly rejuvenated as a result of faulting and subsequent footwall uplift.

In the innermost Hardangerfjord area, Johannessen et al. (2013) conducted apatite fission track and (U-Th)/He analyses along three vertical profiles in order to shed light on the evolution of the hinterland of the passive margin. The study yielded AFT cooling ages in the steep flanks in the innermost Hardangerfjord from late Triassic to late Cretaceous. In the Eidfjord and Ulvik areas the (U-Th)/He analyses yielded Cretaceous single grain ages. From the thermal history modeling two episodes of rapid cooling (2-6 °C/Ma) were recognized. The first in the Permo-Triassic and the second in the latest Cretaceous to Cenozoic. The first, Johannessen et al. (2013) have related to flexural rift-flank uplift and increased onshore tectonics, and the second is related to a combination of tectonic activity, flexural uplift and erosion.

It is beyond the scope of this master project to give a complete review of the details of the previous thermochronological work. A summary of the studies conducted until 2007 is provided by Hendriks et al. (2007).

# 3 METHODOLOGICAL BACKGROUND

---

This project aims to study uplift and erosion histories on both sides of the Røldal Shear Zone. In order to do so, 22 rock samples have been collected and prepared for fission track analysis. Apatite fission track dating is a so-called low temperature thermochronological method (~60-120 °C). It is mostly used to study tectonic and erosional processes of rocks at shallow crustal depths along with  $^{40}\text{Ar}/^{39}\text{Ar}$  and (U-Th)/He thermochronology. However, over the last decades the use of this method has proven to be a helpful tool in provenance studies, thermal history analysis in sedimentary basins and other nonorogenic settings, just to mention a few (Gallagher et al., 1998; Donelick et al., 2005). The method was first recognized as a tool applicable to geological problems by Fleischer, Prize and Walker, whose work yielded a better understanding of the nature and significance of the fission tracks (Fleisher et al., 1975). This led to rapid development of the method. While this chapter provides the theoretical background of the method, the analytical details of the present study are given in chapter 4.

Fission track dating is considered to be a radiometric dating technique; it is based on the spontaneous fission of  $^{238}\text{U}$  into two daughter nuclei. However, it is not a conventional dating technique in that it is not based on the half life of  $^{238}\text{U}$ , but rather the formation of datable tracks (Gallagher et al., 1998). By counting the number of spontaneous tracks and measuring their lengths, the age and thermal history of a sample may be established. The number of tracks depend both on the time of residence at low temperatures and the abundance of  $^{238}\text{U}$ . In order to obtain a fission track age for a sample, the number of tracks and the initial content of  $^{238}\text{U}$  must be established. In addition to this, information about the length of the tracks is needed. The AFT data is utilized in order to produce a thermal model for the samples.

## 3.1 Fission track background

### 3.1.1 Track formation mechanisms

Fission tracks are damage features in the crystal lattice of the mineral created by the projecting nuclei. The details of the mechanism behind the formation of the track itself is not fully understood, but the ion explosion spike model by Fleischer et al. (1965b) is for the time being the most widely accepted one (Figure 3.1). As the two nuclei produced by the spontaneous fission of  $^{238}\text{U}$  project in opposite directions, the Coulomb repulsive forces are greater than the bonding in the crystal lattice. Because of this the projecting nuclei leave a damage trail in the crystal lattice, called a fission track. As the nuclei project they lose energy and eventually come to a halt. As will be further explained in chapter 3.2.1 the fission tracks are metastable features, meaning the damage trail will heal over time and at certain conditions. According to Gallagher et al. (1998), the model must be looked upon as a simplification. Later work by Chadderton (1988) and Vineyard (1976) has yielded another model for the formation of fission tracks, called the thermal spike model. This model suggests tracks are formed by the heating of the area adjacent to the projection path of the fission nuclei, and thus creating defects in the crystal lattice (Chadderton, 1988). A more recent contribution by Chadderton (2003) suggests a compound spike model where both the ion spike and thermal spike models are regarded to be the mechanisms for producing fission tracks. It is evident that the subject matter needs further investigation in order to fully comprehend the track formation mechanisms.

As mentioned, apatite fission track dating is a low temperature thermochronological

method, and thereby very temperature sensitive. The fission tracks will disappear more rapidly at temperatures above 120 °C, and for some samples they will disappear all together. Below this temperature, the tracks will be preserved to a certain extent. This feature will be described later in chapter 3.2.

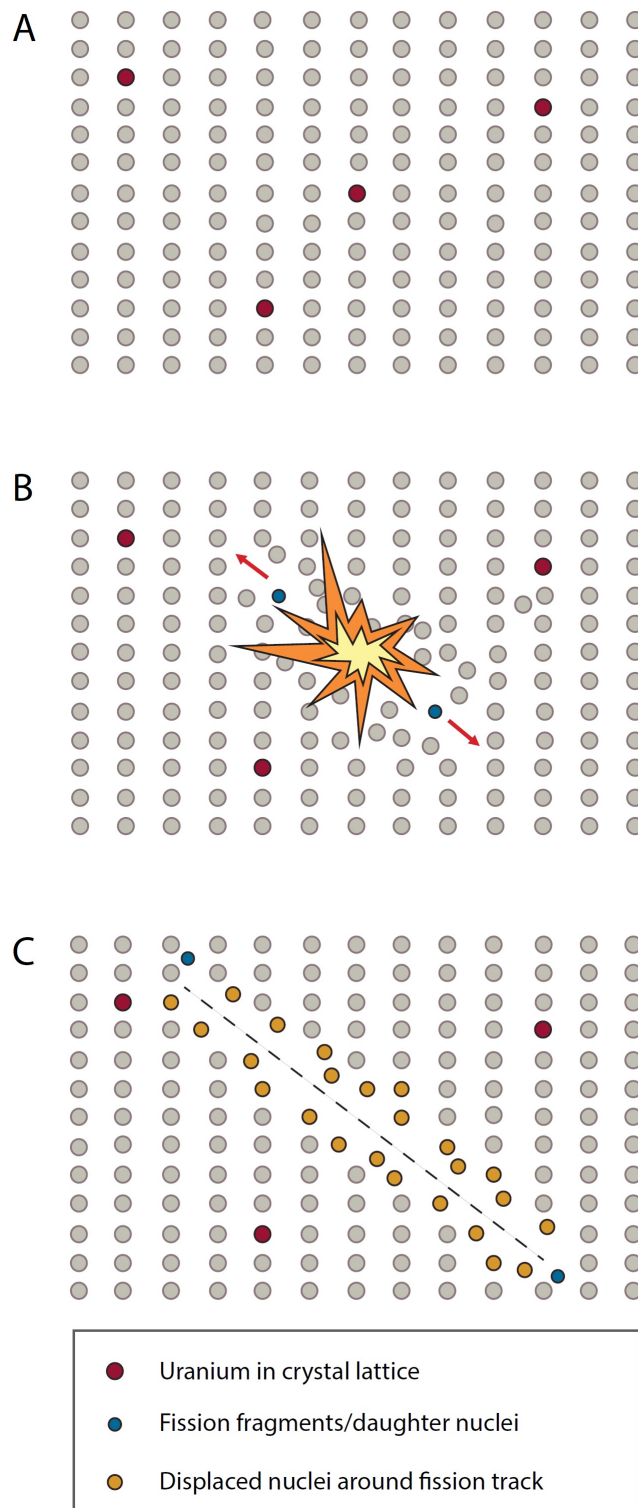


**Figure 3.1:** (a) A small amount of  $^{238}\text{U}$  is present in the mineral. (b) Spontaneous fission of  $^{238}\text{U}$  generates energy, and two daughter nuclei. The daughter nuclei shoot out in opposite directions due to Coulomb repulsion. (c) The daughter nuclei interact with the atoms of the mineral, creating a track in the crystal lattice. Modified from Gallagher et al. (1998) after Fleisher et al. (1975).

### 3.1.2 Track revelation

Latent fission tracks are very small features, usually no more than 14 nm wide (Paul and Fitzgerald, 1992). They were first studied by Silk and Barnes (1959) through transmission electron microscopy. Because they are so narrow they need to be widened in order to make them visible in an optical microscope. The procedure for doing so is to etch the samples in nitric acid. The tracks are attacked by the acid because the atomic structure in the vicinity of the track has been damaged. The tracks then become wider (1-2  $\mu\text{m}$ ) and consequently visible in an optical microscope (Gleadow et al., 2002 in Gleadow and Lovering, 1977). The quality of the etching process is dependent on the orientation of which the apatite grain has been cut. Because apatite is an anisotropic mineral etching is most efficient at surfaces parallel to the c-axis (e.g. Green et al., 1986a; Jonckheere et al., 2007). Also because the etching is more effective on the track tip than in the internal part, the tracks get a needle like appearance (Wagner and Van den Haute, 1992). The quality of the etching is also affected by the temperature and chemical composition of the nitric acid (Fleisher et al., 1975), and naturally the amount of time exposed to the acid.

## 3.2 Factors affecting the appearance and preservation of fission tracks

### 3.2.1 Partial annealing

Fission tracks are not stable after formation because they are at a higher energy level than the surroundings. Because of this the tracks will, over time and with the proper external conditions, fade (Wagner and Van den Haute, 1992). When the tracks fade, or anneal, they become shorter and may eventually heal completely. The process of annealing is proven to be mostly affected by the prevailing temperature conditions (Fleischer et al., 1965a; Fleischer and Price, 1964): above  $120\pm 10$  °C the tracks in apatite are highly unstable; below this temperature the tracks are metastable and will partially anneal; below  $\sim 60$  °C the tracks are relatively stable (meaning the rate of annealing is very slow). Other factors affecting the annealing of tracks are according to Wagner and Van den Haute (1992) time and pressure. The temperature interval between  $60-120\pm 10$  °C is called the partial annealing zone (PAZ) (Gleadow and Duddy, 1981). The temperature range for which the fission tracks anneal partially is naturally different for each mineral. Because of this, different minerals can be used in thermochronological dating, dependent on which geological process is being studied.

### 3.2.2 Chemical composition

Apatite is considered to have a ternary mineral system with three end members: Fluor-apatite ( $\text{Ca}_5(\text{PO}_4)_3\text{F}$ ), hydroxyl-apatite ( $\text{Ca}_5(\text{PO}_4)_3\text{OH}$ ) and chlor-apatite ( $\text{Ca}_5(\text{PO}_4)_3\text{Cl}$ ). These variations in chemical composition lead to different annealing rates (Laslett et al., 1982, 1984, 1987). Since then work by Gallagher et al. (1998) Green et al. (1985) has showed that the more fluor-rich apatites anneal more readily than chlor-rich apatites. The different chemical compositions also appear to have an effect on the closure temperature of the system (Green et al., 1989). According to later work by Ketcham et al. (1999) the closure temperature will increase with higher chlorine content; for apatites with chemical composition close to the fluorine end member, total annealing has been observed at  $\sim 100$  °C, whereas for apatites with chemical composition at the chlorine rich end member the temperature has been 160 °C and more.

### 3.2.3 Dpar

To quantify the annealing a parameter called  $D_{par}$  is applied. It is a measure of the mean, maximum etch pit diameter oriented parallel to the *c*-axis (Donelick et al., 2005). As mentioned above, the effect of the annealing is dependent on the chemical composition. This is also the case for etching: chlorine-rich samples etch more readily than fluorine-rich samples. Because chlorine-rich apatites have slower annealing rates and also etch more readily than fluor-rich samples, they have larger etch pit diameters. For the fluorine-rich samples the etch pit diameter is smaller because they have higher annealing rates and do not etch as easily (e.g. Carlson et al., 1999; Donelick et al., 2005).

### 3.2.4 Crystallography

Due to their anisotropic properties, apatites show different rates of annealing dependent on their crystallographic orientations (Green and Durrani, 1977). Parallel to the crystallographic *c*-axis the rate of annealing is much slower than at planes perpendicular to the *c*-axis. It is essential to understand the importance of this effect: as annealing progresses only portions parallel to the *c*-axis will be visible (Green et al., 1986a; Donelick, 1991). This leads to a reduction in track density and hence the age of the sample will appear to be younger than it actually is (Green, 1988; Laslett et al., 1984). Because of this only grains that are cut parallel to the *c*-axis are to be counted during the analysis (Donelick et al., 2005).

## 3.3 Age determination

### 3.3.1 The external detector method

In order to date a sample it is necessary to know the amount of  $^{238}\text{U}$  (parent) as well as the number of tracks (daughter) per unit volume. In order to establish the concentration of  $^{238}\text{U}$ , the external detector method (EDM) is applied. This is based on the fact that the  $^{238}\text{U}/^{235}\text{U}$  ratio is constant in nature (Steiger and Jäger, 1977). From this follows that the  $^{235}\text{U}$  concentration can be used to establish the  $^{238}\text{U}$  concentration. This procedure, elaborated by Gallagher et al. (1998), is achieved by attaching a clean flake of muscovite onto the polished sample, and irradiating it with low-energy thermal neutrons triggering the fission of  $^{235}\text{U}$ . The induced fission in the sample creates tracks in the muscovite representing the concentration of  $^{235}\text{U}$  in the sample (Figure 3.2). The induced tracks are not visible in the sample because it is being etched prior to radiation, and the muscovite flake is etched subsequent to irradiation to make them visible. Finally, both the spontaneous and induced fission tracks are counted, and the relationship between them provides an age for the sample (Gallagher et al., 1998; Tagami and O'Sullivan, 2005).

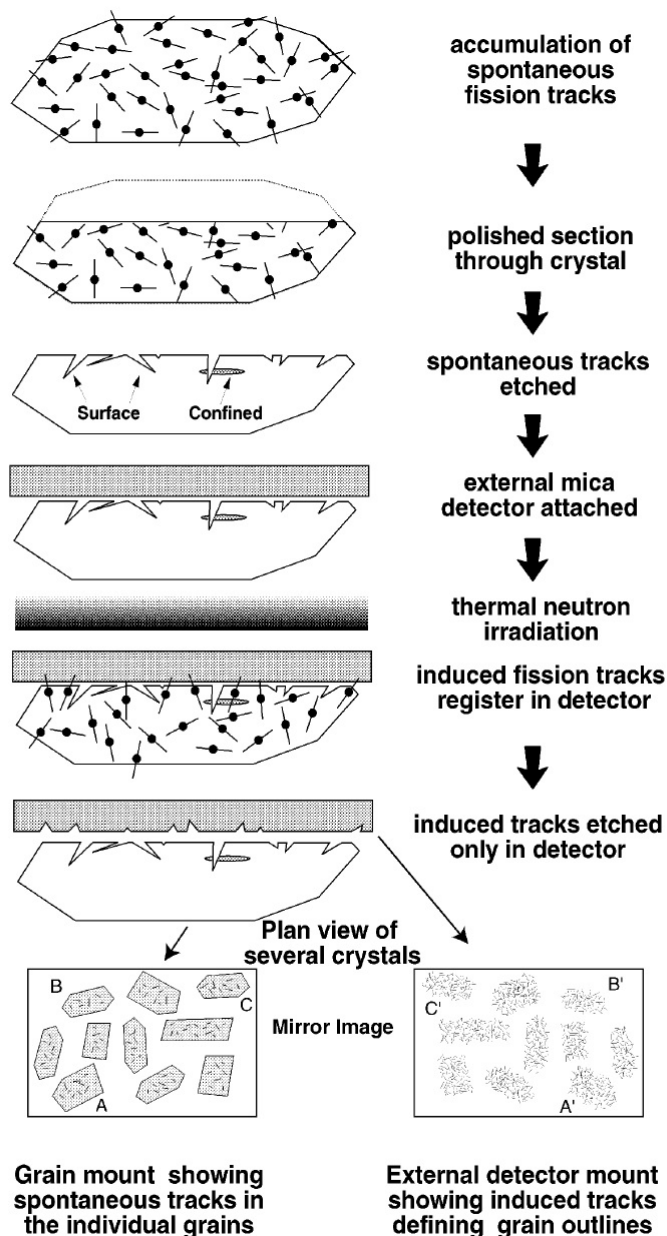


**Figure 3.2:** Principal figure showing the progression of sample preparation with the use of an external detector. See text for further explanation. From Gallagher et al. (1998).

As samples are not irradiated one-by-one but perhaps as many as 30-40 at a time, the neutron flux will weaken as it projects through the samples in the container. Because of this the number of induced fission tracks decrease through the container holding the samples. It is therefore necessary to measure the neutron flux. This is done by placing silicate glass standards of constant and known uranium concentration at regularly spaced intervals in the container together with a muscovite flake (Donelick et al., 2005). These are then counted the same way as the other samples, but finally the average number of induced tracks per sample is divided by the area of the counted field. The number of induced tracks per area on the mica detectors from the standard glasses is called  $\rho_d$ ,



and is a function of the track density corresponding to the position in the container and thus the neutron flux.

### 3.3.2 Age equation

As described by e.g. Tagami and O'Sullivan (2005) and Wagner and Van den Haute (1992), fission track dating is no different from other radiometric dating techniques in that it is based on the decay of a radioactive isotope. The fission track age equation is derived in the following text. The basic equation for calculation of a fission track age is:

$$N_s = \frac{\lambda_F}{\lambda_D} N \{ \exp(\lambda_D t) - 1 \} \quad (3.1)$$

$N_s$  is the number of spontaneous fission tracks in the sample,  $\lambda_F$  is the decay constant of  $^{238}\text{U}$ ,  $\lambda_D$  is the  $\alpha$ -emission also created by the spontaneous fission events,  $^{238}N$  is the number of parent nuclides per unit volume and  $t$  is the age of the sample. In order to determine the  $^{238}\text{U}$ -content, the sample is, as described earlier, irradiated with a thermal neutron flux. This is given by the equation:

$$N_I = {}^{235}N \sigma_F \Phi \quad (3.2)$$

$N_I$  is the number of induced fission tracks,  $^{235}N$  is the number of daughter nuclides per unit volume,  $\sigma_F$  is the transverse section where fission of  $^{235}\text{U}$  is induced and  $\Phi$  is the thermal neutron flux. Further, the age can be calculated by:

$$t = \frac{1}{\lambda_D} \ln \left\{ 1 + \left( \frac{\lambda_D}{\lambda_F} \right) \left( \frac{N_s}{N_I} \right) I \sigma_F \Phi \right\} \quad (3.3)$$

$I$  is the abundance of  $^{235}\text{U}/^{238}\text{U}$  in nature ( $7.2527 \times 10^{-3}$ ), however as only the number of tracks intersecting the surface of the sample mount can be counted the equation becomes:

$$t = \frac{1}{\lambda_D} \ln \left\{ 1 + \left( \frac{\lambda_D}{\lambda_F} \right) \left( \frac{\rho_s}{\rho_I} \right) QGI \sigma_F \Phi \right\} \quad (3.4)$$

$\rho_s$  is the density of countable (i.e. at the surface) spontaneous fission tracks,  $\rho_I$  is the number of induced fission tracks,  $Q$  is an efficiency factor for observation and marking of fission tracks. This factor may be excluded if the same criteria is being used throughout the analysis (see paragraph below). The parameter  $G$  is the internal geometric factor concerning the difference in volume for track production in both the internal surface (spontaneous tracks) and the external surface (induced tracks). The geometry factor is approximately 0.5 due to the differences in etch efficiency and the range of fission tracks (Gleadow and Lovering, 1977).

Some of the parameters in equation (3.4) are difficult to determine, especially the decay constant,  $\lambda_F$ , and the thermal neutron flux  $\Phi$  (Van Den Haute et al., 1998). The neutron flux has previously been established by inducing fission in a standard glass of known uranium content, and measuring the  $\beta$ - or  $\gamma$ - activity caused by this (Hurford and Green, 1983). Because of the difficulties and uncertainties with this method, a new approach has been established by Hurford and Green (1983, 1982) called the zeta calibration. This is a personal zeta factor ( $\zeta$ ) established for each individual person performing the analysis. It is performed by counting standards of known ages, and it obliterates the problems faced with the old method. It is given by the equation:

$$\zeta = B \times \frac{I\sigma_F}{\lambda_F} \quad (3.5)$$

$B$  is a calibration constant empirically determined. By combining equations (3.4) and (3.5) the fission track age of a given sample can be calculated as follows:

$$t = \frac{1}{\lambda_D} \ln \left\{ 1 + \lambda_D \zeta \rho_D \left( \frac{\rho_S}{\rho_I} \right) QG \right\} \quad (3.6)$$

## 3.4 Track lengths

### 3.4.1 Track classification

There are several types of tracks in a grain and not all of them are suitable for length measurements. Some tracks are confined within the grain (confined tracks) and some are cut by the polished grain mount surface (semi - tracks). Earlier it was customary to use semi-tracks for length measurement, but this practice has been abandoned as it does not provide adequate information of cooling styles and the true track lengths (Laslett et al., 1984, 1994). The best practice is to measure tracks that are parallel or sub parallel to the c-axis of the grain because, as described in chapter 3.2.4, the annealing and etching properties differ because of the anisotropic properties of apatite (Gleadow et al., 1986; Laslett et al., 1982). Tracks that are oriented at an angle to the crystallographic c-axis anneal faster and etch slower (Ketcham et al., 2007b; Ketcham, 2005b). Also, parallel to the c-axis the true length of the track is visible. If the track is at an angle to the c-axis it will appear shorter than it actually is.

The confined tracks are dependent on conduits to the surface by either another track, cleavage or defect in order to be etched. Three different types of confined tracks have been described (Figure 3.3): Lal et al. (1969) identified TINT (track in track) and TINCLE (track in cleavage or crack), and Donelick et al. (2005) identified TINDEF (track in defect). Work done by Jonckheere and Wagner (2000); Barbarand et al. (2003b) showed that TINCLES sometimes anneal slower, and because of this the best practice is to measure only TINTs as these are properly etched and well defined.

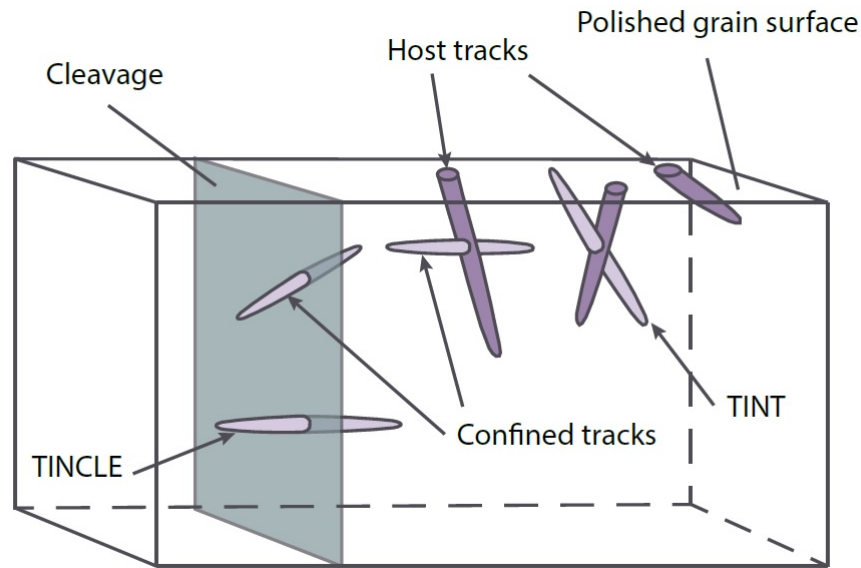


**Figure 3.3:** Different types of tracks in a sample: TINCLE (track-in-track); TINT (track in track). Modified from Tagami and O’Sullivan (2005).

### 3.4.2 Initial track lengths

The use of track lengths for geological interpretation requires knowledge about the nature of the tracks. Three important aspects need to be considered (e.g. Gleadow et al., 2002): (1) Tracks have a quite similar mean initial length which according to Gleadow et al. (1986) is about  $15.8\text{-}16.3\ \mu\text{m}$ , (2) Tracks anneal when exposed to temperatures within the partial annealing zone, (3) Tracks are formed continuously, and the annealing depends on the temperatures the tracks are exposed to since formation.

### 3.4.3 Track length distributions

In order to apply the fission track method, it is very important to understand the meaning of the track lengths; every track tells a story of its thermal path since formation. It is alluring to think that the fission track ages represent the time of which the rock was subjected to temperatures below the zone of total annealing (Wagner and Van den Haute, 1992). However, the picture is not that simple. This statement requires that the rock has remained unaltered after the formation of the fission tracks. Fission track dating is a little different from other conventional dating methods in that the closure temperature can be any temperature below that of total annealing (Wagner and Reimer (1972). There are essentially three different types of ages depending on the thermal history of the host rock: “event ages”, “cooling ages” and “mixed ages” (Gleadow and Brown, 2000). Figure 3.4 show the three different cooling paths and their respective ages, mean track lengths and standard deviation of the track length distribution. All models show cooling over a period of 100 Ma within the partial annealing zone ( $60\text{-}120\ ^\circ\text{C}$ ) and below. In the first case (Figure 3.4A) the rock has cooled rapidly and has not been subjected to heating afterwards. This yields a unimodal distribution of track lengths of  $15\ \mu\text{m}$  and a modeled age of 99.8 Ma which is quite similar to the input age of 100 Ma. This might be called an “event age” according to Gleadow and Brown (2000), however such cooling patterns are quite rare in nature. They may be found in volcanic rocks and rocks that have in other ways been brought rapidly to or near the surface. It

is more common to find rocks with cooling paths as the ones in Figure 3.4b and c. If the rock has cooled slowly, a negatively skewed track length distribution is representative as shown in Figure 3.4B. Here the modeled age of the sample is only 75 Ma, and the track length distribution is much shorter and wider, meaning that the age is a result of the slow cooling through the PAZ. A track distribution like this will not represent the start of an event, but rather a continuous cooling through the partial annealing zone to surface temperatures. Hence, this is called a “cooling age”. Figure 3.4C show samples that have been subjected to elevated temperatures after the initial cooling and therefore show a typical bimodal distribution of track lengths. This is based on the appearance of the tracks; tracks formed before the second heating event will have annealed more than the newest tracks, making them shorter than the latter. Also, the amount of long tracks (i.e. tracks that has not undergone significant annealing) says something about how long the rock was at near-surface temperatures. This is called a “mixed age” because of the short peak representing the elevated temperatures and the high peak representing the rapid cooling that followed. The modeled age found for both Figure 3.4B and C does not represent a specific geological event, but give information of the timing and magnitude of the cooling, as well as the temperature before this happened, and finally the timing of when the rock entered the PAZ (Gleadow and Brown, 2000).

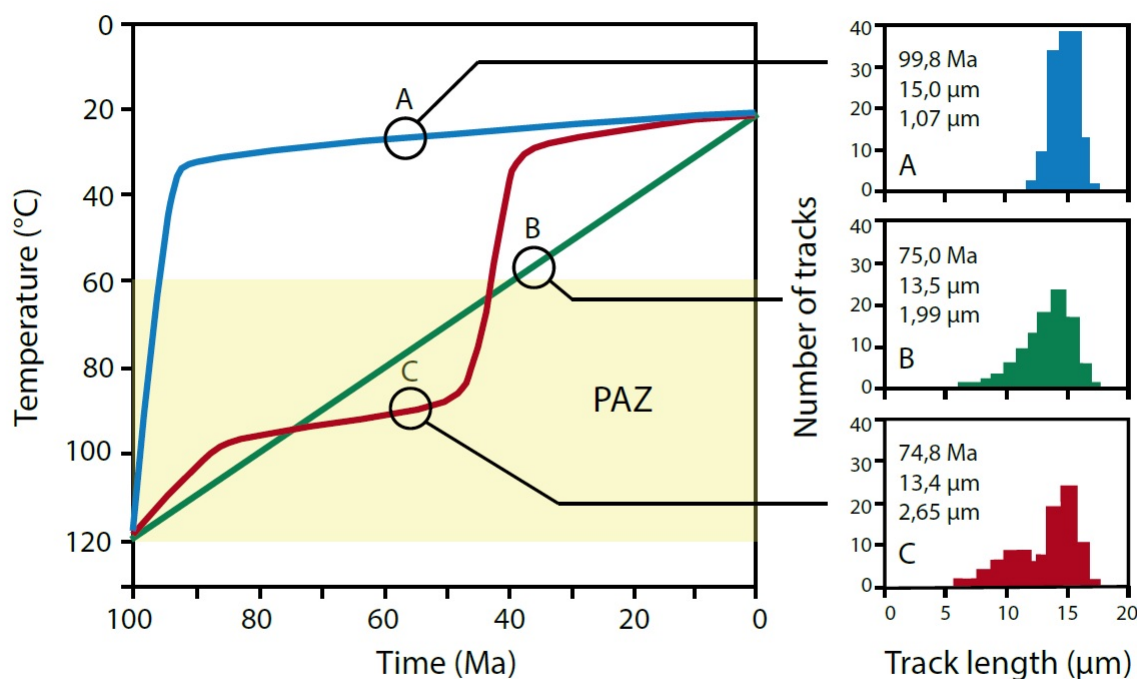


**Figure 3.4:** Three different length distributions showing their respective thermal histories: (a) Rapid cooling; (b) Slow cooling through the PAZ; (c) Interrupted cooling resulting in a typical bimodal distribution of track lengths. From Gleadow et al. (2002) after Gleadow and Brown (2000).

# 4 SAMPLE PREPARATION AND ANALYTICAL PROCEDURE

---

10 rock samples were collected during fieldwork in the area north of Boknafjorden in Rogaland. In addition, 15 partially prepared samples were provided by Tobias Woznitza. 12 of these contained a satisfying amount of apatite and were also prepared for analysis. A total of 22 samples were prepared and irradiated.

## 4.1 Sample preparation

### 4.1.1 Mineral separation

For the mineral separation the following procedure was executed:

1. Approximately 4 kgs of rock were sampled at each of the 10 localities.
2. The rocks were downsized using a hammer and chopping block to fragments < 2 cm in diameter.
3. Samples were crushed with a Pulverisette 300 disk mill (Figure 4.1 A) and sieved.
4. The fraction < 315  $\mu\text{m}$  was put on a Wilfley 800 shaking table (Figure 4.1 B) in order to separate the lighter, rock forming minerals from the heavy fraction which includes the apatites.
5. The samples were dried in a heating cabinet at 45 °C.
6. The samples were separated according to their magnetic properties with a Franz magnetic separator (Figure 4.1 C) set at a slope and sideways tilt of 15 ° and current of 0,3 A.
7. The non-magnetic fraction was put in sodium polytungstate (SPT) with a density of approximately 2,87  $\text{g}/\text{cm}^3$  (Figure 4.1 D). In this process the lighter minerals are separated from the heavier (apatite has a density of approximately 3,19  $\text{g}/\text{cm}^3$  and thus sinks to the bottom of the liquid).
8. The heavy fraction was dried and separated once more in the magnetic separator with a current of 1,2 A.
9. The non-magnetic fraction was put in diiodomethane (DIM) with a density of 3.3  $\text{g}/\text{cm}^3$  (Figure 4.1 E). Here, the apatite is lighter than the liquid and thus floats. This is the final step of the mineral separation and the amount of sample is now dramatically reduced. The samples provided by Tobias Woznitza had already been crushed and separated on a shaking table, but the final work with the magnetic separator and heavy liquids remained.

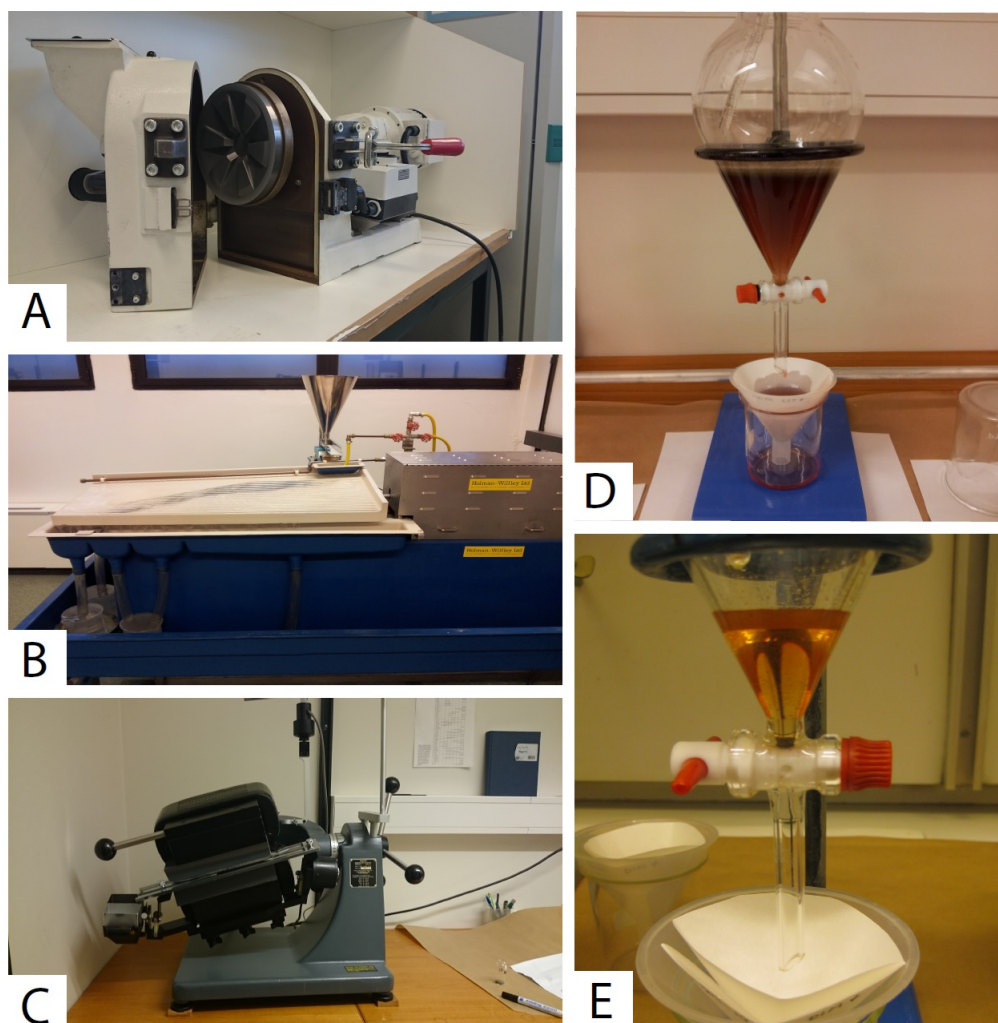


**Figure 4.1:** Mineral separation by means of 300 Pulverisette disc mill (A); Wilfley 800 shaking table (B); Franz magnetic separator (C); SPT (D) and DIM (E).

#### 4.1.2 Grain mount preparation

In order to obtain the largest apatite grains, the sample were sieved with a  $100\ \mu\text{m}$  mesh. Each sample and standard were then mounted (separately) in a plastic ring filled with epoxy. After drying they were ground with silica powder of 800, 1000 and 1200 in order to reveal a large internal area of the grains. When this was achieved, they were polished with 6 and  $3\ \mu\text{m}$  diamond polish to make the grain surfaces smooth. The last stage of polishing was conducted using  $0.05\ \mu\text{m}$   $\text{Al}_2\text{O}_3$  powder. Finally, the mounts were cut in a 1 mm thick slice and ground into a square of approximately  $1\times 1$  cm in order to fit the container used for irradiation.

#### 4.1.3 Etching and irradiation

In order to make the fission tracks visible in an optical microscope the samples were etched for 20 seconds in 5 molar nitric acid ( $\text{HNO}_3$ ) at  $20 \pm 1\ ^\circ\text{C}$ . Afterwards they were thoroughly washed in running water over night and dried. Then, a sheet of muscovite was placed on the polished side of each sample mount and the sample and muscovite were taped together. The sheet of muscovite acts as the external detector as described in chapter 3.3.1. The samples were packed in a cylinder along with a series of

IRMM-540R dosimeter glasses (with a known U-concentration of 15 ppm) and irradiated at the Garching Forschungsreaktor FRM II at the Technical University of Munich. The dosimeter glasses were also paired with an external muscovite detector and are used in order to measure the neutron flux through the cylinder when irradiated. The container positions for the irradiations are listed in Appendix A.

#### 4.1.4 Post irradiation procedure

After irradiation the samples needed approximately 4 months to cool down in order to be handled safely (radioactivity below  $5.0 \mu\text{Sv h}^{-1}$ ). When this level was reached, the samples were marked with five pinholes for reference as the muscovite is the mirror image of the sample, before the tape was removed. The external detectors were then etched for 20 minutes in 40% hydrofluoric acid (HF) at room temperature in order to reveal the induced tracks. Afterwards they were rinsed thoroughly in running water over night in order to remove any leftover acid.

Finally, the samples with their corresponding micas were glued onto a petrographical glass slide together with a copper-grid crosshair used as an additional reference point. (Figure 4.2).

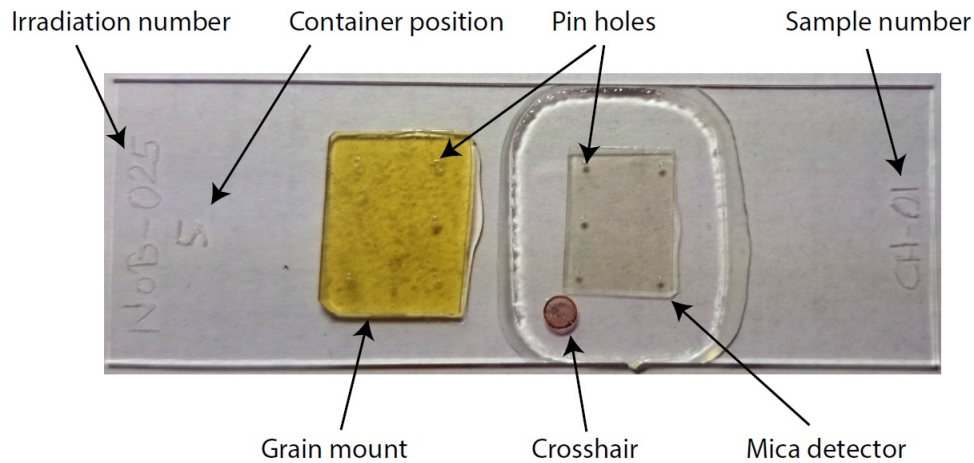


**Figure 4.2:** Sample ready for analysis.

## 4.2 Analytical procedure

### 4.2.1 Equipment

The analysis was conducted at the University of Bergen by means of the following equipment (Figure 4.3) and software:

- Olympus BX51 optical microscope
- CalComp Drawing-board III digitizing tablet
- LED-mouse for length measurement
- Kinetek stage
- FTstage software by Dumitru (1993)
- TrackKey software by Dunkl (2002)
- HeFTy 1.8.0 software by Ketcham and Donelick (2013)

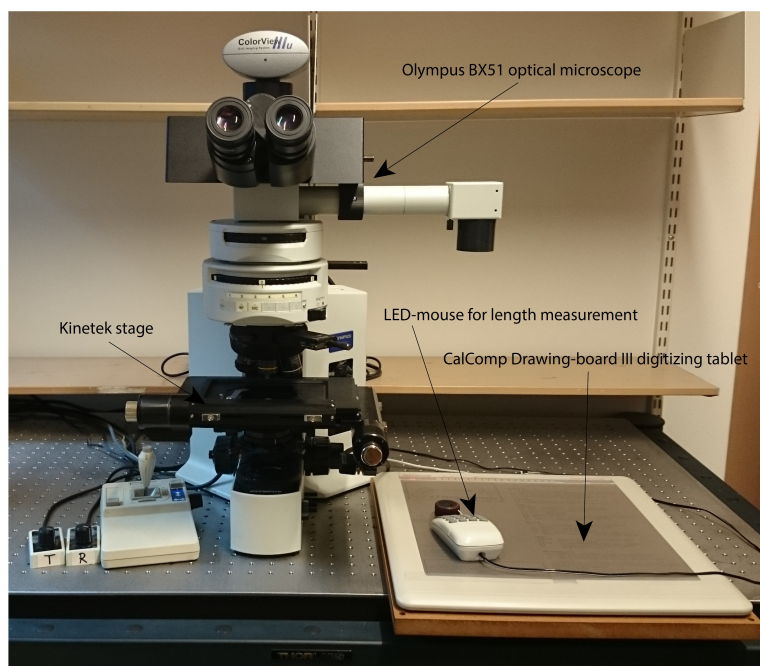


**Figure 4.3:** Equipment used for the analyses.

### 4.2.2 Counting of dosimeter glasses and $\rho_d$ estimation

Before conducting the fission track analysis, the micas of the dosimeter glasses were counted in order to measure the decrease in neutron flux throughout the cylinder. For each glass in the two irradiations 90-120 tracks  $\times$  25 squares were counted three times. The track counts for the glasses were plotted against their position in the container. Linear regression was used to calculate the  $\rho_d$  values for the unknown samples in between the glasses. A trend for the neutron flux was thus determined. For irradiation NoB-023 and NoB-025 four and three IRMM-540R standard glasses were counted, respectively.



#### 4.2.3 Zeta calibration

Because the fission track analysis is done by a person and not a computer, a personal calibration factor is needed in order to ensure reproducible results. In order to achieve this the following recommendations of the IUGS Subcommittee on Geochronology Hurford (1990a,b) were implemented: at least five analyses done from three different irradiations with at least two age standards. In this study, seven Durango and seven Fish Canyon Tuff standards were analysed. For each analysis a zeta-value and standard deviation was calculated by means of the software TrackKey (Dunkl, 2002). A final zeta value was calculated as the weighted mean of the individual zeta values.

#### 4.2.4 Counting technique

When selecting grains for analysis only grains cut parallel to the crystallographic c-axis were used. These grains are recognized in reflected light by their elongated and parallel etch pits. Depending on the distribution and density of tracks within the grain a certain area of the grid is counted (preferably no smaller than ca.  $1400 \mu m^2$ ), and then the same area is counted on the mica detector.

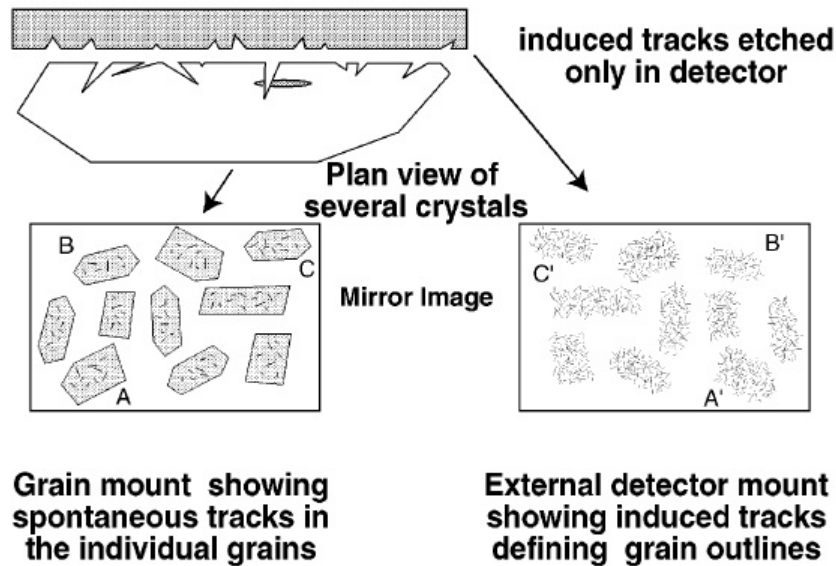


**Figure 4.4:** Figure showing the grain mount and its external detector (print). The print is the mirror image of the grain mount, and shows the outline of the grains (the outline will be clearer if the track density is high). Modified from Gallagher et al. (1998).

#### 4.2.5 Calculation of fission track ages

As for the zeta-calibration, TrackKey was also used for calculation of fission track ages. There are three ways of reporting fission track ages as described by Gallagher et al. (1998), namely the mean, pooled and central ages. The central age is the weighted mean of the log normal distribution of single grain ages, and is the preferred age because it is most robust to outliers and non-Poissonian variation. In order to assess the Poissonian variation a chi-square ( $\chi^2$ ) test is performed. The test indicates if the central age consists of more than one age population by measuring the single grain age dispersion. A  $\chi^2$  value of more than 5% is considered a pass.

#### 4.2.6 Track length and $D_{par}$ measurements

Horizontally confined tracks are used for length measurements, and they are easily recognizable in reflected light as bright elongated features (Figure 4.5). Using a 2000x magnification, track lengths and  $D_{par}$  were measured by utilizing a LED cursor marking the ends of the feature and successively obtaining the lengths. By marking the crystallographic c-axis, the angle between the measured track and c-axis was recorded. Donelick et al. (2005) suggest 100 tracks per sample are to be measured in order to produce a statistically robust thermal model. Because TINCLEs are sometimes resistant to annealing (Jonckheere and Wagner, 2000), only TINTs were measured in this study as is recommended by Barbarand et al. (2003b). For each of the 20 dated grains in every sample, five  $D_{par}$  values were measured, and additionally three  $D_{par}$  values for grains where length measurements were conducted.

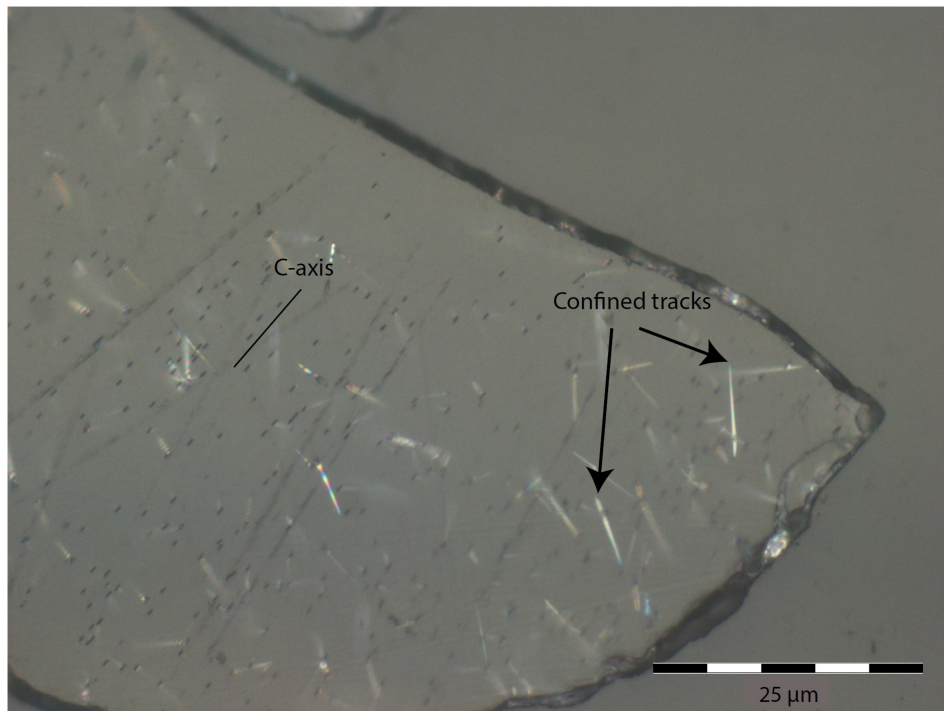


**Figure 4.5:** Grain cut parallel to the c-axis as shown by the elongated etch pits, and confined tracks suitable for length measurements.

#### 4.2.7 Thermal history modeling

Thermal history modeling was performed by the use of the software HeFTy 1.8.0 developed by Dr. Richard A. Ketcham. It utilizes the parameters so far produced in the study; single grain age data, track lengths and their corresponding  $D_{par}$  values. In addition, for estimation of kinetic behavior the annealing model of Ketcham et al. (2007a) was used and  $D_{par}$  was selected as kinetic parameter. As proposed by Ketcham et al. (2007b) confined tracks were corrected by c-axis projection in order to strengthen the reproducibility of the data. For the calculation of the default initial mean track length, the  $D_{par}$  values were used. The software utilizes these parameters to produce a forward model (chapter 3.4.3) and an inverse model. The inverse modeling creates a range of possible cooling paths for the sample and compares them to the data. Paths with good or acceptable fits to the data are kept whilst paths with a poor fit to the data are

discarded. The cloud of good and acceptable cooling paths constrains possible cooling paths for the sample. In this study, the Monte Carlo search method was applied. Thermal constraints forcing the paths through a certain temperature at a certain age was also utilized. All samples with length measurements were modeled with start and end constraints. Start constraints were set to the time and temperature corresponding to the Caledonian orogeny and end constraints were set to average surface temperatures of today ( $8 \pm 5$  °C). Additional modeling constraints are discussed in chapter 5.4.



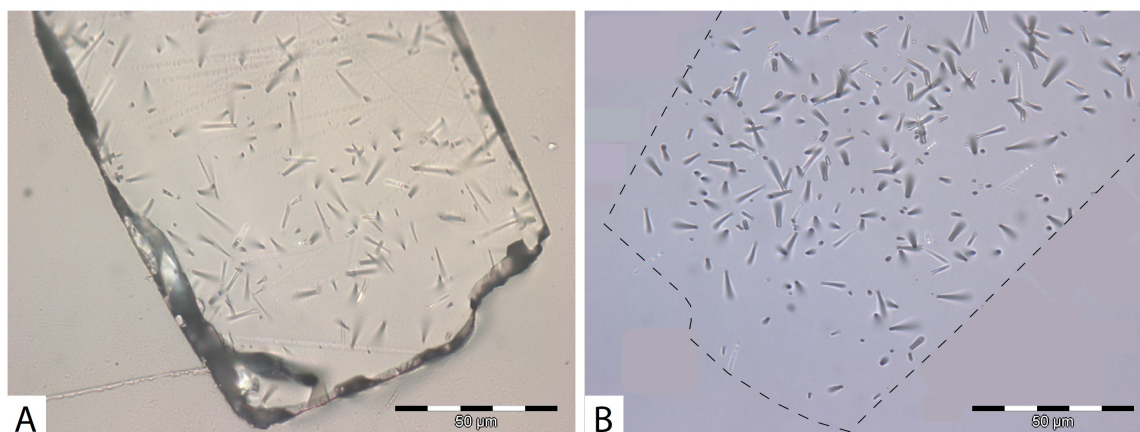
# 5 RESULTS

## 5.1 Sample quality

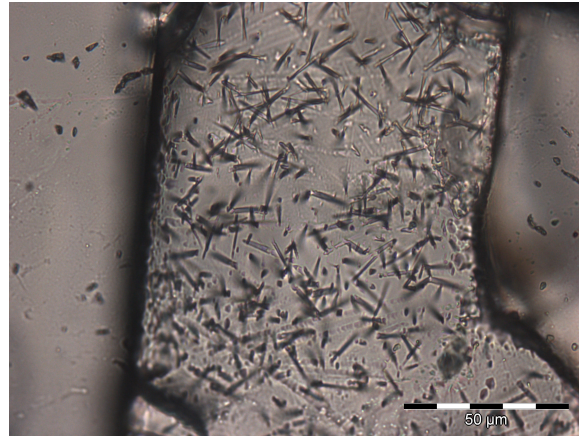
The overall grain quality is quite good. However, the samples from the southeastern side of the RSZ are generally of higher quality (Figure 5.1) than those from the northwestern side (Figure 5.2). The reason for this however, is not known, but it might be related to the lithology. The CH samples are gneisses, whereas the NTW samples are mostly granites and granodiorites. The quality of the apatites in this study seems to be better in the magmatic rocks. A complete overview of the individual sample quality is listed in Table 5.1.

Table 5.1: Table of the general grain quality of the individual samples.

Sample no.	General grain quality	Zoning	Cracks and scratches	Inclusions	U (ppm)
CH-01	Intermediate	-	-	X	20
CH-02	Intermediate	X	X	X	36
CH-03	Good	-	-	-	24
CH-04	Poor	X	X	-	33
CH-05	Intermediate	-	X	X	5
CH-06	Intermediate	-	X	X	9
CH-07	Poor	X	X	X	39
NTW-16-13	Good	-	-	X	24
NTW-17-13	Good	-	-	-	4
NTW-19-13	Good	-	-	X	17
NTW-24-13	Good	-	-	X	31
NTW-27-13	Good	-	X	X	35
NTW-28-13	Intermediate	X	X	X	20
NTW-29-13	Good	-	-	X	27
NTW-30-13	Good	X	X	-	24
NTW-31-13	Intermediate	-	X	X	50
NTW-32-13	Intermediate	X	-	X	31



**Figure 5.1:** A typical good sample, NTW-16-13, (A) with its corresponding print (B). The dotted line represents the approximate edge of the grain.



**Figure 5.2:** A poor sample, CH-07, with a poor surface, fluid inclusions, mineral inclusions and dislocations.

## 5.2 Calculations and calibrations

### 5.2.1 Counting of dosimeter glasses and estimation of $\rho_d$

The counting of the mica detectors of the IRMM-540R standard glasses yielded  $\sim 2500$ - $3000$  tracks in each glass per count. This was used in order to establish a track density gradient and  $\rho_d$  values for the individual samples and standards in their respective irradiations (Figure 5.3). In Appendix A the samples' position in the container and  $\rho_d$  values are listed.

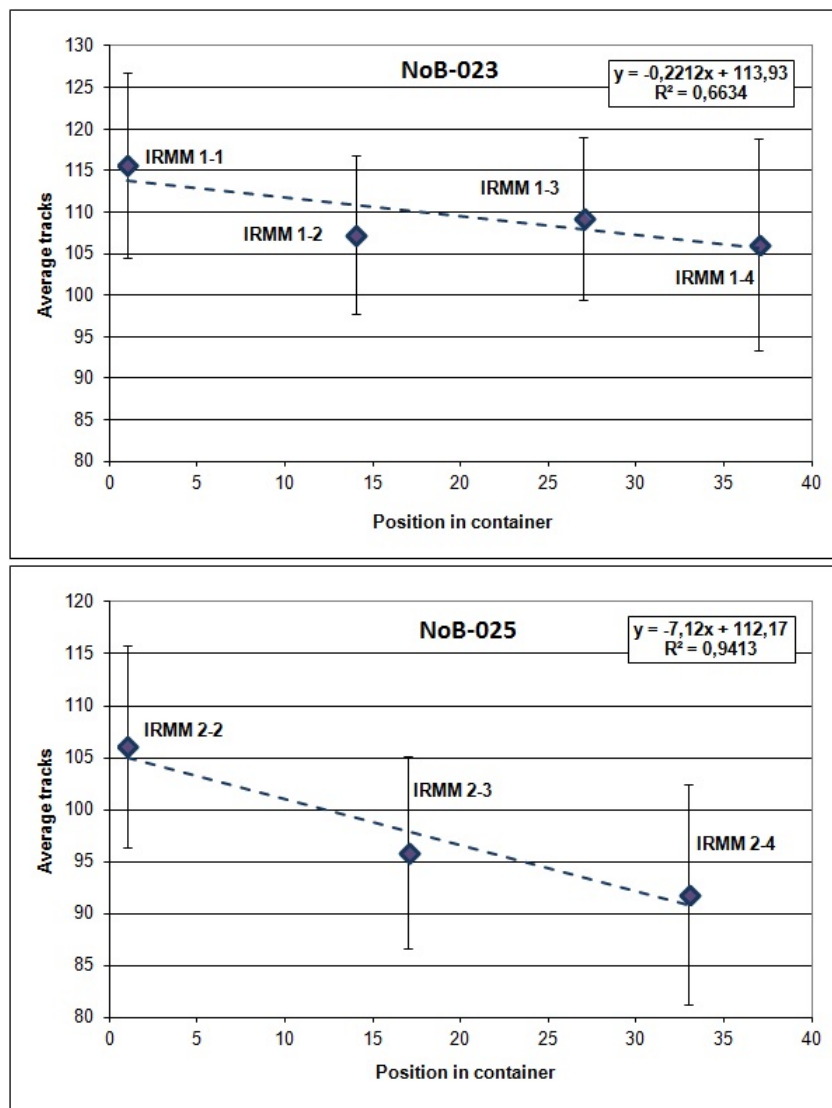


**Figure 5.3:** Average number of tracks in one grid unit plotted against position in the container (NoB-023 and NoB-025). IRMM 1-1 and IRMM 2-2 were closest to the neutron source. With increasing distance from the source, the number of tracks decrease. The formulae in the boxes are used for calculating  $\rho_d$  values for each sample in their respective container.

### 5.2.2 Zeta calibration

The zeta calibration was performed by analysing seven Durango and five Fish Canyon Tuff standards from seven different irradiations. The final zeta yielded a value of  $258,9 \pm 6,2$  (Table 5.2 and Figure 5.4).

Table 5.2: Zeta calibration results.

Irradiation no.	Standard no.	n (G)	Dosimeter		Spontaneous		Induced		Zeta
			$\rho_d (10^5)$	Nd	$\rho_s (10^5)$	Ns	$\rho_i (10^5)$	Ni	
NoB-002	DUR 1	20	16.701	9168	1.454	136	10.596	991	274.6 ± 25.7
NoB-002	DUR 2	20	16.729	9168	1.576	136	9.351	807	223.3 ± 21.1
NoB-002	FC-1	20	16.675	9168	2.481	175	17.964	1267	242.8 ± 20.2
NoB-003	Dur	20	18.016	9849	1.460	146	10.891	1089	246.9 ± 22.3
NoB-003	FC	20	17.940	9849	2.488	129	17.606	913	220.7 ± 21.2
NoB-014	Dur	20	14.634	32181	2.730	298	18.271	2011	290.3 ± 18.7
NoB-014	FCT	20	14.576	32181	2.107	202	14.882	1422	270.1 ± 20.9
NoB-017	FCT 1	20	18.912	18016	2.100	119	19.373	1098	272.8 ± 26.9
NoB-021	DUR	20	19.760	32405	3.050	245	21.212	1704	221.6 ± 15.6
NoB-021	FCT	20	19.691	32405	1.871	168	16.814	1510	255.3 ± 21.3
NoB-023	DUR	20	20.227	30239	2.443	259	25.110	2662	319.9 ± 21.5
NoB-025	DUR	20	18.047	14690	2.396	214	21.285	1901	309.9 ± 23.0
<b>Weighted mean zeta</b>									<b>258.9 ± 6.2</b>

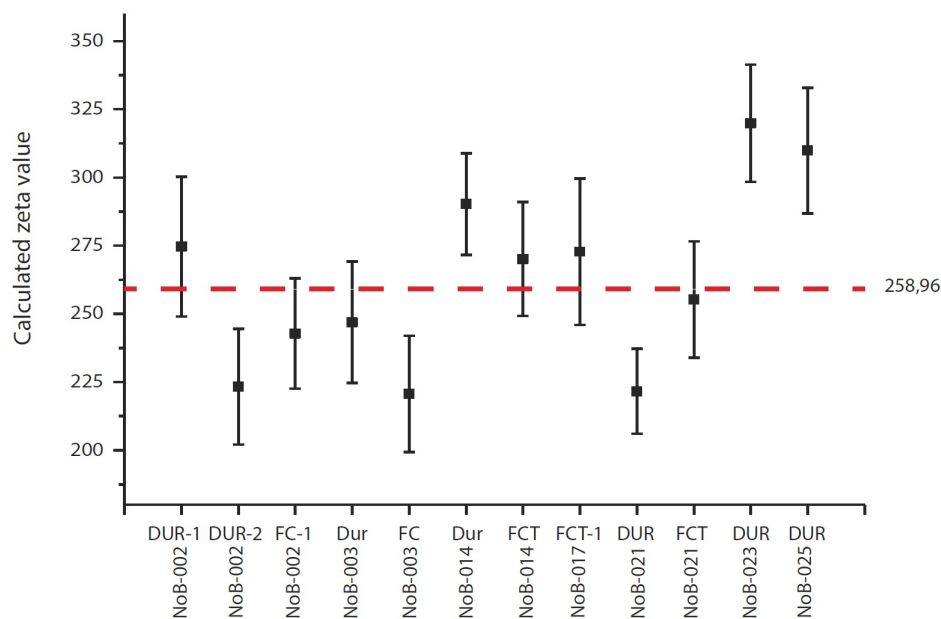


**Figure 5.4:** Plot showing the individual zetas and the weighted mean zeta (red dashed line).

### 5.3 AFT analysis

Apatite fission track analyses were performed on 17 samples. The ages range from Permian (260 Ma) to early Cretaceous (141 Ma) with a majority of ages in the Jurassic between 149 and 195 Ma. The samples from the NW side of the Røldal Shear Zone are generally older than the samples from the SE side. One sample, CH-05, is quite a lot older than the other samples and other thermochronological data in the area (Woznitza,



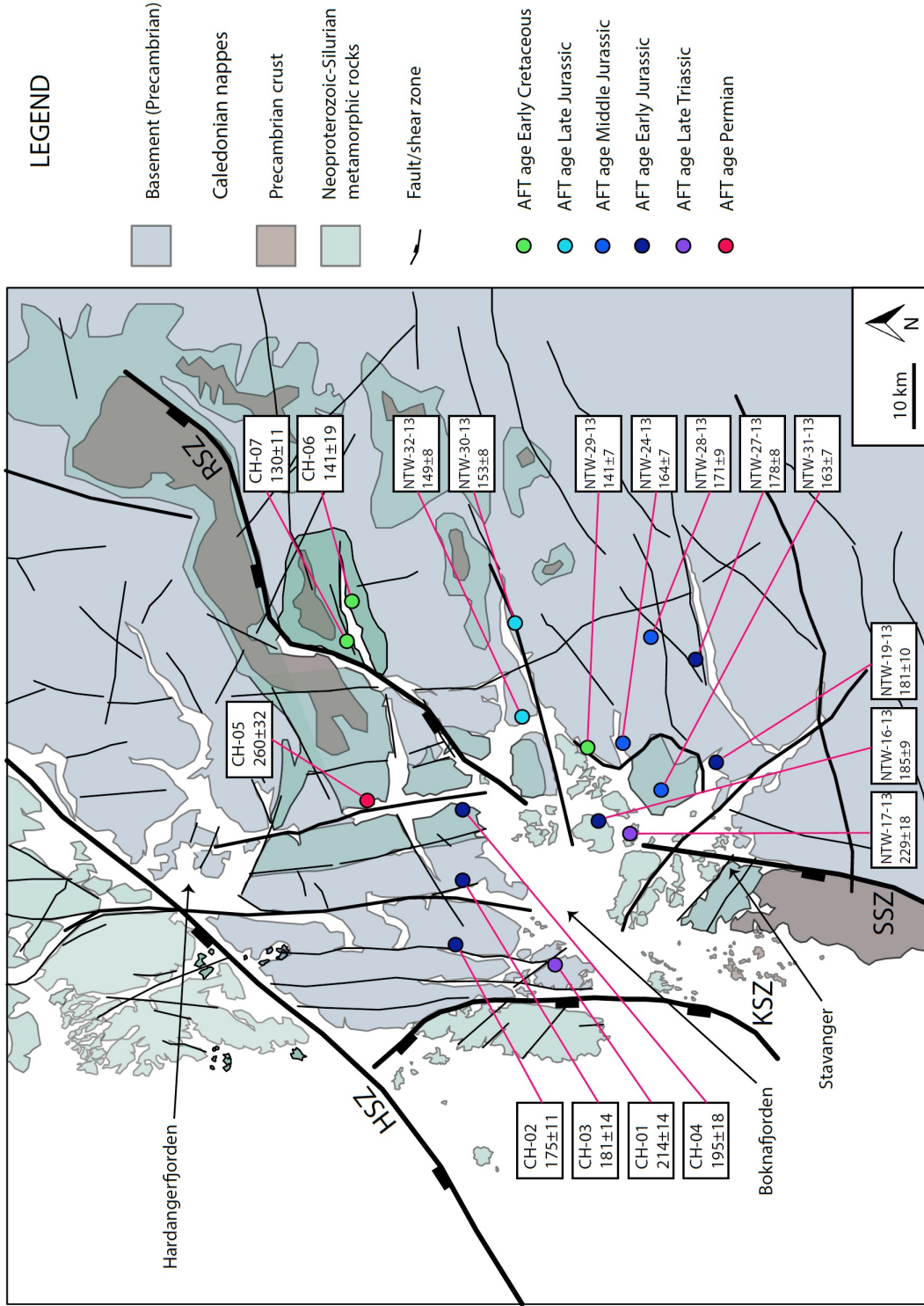
2014). Also, it has one of the lowest U-concentrations and only 13 grains were counted. This is the sample with the lowest number induced tracks and also the highest error. It must therefore be interpreted with caution. The results of the apatite fission track analyses is presented in Table 5.3, and a map with sample locations and corresponding central ages is presented in Figure 5.5. Radial plots are listed in Appendix B.

Figure 5.6 is showing the comparison between the AFT with Dpar, U-concentration, easting and elevation. There is no correlation between age and mean Dpar as seen from the red regression line (Figure 5.6 A). There is a very weak correlation between age and U-concentration (Figure 5.6 B). The ages are younger in the footwall (grey) on the southeastern side of the RSZ (mean age where CH-05 is excluded: 163 Ma) than in the hangingwall (pink) on the northwestern side (mean age: 181 Ma) (Figure 5.6 C). Samples below 100 m (yellow) have ages ranging from Permian to Cretaceous, whereas the samples at the highest elevations (green) are younger with ages ranging from early Jurassic to early Cretaceous (Figure 5.6 D). There is also a general trend for the ages to become younger inland (Figure 5.5).

Table 5.3: Apatite fission track data.

Sample no.	Irradiation	UTM (zone 32V)		Lithology	Elevation (masl)	n	Dosimeter		Spontaneous		Induced		Central age $\pm 1\sigma$ (Ma)	P ( $\chi^2$ ) %	Measured		C-axis projection		n	Dpar (mean) ( $\mu\text{m}$ )	$\pm 1\sigma$ ( $\mu\text{m}$ )	U (ppm)
		Easting	Northing				Nd	ps ( $10^5$ )	Ns	ps ( $10^5$ )	Ni	MTL ( $\mu\text{m}$ )			$\pm 1\sigma$ ( $\mu\text{m}$ )	MTL ( $\mu\text{m}$ )	$\pm 1\sigma$ ( $\mu\text{m}$ )	(TL)				
CH-01	NoB-025	297550	6569072	Gneiss	68	20	18.860	14690	24.381	1012	27.561	1144	214 $\pm$ 14	3.3	-	-	-	-	100	1.17	0.06	20
CH-02	"	299766	6586213	Gneiss	21	20	18.778	14690	36.014	919	49.808	1271	175 $\pm$ 11	5.9	11.28	3.01	13.09	1.50	100	1.35	0.05	36
CH-03	"	310550	6583261	Gneiss	48	7	18.697	14690	23.628	339	31.086	446	181 $\pm$ 14	80.6	-	-	-	-	1.20	0.09	24	
CH-04	"	321928	6582793	Gneiss	13	6	18.616	14690	34.593	233	42.165	284	195 $\pm$ 18	29.7	-	-	-	-	1.35	0.08	33	
CH-05	"	324012	6599580	Gneiss	26	13	18.535	14690	6.228	147	5.635	133	260 $\pm$ 32	76.4	-	-	-	-	1.14	0.07	5	
CH-06	"	354814	6602532	Gneiss	243	11	18.453	14690	6.498	95	10.875	159	141 $\pm$ 19	87.2	-	-	-	-	1.15	0.07	9	
CH-07	"	349157	6603536	Gneiss	183	14	18.372	14690	27.304	462	49.702	841	130 $\pm$ 11	0.8	11.03	2.06	12.66	1.21	100	1.32	0.1	39
NTW-16-13	NoB-023	320899	6562557	Granitic intr.	41	19	21.084	32946	24.453	1402	35.808	2053	185 $\pm$ 9	13.9	-	-	-	-	1.12	0.08	24	
NTW-17-13	"	317933	6557115	Pegmatite	11	19	20.037	32946	5.256	392	5.846	436	229 $\pm$ 18	32.4	-	-	-	-	1.36	0.07	4	
NTW-19-13	"	329677	6542961	Biotite gneiss	16	19	20.989	32946	18.094	755	26.745	1116	181 $\pm$ 10	65.1	-	-	-	-	1.04	0.07	17	
NTW-24-13	"	333929	6559737	Granite	81	20	20.894	32946	28.725	1444	46.708	2348	164 $\pm$ 7	73.7	-	-	-	-	1.13	0.13	31	
NTW-27-13	"	350333	6547143	Catacl. granite	264	18	20.799	32946	32.250	1351	48.220	2020	178 $\pm$ 8	30.8	9.24	3.41	12.1	1.64	100	1.09	0.06	35
NTW-28-13	"	351361	6553664	Granodiorite	607	20	20.751	32946	19.310	1123	29.972	1743	171 $\pm$ 9	4.8	11.93	1.57	11.93	1.58	100	1.11	0.07	20
NTW-29-13	"	332499	6564421	Granodiorite	37	20	20.703	32946	19.421	1005	36.484	1888	141 $\pm$ 7	21.4	-	-	-	-	1.00	0.14	27	
NTW-30-13	"	352255	6574928	Granite	346	20	20.656	32946	19.861	1006	33.897	1717	153 $\pm$ 8	19.9	-	-	-	-	1.23	0.06	24	
NTW-31-13	"	327861	6550582	Granite	43	19	20.608	32946	43.900	1577	71.097	2554	163 $\pm$ 7	39.6	-	-	-	-	1.18	0.05	50	
NTW-32-13	"	337809	6574086	Granite	62	20	20.560	32946	24.293	721	43.059	1278	149 $\pm$ 8	25.7	-	-	-	-	1.15	0.09	31	

n (G), number of grains; Nd, Ns, Ni, number of tracks counted; pd, ps, pi, track densities in  $1 \times 10^5$  tracks  $\text{cm}^{-2}$ ; P( $\chi^2$ ), p-value of the chi-square age homogeneity test (Galbraith, 2005); MTL, mean track length; n (TL), number of track lengths



**Figure 5.5:** Simplified geological map of the study area showing AFT ages, shear zones and some selected faults (note that the width of the shear zones and faults are not to scale). AFT ages are reported as central ages with a  $1\sigma$  error. HSZ, Hardangerfjord Shear Zone; KSZ, Karmøy Shear Zone; SSZ, Stavanger Shear Zone; RSZ, Røldal Shear Zone.

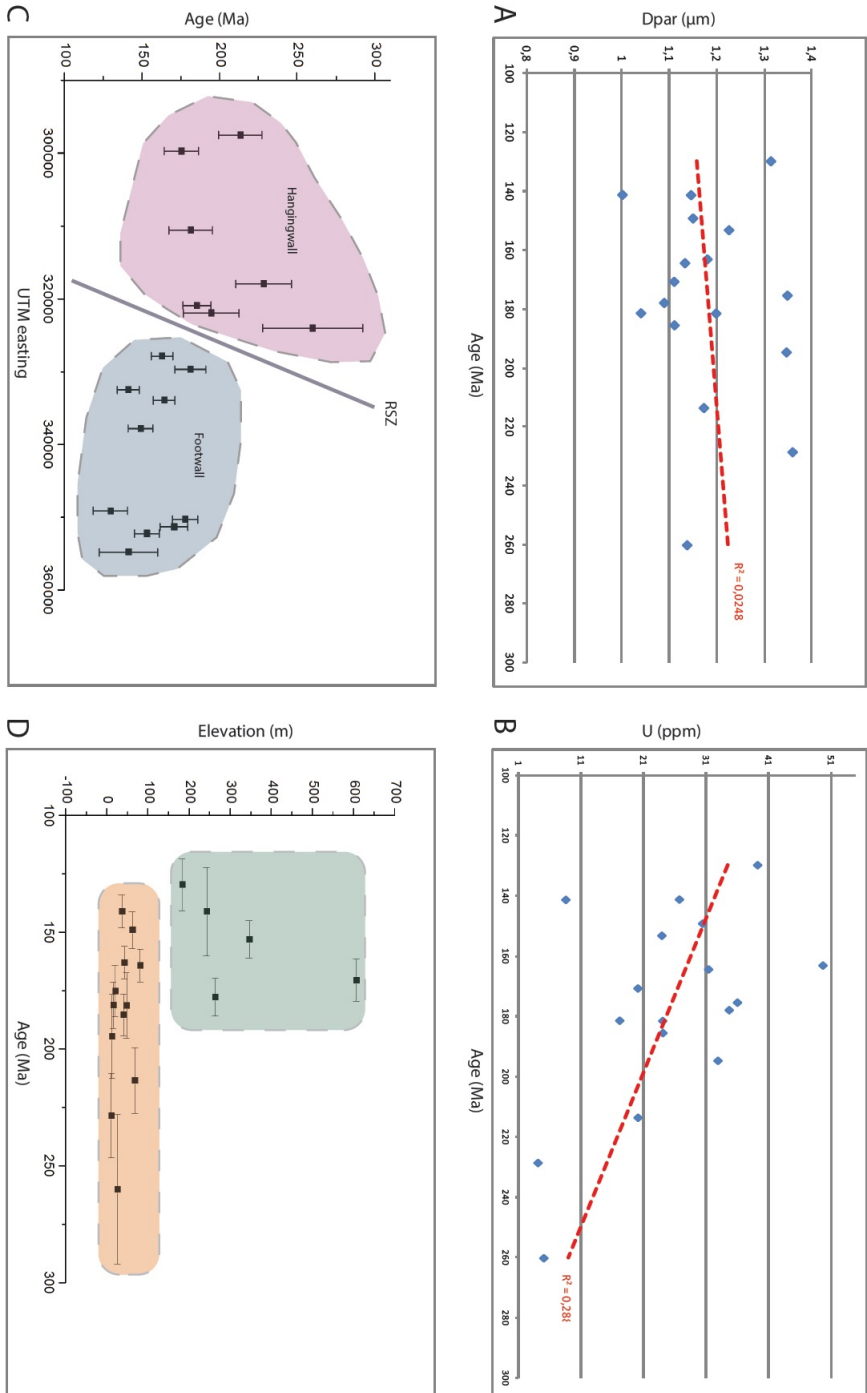


**Figure 5.6:** Apatite fission track ages of the 17 analysed samples plotted against (A) Dpar; (B) U-concentration; (C) UTM easting and (D) Elevation. See text for further explanation.

## 5.4 Inverse thermal history modeling

Inverse thermal history modeling was applied to four samples (CH-02, CH-07, NTW-24-13 and NTW-27-13) distributed as evenly as possible in the study area. CH-07 is from the inland, and the three remaining samples are from the coastal area. Track length distributions for the samples are shown in Figure 5.7, and are plotted against age and elevation in Figure 5.8. The mean track length increases with the age apart from sample CH-07 from the inland which has a different cooling history than the coastal samples. There does not seem to be any correlation between mean track length and the elevation.

The modeling was performed in several steps: (1) All four samples were run using only start- and end constraints (termed unconstrained). The start constraint was set to temperatures representative for the time shortly following Caledonian orogenesis and the end constraint was set to today's average surface temperature ( $8 \pm 5$  °C); (2) The samples were run again with additional constraints between the start and end constraints (termed Jurassic models). Following Ksienzyk et al. (2014), the samples were forced to the surface in the Jurassic and subsequently reburied in the Jurassic modeling. This is due to the discovery of Jurassic sediments in a tunnel close to the island of Bjorøy in the Hjeltefjord fault zone west of Bergen (Fossen et al., 1997). Based on the dinocyst assemblage, the age of the sediments is set to Oxfordian (155-161 Ma). The temperature of the following reburial reached no more than 50 °C based on vitrinite reflectance from coal fragments. The extent of the Jurassic sediments is somewhat established by means of seismic surveying. It indicates that above the tunnel in the Vatilestraumen area a 50-60 m thick sediment layer may be present. This shows that the area was at or close to the surface in the Jurassic, and was subsequently reburied.

The weighted mean paths for the three coastal samples are assembled in one diagram in Figure 5.13 for easy comparison.

Cooling rates were established by dividing the difference in temperature by the difference in age.

- **CH-02:**

- (1) Rapid post-Caledonian cooling that continued as the sample entered the PAZ in the Permian. During the late Triassic-early Jurassic cooling slows down (Figure 5.9 A).

- (2) Fast cooling rate into the PAZ in the middle Triassic that continued as the sample exited the PAZ in the early Jurassic. Re-burial in the Jurassic to early Cretaceous with re-heating to temperatures of max. 80 °C. The sample is cooling again since the early Cretaceous. While the few good fit paths show initial fast cooling, then slow cooling until the Neogene and a significant increase in cooling rates in the Neogene, most of the acceptable paths show relatively constant cooling since the early Cretaceous (Figure 5.9 B).

- **CH-07:**

- (1) The post-Caledonian cooling is much slower and the sample enters the PAZ later. In the Pliocene the cooling rate accelerated dramatically (Figure 5.10). This sample was also run with additional constraints, but the modeling was unsuccessful.

- **NTW-24-13:**

(1) Very rapid post-Caledonian cooling. The sample enters the PAZ already in the Carboniferous and remains at temperatures around 70 °C until the late Cretaceous (Figure 5.11 A).

(2) Rapid cooling until the Carboniferous when the sample enters the PAZ. Slight decrease in cooling rates during the Permian-Triassic. In the early-Jurassic the sample reached near-surface conditions, followed by re-burial and consequently re-heating to ca. 80 °C in the mid-Cretaceous. Renewed uplift from mid-Cretaceous to the present time brought the sample to the surface (Figure 5.11 B).

- **NTW-27-13:**

(1) Rapid cooling until the late Triassic. The sample enters the PAZ in the Triassic and cooled slowly out of the PAZ in the Jurassic-Cretaceous. Very slow cooling during Jurassic to early Paleogene times. Increase in cooling rates in the last 30 Ma (Figure 5.12 A).

(2) Rapid cooling until the Jurassic when the sample reached near-surface temperatures, followed by re-burial in the late Jurassic to early Paleogene. Max. temperatures of ca. 60 °C are reached around the Cretaceous-Paleogene boundary. Renewed uplift and cooling in the Paleogene-Neogene (Figure 5.12 B).

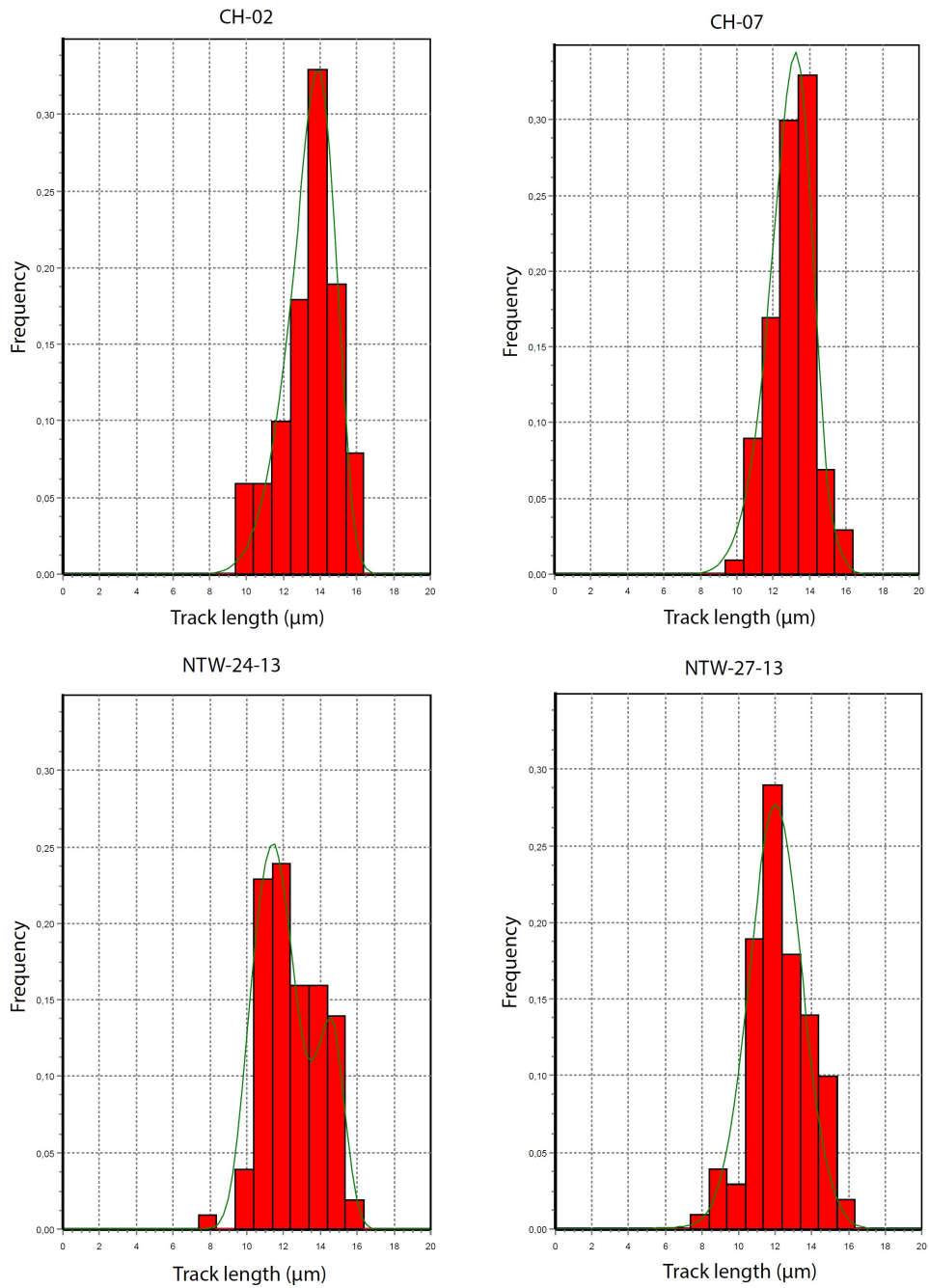


**Figure 5.7:** C-axis projected length distributions for all modeled samples. Modeled length distributions are shown by green curve.

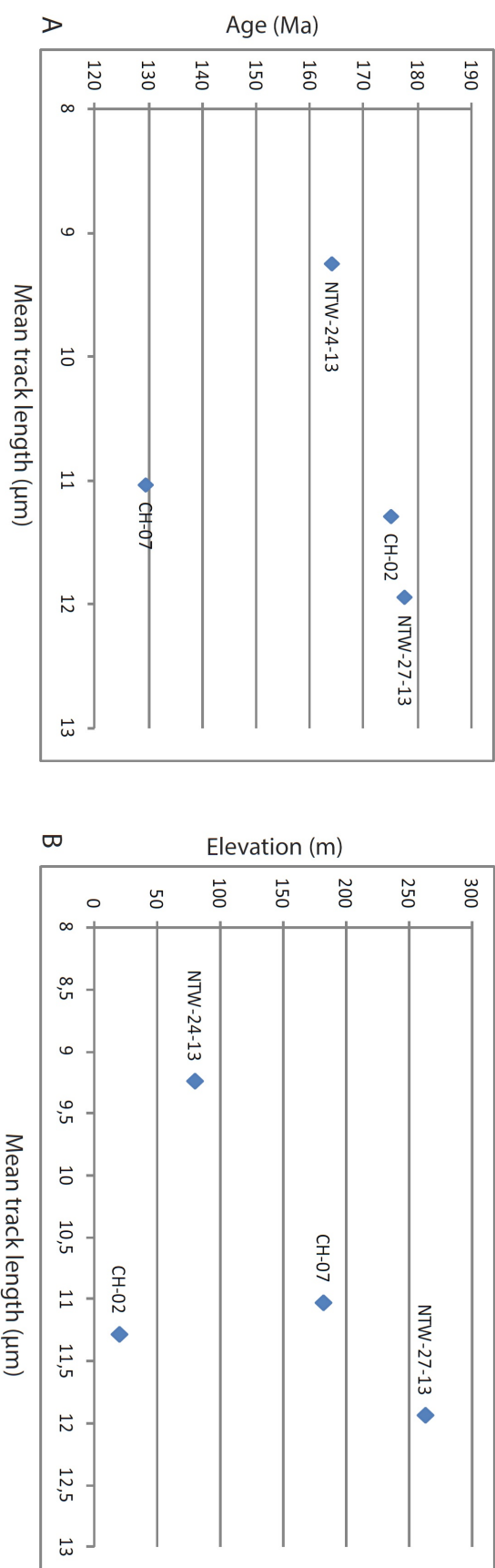


**Figure 5.8:** Mean track lengths of the four samples used for thermal history modeling plotted against (A) Age; (B) Elevation.



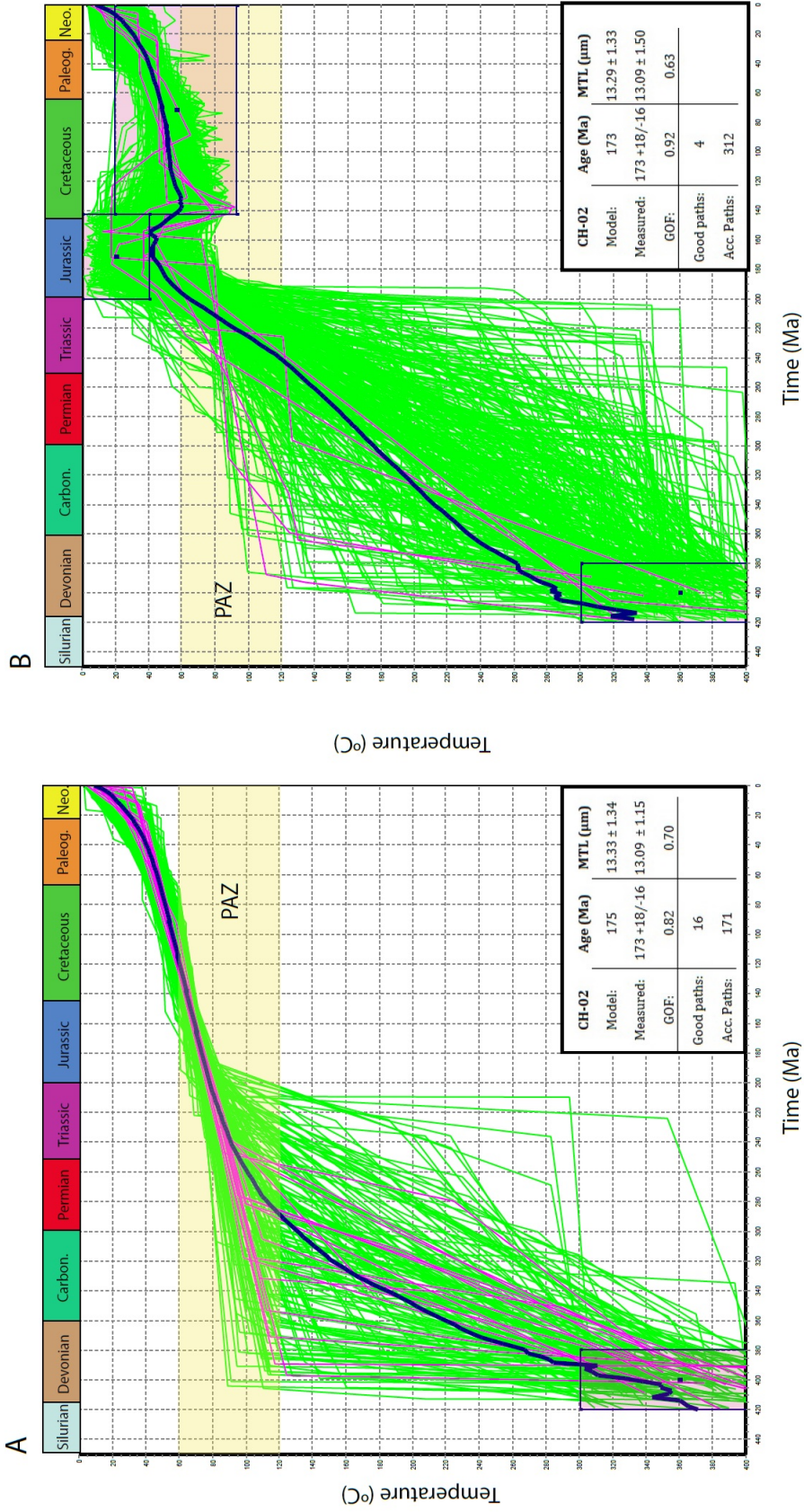


**Figure 5.9:** Unconstrained (A) and Jurassic model (B) inverse models for sample CH-02. Good paths are shown in purple and acceptable paths are shown in green. Weighted mean path is shown in black. The modeling was run using 100,000 tried paths.

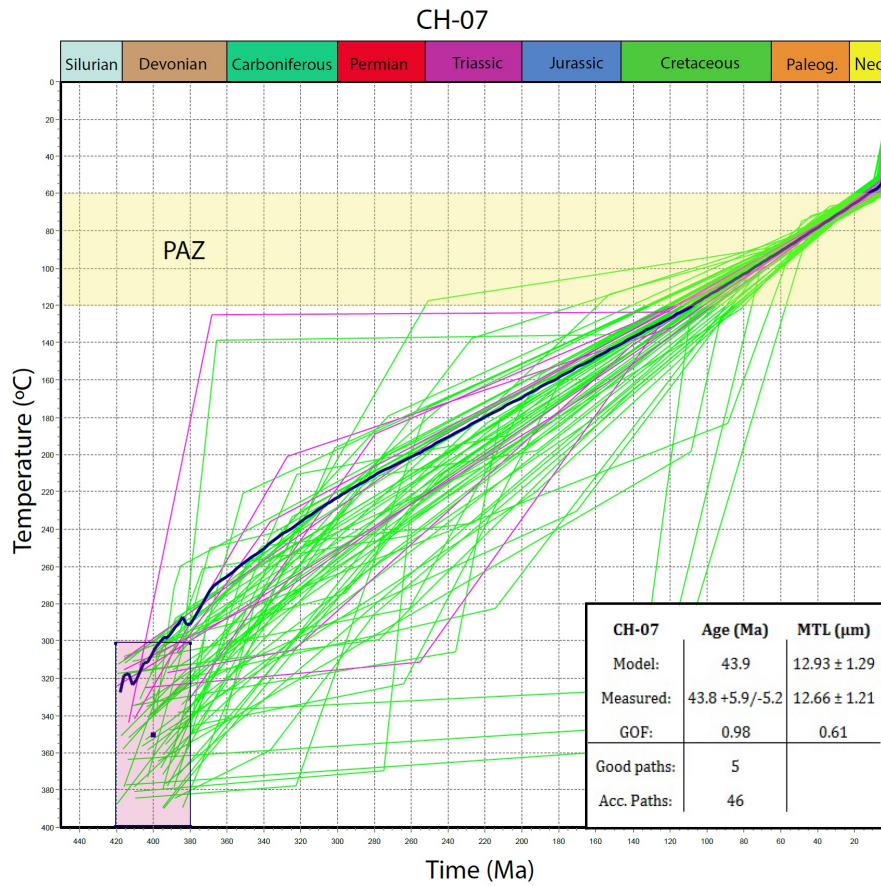


**Figure 5.10:** Unconstrained inverse model for sample CH-07. Good paths are shown in purple and acceptable paths are shown in green. Weighted mean path is shown in black. The modeling was run using 100.000 tried paths.

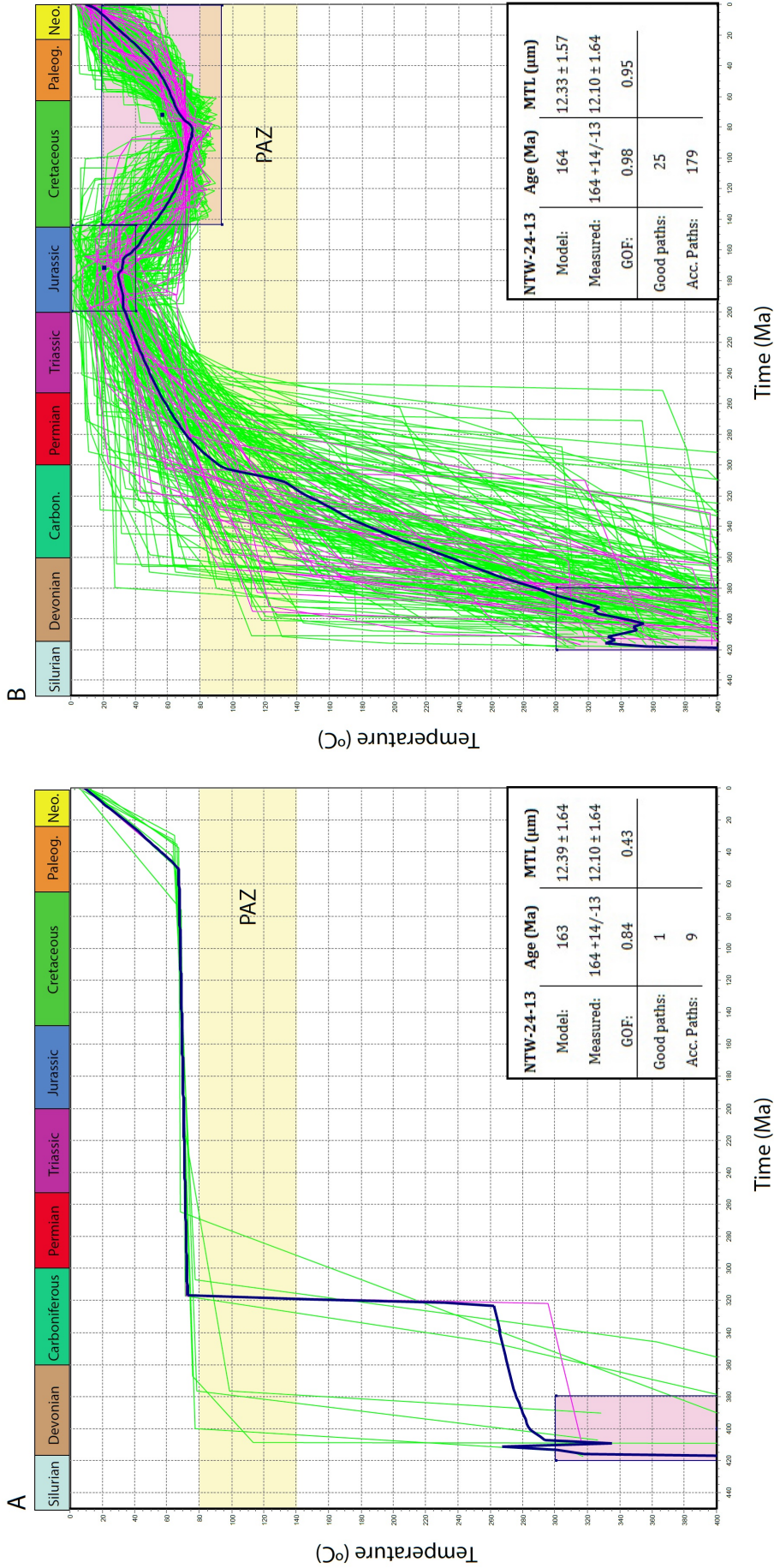


**Figure 5.11:** Unconstrained (A) and Jurassic model (B) inverse models for sample NTW-24-13. Good paths are shown in purple and acceptable paths are shown in green. Weighted mean path is shown in black. The modeling was run using 100,000 tried paths.

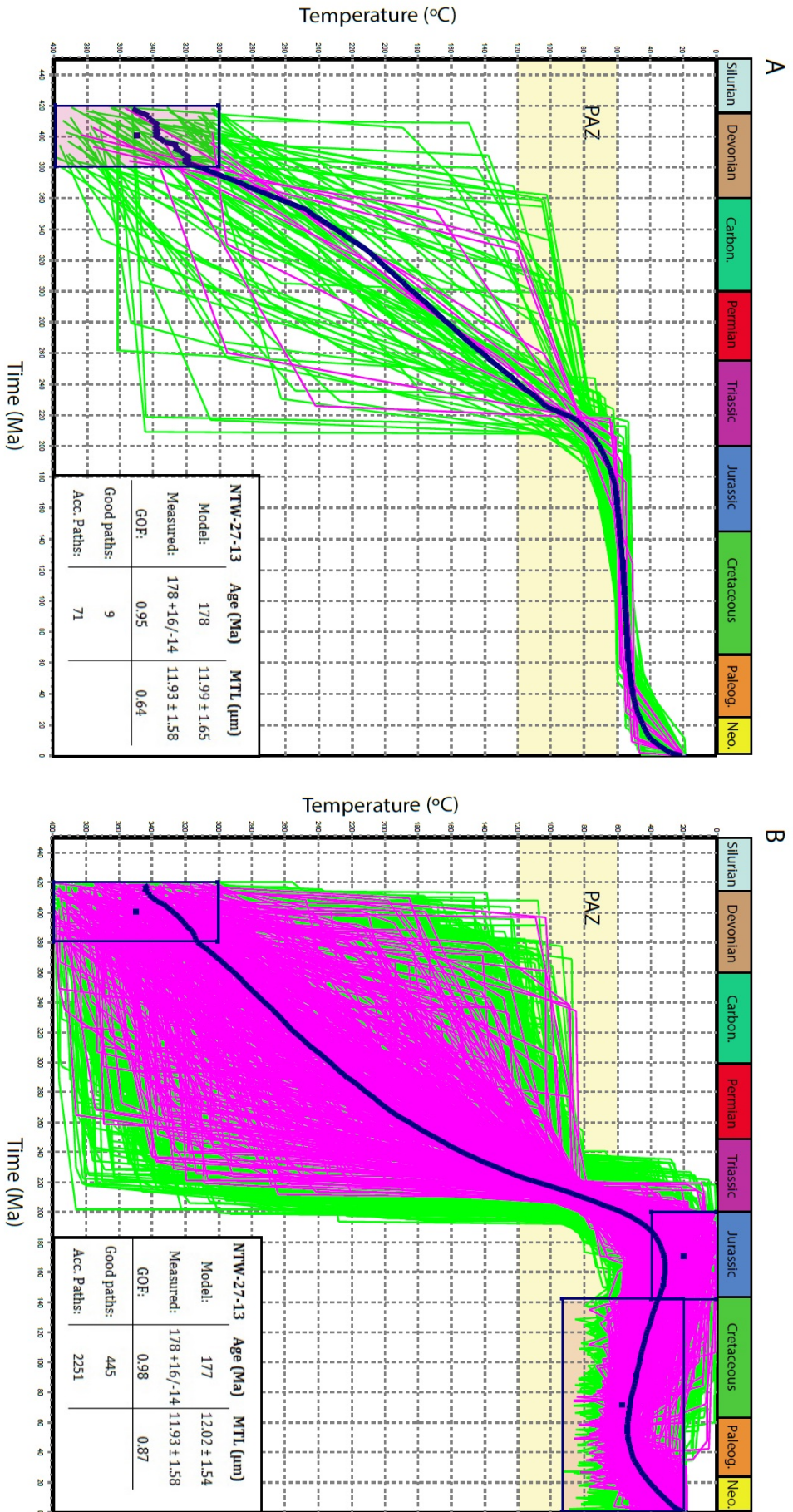


**Figure 5.12:** Unconstrained (A) and Jurassic model (B) inverse models for sample NTW-27-13. Good paths are shown in purple and acceptable paths are shown in green. Weighted mean path is shown in black. The modeling was run using 100,000 tried paths.

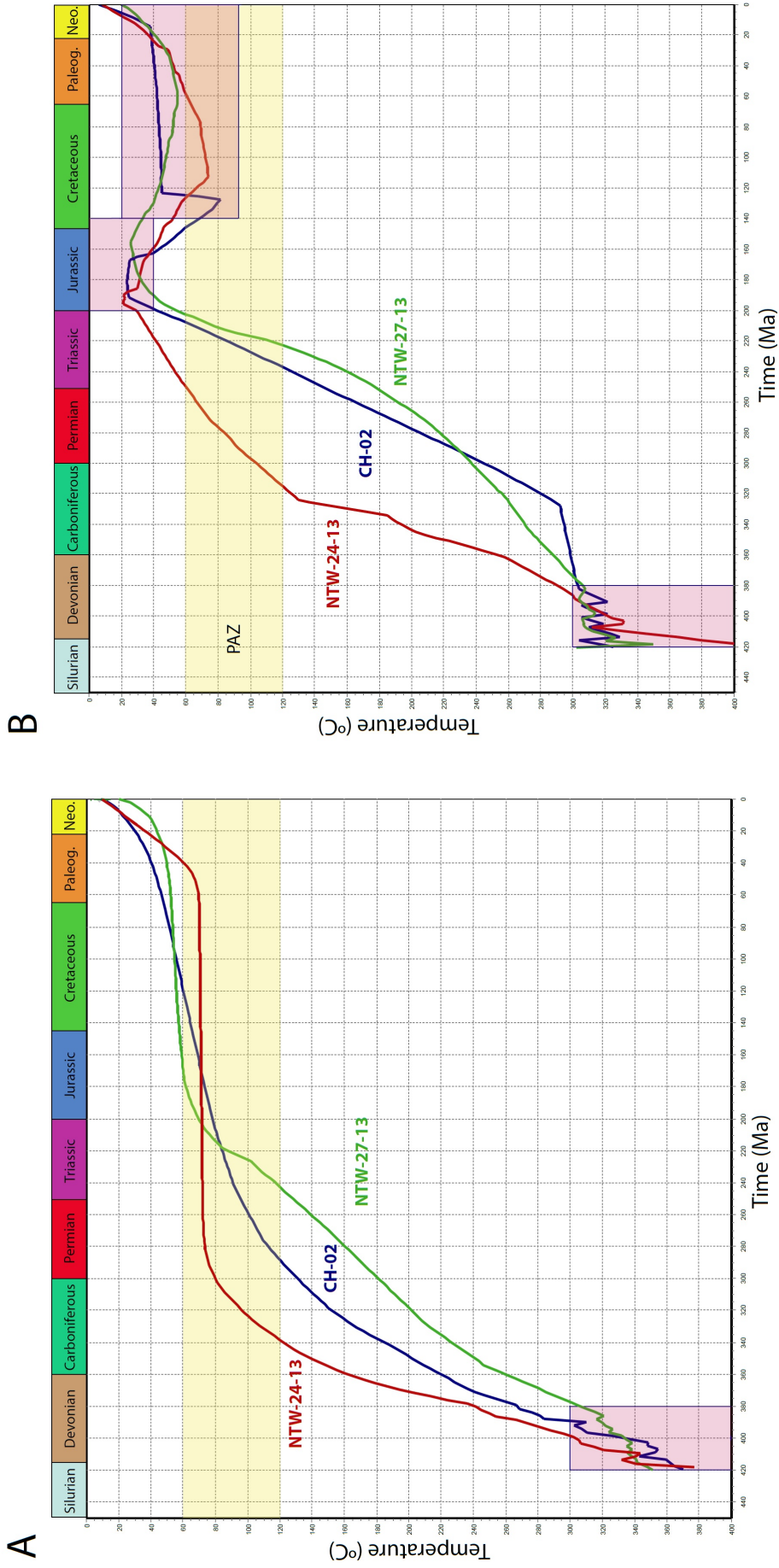


**Figure 5.13:** Weighted mean paths for (near) coastal samples for unconstrained (A) and Jurassic models (B) inverse thermal modeling.



# 6 INTERPRETATION AND DISCUSSION

---

## 6.1 Assessment of data quality

In this chapter, the data quality and possible errors of the apatite fission track analyses of the 17 samples and four inverse thermal models are assessed.

### 6.1.1 Zeta calibration

The calibration was performed in accordance with the recommendation of the IUGS subcommission on geochronology (cf. chapter 4.2.3). The zeta-calibration was executed during training and so the counting behaviour changed as more experience was gained. This resulted in a high zeta value ( $258.9 \pm 6.2$ ), however its validity was tested with selected samples and compared to the results of others in the research group at the University of Bergen.

### 6.1.2 AFT ages

The quality of the samples was variable as illustrated in Figures 5.1 and 5.2, but most of the samples were of good quality, resulting in an overall high confidence in the ages. Samples of poor quality are more difficult to analyse and hence the possibility of making mistakes is greater. The main issue affecting sample quality in the present study were surface pits and roughness that can easily be confused with very short tracks. The surface irregularities were partly due to fluid inclusions and partly due to polishing problems. The effect of such features are usually reflected in the  $1\sigma$  errors of the individual ages. The error is relatively low (4-10 %) for all samples, except for samples CH-05 and CH-06 where the error is 12-13 %. As seen from Table 5.1 this is likely related to the low U-concentration. In a sample with a low U-concentration there are fewer countable tracks and so it is more vulnerable to analytical errors. This could be due to a poor alignment, if the analyst misses a track or simply failing to distinguish a track from another feature. This would cause the ratio of spontaneous and induced tracks to be inaccurate, which is directly transferred to the age. Sample CH-05 is very old ( $260 \pm 32$  Ma) compared to the other samples (Figure 5.5). Because of this, the low U-concentration and relatively high error (12 %) it is regarded with caution. Sample CH-06, on the other hand, has a similar age to the surrounding samples ( $141 \pm 19$  Ma) and so it is more likely that the age is within the right range. Overall, with the possible exception of sample CH-05, there is no reason to suspect any problems with the results of the AFT dating.

### 6.1.3 The failure of the $\chi^2$ test

In order to pass the  $\chi^2$  test  $P_{\chi^2}$  should be  $\geq 5\%$ . All samples passed the test except for samples CH-01, CH-07 and NTW-28.13. When the test is failed, it is possible that there is more than one age population in the sample; hence more than one cooling history. Also, populations with slightly different chemistry could have different annealing behaviours and hence produce different ages. However, there are other factors that cause the test to fail. This is illustrated in Figure 6.1. If the sample is of good quality and has a high U-concentration, the single grain ages are more precise which is reflected by the small errors. The errors overlap, and so the test is passed (Figure 6.1 A). In a good sample with low U-concentration, the test is also passed because even though the errors are larger they still overlap (Figure 6.1 B). As for a poor sample with high U-concentration, the ages are precise but scattered resulting in small errors that do not

overlap. This causes the test to fail (Figure 6.1 C). If however a poor sample has a low U-concentration and the errors still overlap despite the scatter in single grain ages, the test is passed (Figure 6.1 D). In effect, the passing of the  $\chi^2$  test is largely dependent on the errors, and the likeliness of passing the test increase when the U-concentration is low (hence, the errors are large and possibly overlapping).

This is a possible cause for the failure of the  $\chi^2$  test for the three mentioned samples. They are all of intermediate to poor quality and have high U-concentrations.

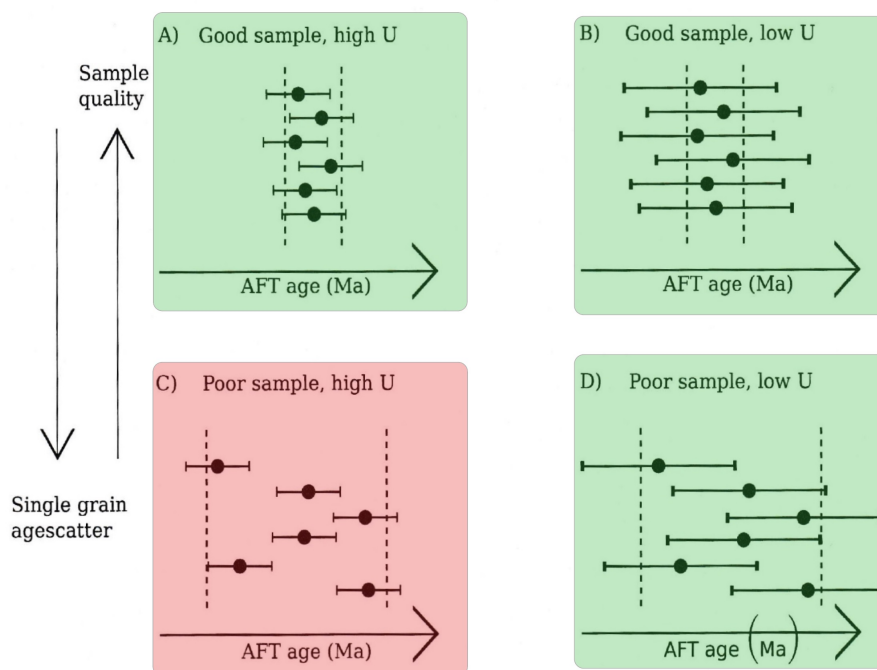


**Figure 6.1:** Principal figure of the passing (green) or failing (red) of the  $\chi^2$  test. See text for further explanation. Modified from Angell (2013).

#### 6.1.4 Mean track lengths and $D_{par}$

In all four samples selected for track length measurements, 100 confined tracks (TINTs) were measured. The track lengths were  $\sim 11 \mu m$  for samples CH-02, CH-07 and NTW-27-13, and a little shorter ( $\sim 9 \mu m$ ) for sample NTW-24-13. The validity of the measurements from this sample was tested by measuring a selection of tracks a second time. The results were entirely reproducible.

The reproducibility of length measurements between analysts is poor according to a study conducted by Ketcham et al. (2009). A group of scientists were invited to the study, and measured lengths from the same sample. The result showed a great scatter in the lengths which is caused by personal bias such as selection of tracks and precision. Also, the study found that there is a general trend to overlook the smaller tracks, and so the mean track length appear to be greater than it actually is. The length measurement procedure is therefore in need of a personal calibration, but no routine for this has been established so far. As the mean track lengths in this study are quite short, the problem of overestimating the length could be avoided. However, there is another factor affecting the lengths, that is the chemical composition of the sample. This is represented by the



$D_{par}$  values (cf. 3.2.3). If the  $D_{par}$  value is small, the sample is most likely a fluorine-rich sample that is more resistant to etching. Fluorine-rich samples also anneal faster than chlorine-rich samples. This could also be the reason as to why the mean track lengths in this study are quite short.

### 6.1.5 Inverse thermal history modeling

The inverse thermal history models provide possible cooling paths based on the AFT data and the constraints introduced by the analyst. The resulting best-fit or weighted-mean cooling paths are therefore necessarily the only possible cooling history for the sample. The model is strongly dependent on the quality of the AFT analyses and on the assumptions, made by the analyst, that constitute the constraints. The track length measurements play an important role in the modeling as too short lengths will force the sample to reside in the partial annealing zone longer than it actually did. Vice versa, too long lengths will cause a fast cooling rate, and a short residence in the partial annealing zone.

In this study two thermal models have been run for the coastal samples. The first had only start- and end constraints, and so a vast range of possible paths were produced as the paths were controlled mostly by the AFT data. The second model had constraints forcing the sample to (or close to) the surface in the Jurassic and subsequently allowing it to be re-buried. These constraints were introduced to the modeling in order to test if the samples could have experienced such a cooling path, which have been inferred by other studies in southwestern Norway. For sample CH-02 the Jurassic model yielded less good paths but still has a better goodness of fit for the age than the unconstrained model (Figure 5.9). The Jurassic model fits much better for sample NTW-24-13. It yielded more paths and much better values of goodness of fit (Figure 5.11). The Jurassic modeling for sample NTW-27-13 also fits better (Figure 5.12). In conclusion, the Jurassic models for samples NTW-24-13 and NTW-27-13 fits much better and sample CH-02 is somewhat undecided. For the inland sample (CH-07), however, the Jurassic model is entirely incompatible with the data and can therefore be ruled out.

## 6.2 Discussion of the results

### 6.2.1 Interpretation of the AFT ages

As mentioned earlier, the ages are getting younger from the coastal areas towards the inland (Figure 5.5). If the area was uplifted as a single coherent block, the ages would increase with elevation from the coast towards the inland. This is not the case for a rifted margin as the continental margin is not uplifted as one rigid block. Scarp retreat or downwarping is expected, and thus different cooling histories at the coast and inland. Leighton (2007) suggests in his study that fault activity must have influenced the topography by separating areas of different relief. This is supported by the age-elevation distribution of this study (Figure 5.6 D) where the samples in the higher areas have relatively young ages, and the samples at the lower elevations have older ages. The young ages at the lower elevations are a result of the erosion of the uplifted footwall which is suggested, following Leighton (2007), to be related to Permo-Triassic continental rifting and faulting. This interpretation is supported by the age offset across the Røldal Shear Zone (Figure 5.6 C) which is discussed further below. For practical reasons the discussion of the AFT ages are divided in two parts concerning the coastal samples and the inland sample separately.

- **Coastal samples:** The samples in the coastal areas have experienced rapid Permo-Triassic uplift followed by sedimentary burial up to 50-80 °C in the Jurassic to Cretaceous.

The ages are offset across the RSZ proving the importance of active faulting throughout the Mesozoic. The ages in the footwall are younger than the samples in the hangingwall. This is explained by the rejuvenation of the material available for erosion caused by isostatic uplift as the faulting occurred. The isostatic uplift created a higher relief in the footwall, making it more susceptible to erosion than the rocks in the hangingwall (Figure 6.2).

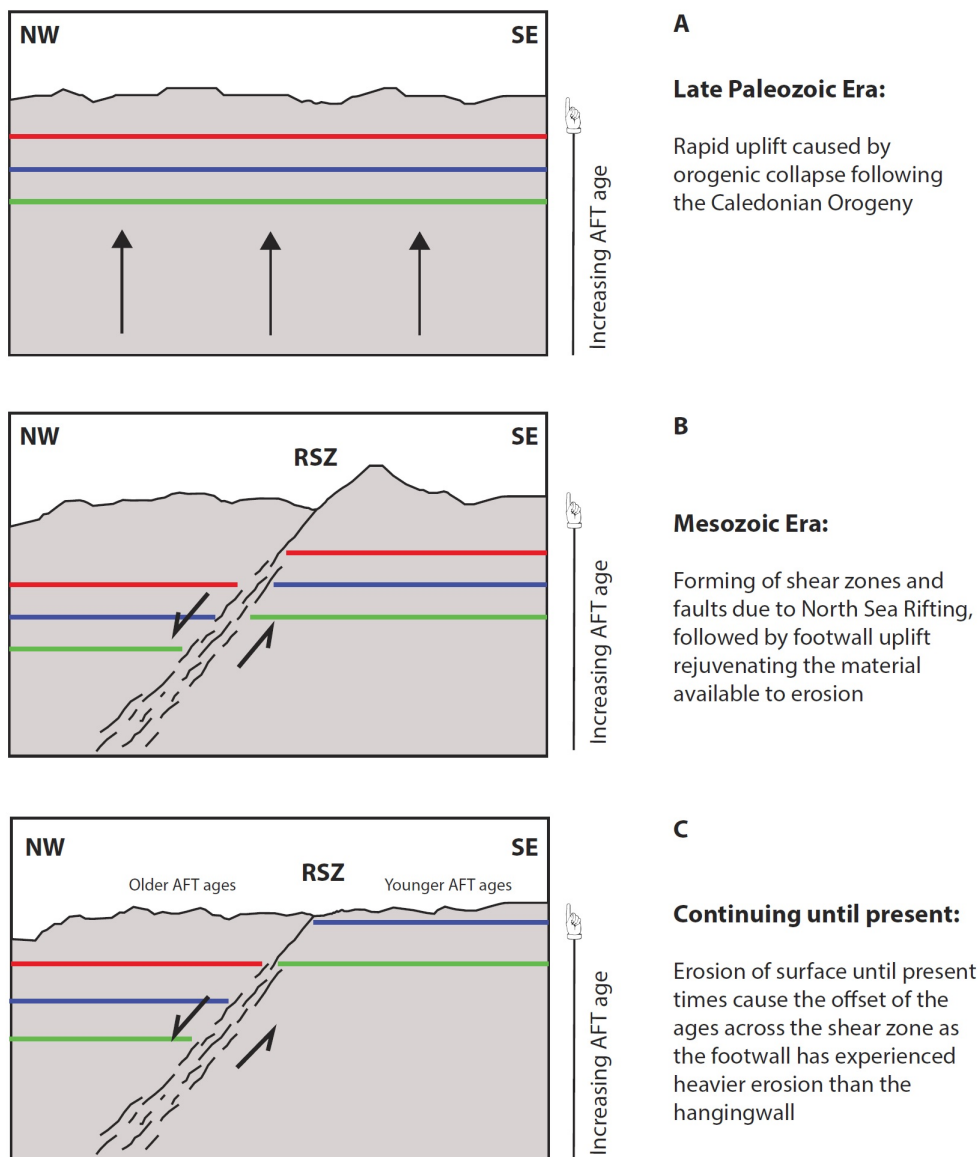


**Figure 6.2:** A proposed structural evolution of the Røldal Shear Zone area. In the late Paleozoic rapid uplift occurred as a result of the orogenic collapse (A). In the Mesozoic the RSZ was developed. Its movements caused the footwall to be uplifted, rejuvenating the material available for erosion (B). Continuous erosion to the present day caused the footwall to be of younger age than the hangingwall as it was eroded more extensively (C). Note that this figure does not include the Cretaceous re-burial.

- Inland sample:** The inland sample is taken from the headland of two intersecting fjords and is quite young ( $130 \pm 11$  Ma). In a previous study by Angell (2013) analysis of a headland sample also yielded a younger age than the surrounding samples. The reason for this is not known, but a possible explanation is put forward, following Angell (2013), as seen in Figure 6.3: In a normal age distribution the AFT ages are increasingly older towards the surface (A), however as this sample is located at a headland, the erosion exerted by glaciers has played an important role. The thick ice sheet is forcing the rock column downwards and at the same time carving out the valleys/fjords (B). When the ice melts, the area is uplifted, but more so in the areas closest to the valleys/fjords, causing a domal uplift (C). As the surface is eroded, the AFT ages at the headland are younger than further away from the valleys/fjords.

Another possible explanation to the young age is that the fjords follow large faults (as is clearly the case here) and the fluid circulation along the faults could have affected the age, being particularly intense in the areas where large fault systems intersect.

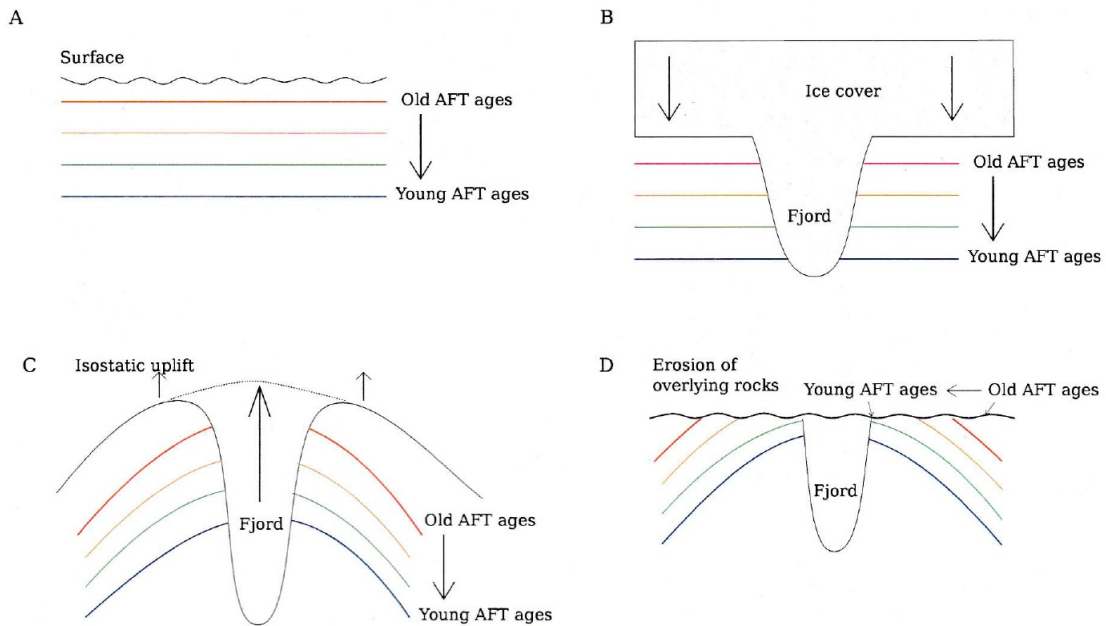


**Figure 6.3:** Principal figure of the isostatic uplift resulting from the glacial erosion creating a fjord: (A) In the crust the ages are getting older towards the surface and will have a normal age distribution; (B) The ice exerts downward pressure on the crust and carves out a valley/fjord; (C) When the ice melts the area is uplifted the most closest to the valley/fjord where the erosion was strongest. This causes a domal uplift of the area; (D) Subsequently, when the isostatic uplift ceases, the dome is eroded to the same level as the surrounding area. Because of this, the young AFT ages are in the area close to the fjord. From Angell 2013.

### 6.2.2 Interpretation of inverse thermal history models

- Coastal samples:** Comparing the thermal models of CH-02 and NTW-27-13 (Figure 5.13 B) on the northwestern and southeastern side of the RSZ, respectively,

it is evident that the footwall sample reached shallow crustal depths later than the hangingwall sample. This is suggested to be related to a rejuvenation of the relief of the footwall due to Mesozoic fault activity in the Røldal Shear Zone and other major shear zones and faults. NTW-24-13 reached the surface earlier than CH-02 which is the opposite of what is expected. However, this sample is further inland and closer to other faults and may therefore have been uplifted earlier. As the Jurassic modeling of CH-02 only produced 4 good paths it is a slight possibility that this particular sample was not uplifted in the Jurassic and subsequently re-buried. This could be due to the activity of the Røldal Shear Zone. However, this is difficult to resolve due to the lack of other inverse models in the hangingwall. It is, however, reasonable to suggest that it was uplifted in the Jurassic (and re-buried in the Cretaceous) because that is the general trend for the coastal samples in the studies conducted in southwestern Norway.

All modeled samples at the coast were exhumed to (or close to) the surface in the Jurassic and subsequently re-buried in the Cretaceous. This is supported by the offshore sediment-record where clastic sedimentary units originating from the Norwegian mainland propagated in the Cretaceous. The sedimentary units were transported through the major feeder systems which are corresponding to the large fjords (e.g. Sognefjorden, Hardangerfjorden and Boknafjorden) (Gabrielsen et al., 2010a). It is suggested that the increased sedimentation rates are a result of more material made available for erosion caused by the faulting, and hence a rejuvenation of the relief in the Jurassic. Gabrielsen et al. (2010a) explain the increased sedimentation rates to be a result of a major uplift event in southwestern Norway, but fail to consider the effect of faulting in the Jurassic. As faulting is known to enhance relief, it is reasonable to suggest both mechanisms played an important role to increase sedimentation rates.

- **Inland sample:** Experienced lesser Permo-Triassic uplift, and cooled slowly until the Neogene when cooling rates increased. The increased cooling rates is related to higher erosion rates, also reflected by the high sediment accumulation in the North Sea (Huuse, 2002). Looking at the thermal model for sample CH-07, it is obvious that the cooling rate in the Neogene is too high to be explained exclusively by uplift. However, erosion exerted by glaciers produce quite high erosion rates ( $\sim 100\text{-}200$  m/Ma) as is expected in the Quaternary (Hallet et al., 1996). Following Leighton (2007) it is therefore suggested that the increased cooling rate is connected to the change to a colder global climate. A colder climate causes increased erosion rates as the relative sea level sinks exposing large areas of the continental shelves, scarcity of vegetation cover and expanding ice sheets. There is therefore no need to conclude with Neogene uplift as the only reason for increased erosion rates as is suggested by e.g. Gabrielsen et al. (2010a).

### 6.3 Comparison to previous studies

The Røldal Shear Zone area has never been explored by means of thermochronological methods. However, in a recent contribution by Woznitza (2014), the adjacent area north of this study area was explored by means of (U-Th)/He and K/Ar thermochronology. In that study a profile going all the way from the island Utsira at the coast west of Karmøy to Lake Totak on the Hardangervidda in the inland was studied. The aim of the study was to investigate upper crustal movements and periods of active faulting. The analyses yielded ages ranging from Permian to late Cretaceous, with the majority of ages ranging from late Triassic to early Cretaceous. The ages were clearly offset across faults and

lineaments, clearly showing the importance of active faulting for the age distribution and hence the landscape evolution. This is further substantiated by the results of the K/Ar analyses which show that the faults were indeed active since the Silurian to the Cretaceous.

The inverse thermal modeling performed in the study by Woznitza (2014) also showed rapid Permo-Triassic cooling rates for the coastal samples, and is interpreted to be connected to rift flank uplift. Constraints forcing the coastal samples to (or close to) the surface in the Jurassic and to be subsequently re-buried and re-heated to temperatures of 40-60 °C were added to the modeling. In mid-Cretaceous times the samples were exhumed once more. For the inland samples, the Permo-Triassic cooling was slower and steady throughout the Mesozoic and Paleocene times. The inland samples reached the surface in the Cenozoic, much later than the coastal samples. Woznitza (2014) argues that the (U-Th)/He and K/Ar data reveal a dynamic evolution of southwestern Scandinavia by a combination of faulting induced uplift resulting in enhanced erosion.

Further north in an area around Bergen, Ksienzyk et al. (2014) conducted a study utilizing apatite fission track analysis, and apatite and zircon (U-Th)/He thermochronology. Samples were collected mainly on the islands close to Bergen, but also some samples were collected northeast and southeast of Bergen. The samples yielded Permian to Jurassic ages for the AFT analyses, Triassic to Cretaceous ages for the apatite (U-Th)/He analyses, and Carboniferous to Triassic ages for the zircon (U-Th)/He analyses. Also here, the analyses showed that ages were clearly offset across faults once again proving that faults were active in the Mesozoic. Based on the discovery of unfaulted Jurassic sediments by Fossen et al. (1997), proving that the area must have been at the surface in the Jurassic and subsequently re-buried to temperatures of max. 50 °C (cf. chapter 5.4), Ksienzyk et al. (2014) added constraints forcing the samples to the surface (or close to the surface) in the Jurassic and subsequently re-burying them. It is suggested that the age distribution is a result of rift- and post-rift tectonics related to the rifting in the North Sea and North Atlantic.

#### 6.4 Proposed exhumation history for the Røldal Shear Zone area

The models attempting to explain the evolution of a passive margin as illustrated in Figure A-C (Gilchrist and Summerfield, 1990; Kooi and Beaumont, 1994; Ollier and Pain, 1997) are too simple when considering the Norwegian margin. The downwarp model (Figure 6.4 A) suggests that the margin is created by flexure of the lithosphere without faulting. This would create an extremely shallowly dipping monocline. Gallagher et al. (1998) points out that in order for this model to be geologically plausible, the lithosphere would have to be infinitely rigid. In addition, they do not account for the isostatic response to the denudational unloading. The scarp retreat model (Figure 6.4 B) explains the margin to be a result of extensional faulting followed by landward retreat of the escarpment. In this model, erosion occurs in the area between the new escarpment and the ocean. Only little erosion is expected inland of the escarpment (Gallagher et al., 1998). The pinned divide model is similar to the scarp retreat model, but includes a parameter of the drainage divide inland of the escarpment. Rivers running towards the coast exert erosion on the escarpment. The major difference between the two models is thus that instead of a retreating scarp, the escarpment is being worn downwards by rivers. In addition, if the base level of the drainage divide is lowered during the formation of the escarpment, and the inland experiences significant denudation, the evolution of the new escarpment is pinned at the initial drainage divide.

The evolution of the Norwegian margin is one of great complexity, and the thermochronological studies conducted in this contribution and others (compiled in Hendriks et al., 2007) in southwestern Norway, clearly show the importance and absolute need to take active faulting into consideration when producing such a model. The Norwegian margin has been affected by several rift phases which ended with the opening of the Atlantic Ocean (Lundin and Dore, 1997). Johannessen et al. (2013) point out the importance of accounting for the pre-rift structural inheritance, which the simple models fail to do. Further, Johannessen et al. (2013) highlight the importance of this as the evolution of the North Sea Rift has been strongly determined by the heritage of the Precambrian structural grain (Færseth et al., 1996; Gabrielsen et al., 2002). It is therefore suggested, following Johannessen et al. (2013), that the evolution of southwestern Norway is a result of sustained elevated topography shaped by rift-related uplift, extensional faulting and erosion (Figure 6.4 D). This is evident from the thermochronological record (Figure 6.4 E).

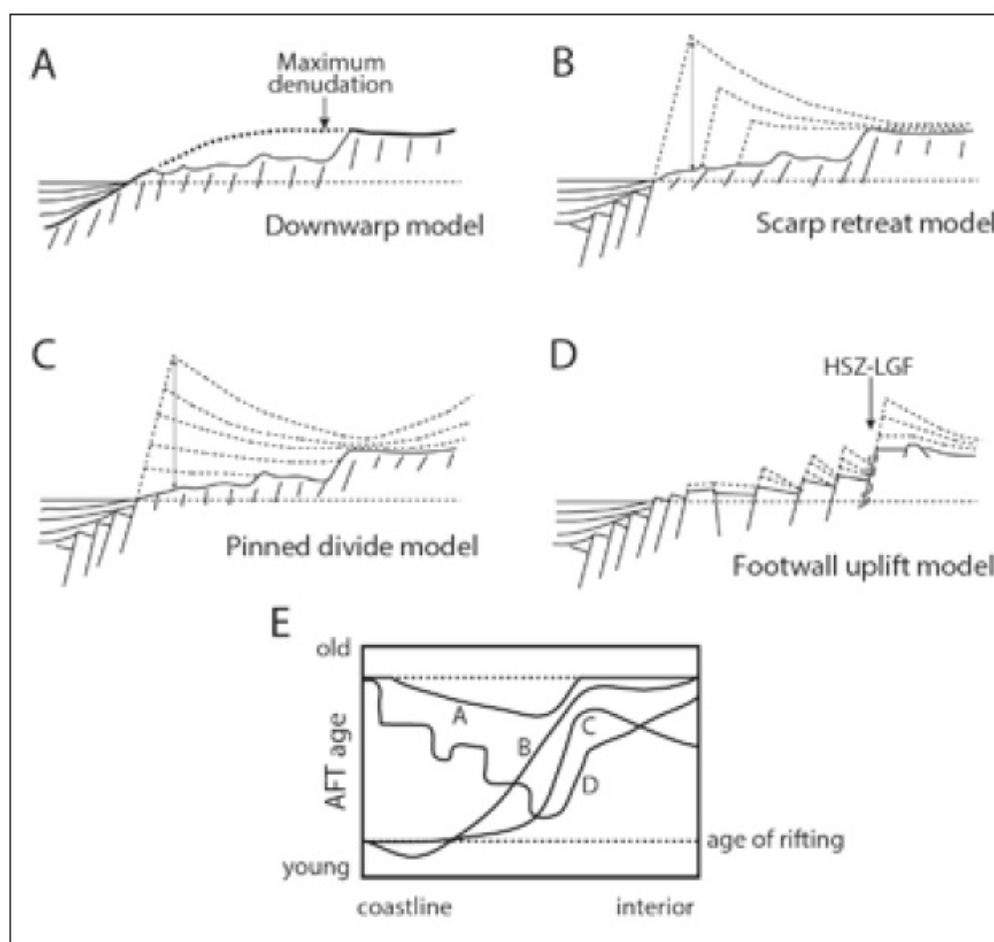


**Figure 6.4:** Figure showing the different models for the evolution of passive margins. (A) The downwarp model connects it to a denudational response to lithospheric flexure. (B) The scarp retreat model connects it to extensional faulting followed by landward retreat of the escarpment. (C) The pinned divide model connecting it to fluvial erosion of the rift flank. (D) Footwall uplift model connecting it to vertical fault movements as seen from the AFT ages. (E) AFT ages for the different models. From Johannessen et al. (2013).

# 7 SUMMARY AND OUTLOOK

---

From this study the following main conclusions are drawn:

- The AFT ages are ranging from Permian to early Cretaceous, with the majority of Jurassic ages.
- The ages are getting younger from the coast towards the inland.
- Across the Røldal Shear Zone there is an age offset related to active faulting in the Mesozoic.
- Samples in the coastal area (CH-02, NTW-24-13 and NTW-27-13) experienced rapid Permo-Triassic uplift and have been brought to (or close to) the surface in the Jurassic, and were subsequently re-buried.
- The inland sample (CH-07) experienced slower and steady cooling until the Neogene when cooling rates increased dramatically. This is related to the shift to a colder climate and hence the enhanced erosion exerted by glaciers, scarcer vegetation cover and exposing of shelf areas.
- It is suggested that the evolution of the landscape of southwestern Norway is a result of sustained elevated topography shaped by rift-related uplift, extensional faulting and erosion.

This contribution is the first thermochronological study in the Røldal Shear Zone area, and thus provides new information to the thermochronological record of southwestern Norway. In order to enhance the validity of the study more samples ought to be analysed and more track length measurements are needed (especially in the hangingwall).





# References

---

- Andersen, T., 1998, Extensional tectonics in the Caledonides of southern Norway, an overview: *Tectonophysics*, v. 285, no. 3, p. 333–351.
- Andersen, T., Andresen, A., and Sylvester, A., 2002, Timing of late-to post-tectonic Sveconorwegian granitic magmatism in South Norway: *Bulletin 440 Miscellaneous research papers*.
- Andersen, T., and Jamtveit, B., 1990, Uplift of deep crust during orogenic extensional collapse: A model based on field studies in the Sogn-Sunnfjord Region of western Norway: *Tectonics*, v. 9, no. 5, p. 1097–1111.
- Andersen, T., Jamtveit, B., Dewey, J., and Swensson, E., 1991, Subduction and eduction of continental crust: major mechanisms during continent-continent collision and orogenic extensional collapse, a model based on the south Norwegian Caledonides: *Terra Nova*, v. 3, no. 3, p. 303–310.
- Andersen, T., Torsvik, T., Eide, E., Osmundsen, P., and Faleide, J., 1999, Permian and Mesozoic extensional faulting within the Caledonides of central south Norway: *Journal of the Geological Society*, v. 156, no. 6, p. 1073–1080.
- Andréasson, P., Gee, D., Whitehouse, M., and Schöberg, H., 2003, Subduction-flip during Iapetus Ocean closure and Baltica–Laurentia collision, Scandinavian Caledonides: *Terra Nova*, v. 15, no. 6, p. 362–369.
- Andriessen, P., 1990, Anomalous fission track apatite ages of the Precambrian basement in the Hunnedalen region, south-western Norway: *International Journal of Radiation Applications and Instrumentation. Part D. Nuclear Tracks and Radiation Measurements*, v. 17, no. 3, p. 285–291.
- Andriessen, P., and Bos, A., 1986, Post-Caledonian thermal evolution and crustal uplift in the Eidfjord area, western Norway: *Norsk geologisk tidsskrift*, v. 66, no. 3, p. 243–250.
- Angell, H., 2013, Exhumation history and fault tectonics between the Sognefjord and the Fordefjord applying low-temperature thermochronology [Master's thesis]: University of Bergen.
- Badley, M., Price, J., Dahl, C., and Agdestein, T., 1988, The structural evolution of the northern Viking Graben and its bearing upon extensional modes of basin formation: *Journal of the Geological Society*, v. 145, no. 3, p. 455–472.
- Barbarand, J., Carter, A., Wood, I., and Hurford, T., 2003a, Compositional and structural control of fission-track annealing in apatite: *Chemical Geology*, v. 198, p. 107–137.
- Barbarand, J., Hurford, T., and Carter, A., 2003b, Variation in apatite fission-track length measurement: implications for thermal history modelling: *Chemical Geology*, v. 198, p. 77–106.
- Bhandari, N., Bhat, S., Lal, D., Rajagopalan, G., Tamhane, A., and Venkatavaradan, V., 1971, Fission fragment tracks in apatite: recordable track lengths: *Earth and Planetary Science Letters*, v. 13, no. 1, p. 191–199.

- Bingen, B., Nordgulen, Ø., and Giulio, V., 2008, A four-phase model for the Sveconorwegian orogeny, SW Scandinavia: *Norsk Geologisk Tidsskrift*, v. 88, no. 1, p. 43.
- Bingen, B., Skår, Ø., Marker, M., Sigmond, E., Nordgulen, Ø., Ragnhildstveit, J., Mansfeld, J., Tucker, R., and Liégeois, J., 2005, Timing of continental building in the Sveconorwegian orogen, SW Scandinavia: *Norwegian Journal of Geology*, v. 85, no. 1-2, p. 87–116.
- Brekke, H., et al., 2000, The tectonic evolution of the Norwegian Sea continental margin, with emphasis on the Voring and More basins: *Special Publication-Geological Society of London*, v. 167, p. 327–378.
- Brueckner, H., and Cuthbert, S., 2013, Extension, disruption, and translation of an orogenic wedge by exhumation of large ultrahigh-pressure terranes: Examples from the Norwegian Caledonides: *Lithosphere*, v. 5, no. 3, p. 277–289.
- Bryhni, I., Nøttvedt, A., Ramberg, I., Solli, A., and Nordgulen, Ø., 2006, Landet blir til - Norges geologi: *Norsk geologisk forening*.
- Burchart, J., Butkiewicz, T., Dakowski, M., and Galazka-Friedman, J., 1979, Fission track retention in minerals as a function of heating time during isothermal experiments: A discussion: *Nuclear Tracks*, v. 3, no. 3, p. 109–117.
- Carlson, W., Donelick, R., and Ketcham, R., 1999, Variability of apatite fission-track annealing kinetics: I. Experimental results: *American mineralogist*, v. 84, p. 1213–1223.
- Chadderton, L.T., 1988, On the anatomy of a fission fragment track: *International Journal of Radiation Applications and Instrumentation. Part D. Nuclear Tracks and Radiation Measurements*, v. 15, p. 11–29.
- Chadderton, L.T., 2003, Nuclear tracks in solids: registration physics and the compound spike: *Radiation measurements*, v. 36, no. 1, p. 13–34.
- Chalmers, J., Green, P., Japsen, P., and Rasmussen, E., 2010, The Scandinavian mountains have not persisted since the Caledonian orogeny. A comment on Nielsen et al. (2009a): *Journal of Geodynamics*, v. 50, no. 2, p. 94–101.
- Chauvet, A., and Séranne, M., 1994, Extension-parallel folding in the Scandinavian Caledonides: implications for late-orogenic processes: *Tectonophysics*, v. 238, no. 1, p. 31–54.
- Cockburn, H., Brown, R., Summerfield, M., and Seidl, M., 2000, Quantifying passive margin denudation and landscape development using a combined fission-track thermochronology and cosmogenic isotope analysis approach: *Earth and Planetary Science Letters*, v. 179, no. 3, p. 429–435.
- Cocks, L., McKerrow, W., and Van Staal, C., 1997, The margins of Avalonia: *Geological Magazine*, v. 134, no. 05, p. 627–636.
- Cocks, L., and Torsvik, T., 2002, Earth geography from 500 to 400 million years ago: a faunal and palaeomagnetic review: *Journal of the Geological Society*, v. 159, no. 6, p. 631–644.

- Cocks, L., and Torsvik, T., 2005, Baltica from the late Precambrian to mid-Palaeozoic times: the gain and loss of a terrane's identity: *Earth-Science Reviews*, v. 72, no. 1, p. 39–66.
- Cocks, L., and Torsvik, T., 2006, European geography in a global context from the Vendian to the end of the Palaeozoic: *Memoirs-Geological Society of London*, v. 32, p. 83.
- Coward, M., 1995, Structural and tectonic setting of the Permo-Triassic basins of northwest Europe: *Geological Society, London, Special Publications*, v. 91, no. 1, p. 7–39.
- Crowley, K., Cameron, M., and Schaefer, R.I., 1991, Experimental studies of annealing of etched fission tracks in fluorapatite: *Geochimica et Cosmochimica Acta*, v. 55, no. 5, p. 1449–1465.
- Davis, W.M., 1889, *The rivers and valleys of Pennsylvania*: National Geographic Society.
- Dietler, T.N., Koestler, A.G., and Milnes, A.G., 1985a, A preliminary structural profile through the Western Gneiss Complex, Sognefjord, southwestern Norway: *Nors*, v. 65, p. 233–235.
- Dietler, T., Koestler, A., and Milnes, A., 1985b, A preliminary structural profile through the Western Gneiss Complex, Sognefjord, southwestern Norway: *Nor. Geol. Tidsskr.*, v. 65, p. 233–235.
- Dobrzhinetskaya, L., Eide, E., Larsen, R., Sturt, B., Trønnes, R., Smith, D., Taylor, W., and Posukhova, T., 1995, Microdiamond in high-grade metamorphic rocks of the Western Gneiss region, Norway: *Geology*, v. 23, no. 7, p. 597–600.
- Donelick, R.A., 1991, Crystallographic orientation dependence of mean etchable fission track length in apatite: An empirical model and experimental observations: *American Mineralogist*, v. 76, p. 83–91.
- Donelick, R.A., O'Sullivan, P., and Ketcham, R., 2005, Apatite fission-track analysis: *Reviews in Mineralogy and Geochemistry*, v. 58, no. 1, p. 49–94.
- Doré, A., 1992, Synoptic palaeogeography of the northeast Atlantic seaway: Late Permian to Cretaceous: *Geological Society, London, Special Publications*, v. 62, no. 1, p. 421–446.
- Doré, A., Lundin, E., Fichler, C., and Olesen, O., 1997, Patterns of basement structure and reactivation along the NE Atlantic margin: *Journal of the Geological Society*, v. 154, no. 1, p. 85–92.
- Doré, A., Lundin, E., Jensen, L., Birkeland, Ø., Eliassen, P., and Fichler, C., 1999, Principal tectonic events in the evolution of the northwest European Atlantic margin, *in Geological society, london, petroleum geology conference series*, v. 5: Geological Society of London, p. 41–61.
- Dumitru, T., 1993, A new computer-automated microscope stage system for fission-track analysis: *Nuclear Tracks and Radiation Measurements*, v. 21, no. 4, p. 575–580.
- Dunkl, I., 2002, TRACKKEY: a Windows program for calculation and graphical presentation of fission track data: *Computers & Geosciences*, v. 28, no. 1, p. 3–12.

- Dunlap, W., and Fossen, H., 1998, Early Paleozoic orogenic collapse, tectonic stability, and late Paleozoic continental rifting revealed through thermochronology of K-feldspars, southern Norway: *Tectonics*, v. 17, no. 4, p. 604–620.
- Eide, E., Torsvik, T., and Andersen, T., 1997, Absolute dating of brittle fault movements: Late Permian and late Jurassic extensional fault breccias in western Norway: *Terra Nova*, v. 9, no. 3, p. 135–139.
- Erratt, D., Thomas, G., and Wall, G., 1999, The evolution of the central North Sea Rift, *in* Geological society, london, petroleum geology conference series, v. 5: Geological Society of London, p. 63–82.
- Færseth, R., 1996, Interaction of Permo-Triassic and Jurassic extensional fault-blocks during the development of the northern North Sea: *Journal of the Geological Society*, v. 153, no. 6, p. 931–944.
- Færseth, R., Gabrielsen, R., and Hurich, C., 1996, Influence of basement in structuring of the North Sea basin, offshore southwest Norway: *Oceanographic Literature Review*, v. 43, no. 8.
- Faleide, J., Kyrkjebø, R., Kjennerud, T., Gabrielsen, R., Jordt, H., Fanavoll, S., and Bjerke, M., 2002, Tectonic impact on sedimentary processes during Cenozoic evolution of the northern North Sea and surrounding areas: Geological Society, London, Special Publications, v. 196, no. 1, p. 235–269.
- Fjeldskaar, W., Lindholm, C., Dehls, J.F., and Fjeldskaar, I., 2000, Postglacial uplift, neotectonics and seismicity in Fennoscandia: *Quaternary Science Reviews*, v. 19, no. 14, p. 1413–1422.
- Fleischer, R., and Price, P., 1964, Techniques for geological dating of minerals by chemical etching of fission fragment tracks: *Geochimica et Cosmochimica Acta*, v. 28, p. 1705–1714.
- Fleischer, R., Price, P., and Walker, R., 1965a, Effects of temperature, pressure, and ionization of the formation and stability of fission tracks in minerals and glasses: *Journal of Geophysical Research*, v. 70, no. 6, p. 1497–1502.
- Fleischer, R., Price, P., and Walker, R., 1965b, Ion Explosion Spike Mechanism for Formation of Charged-Particle Tracks in Solids: *Journal of Applied Physics*, v. 36, no. 11, p. 3645–3652.
- Fleisher, R., Price, P., and Walker, R., 1975, Nuclear tracks in solids: Principles and applications: Berkeley, California, University of California Press, v. 1, p. 626.
- Fossen, H., 1992, The role of extensional tectonics in the Caledonides of south Norway: *Journal of structural geology*, v. 14, no. 8, p. 1033–1046.
- Fossen, H., 1998, Advances in understanding the post-Caledonian structural evolution of the Bergen area, West Norway: *Norsk Geologisk Tidsskrift*, v. 78, no. 1, p. 33–46.
- Fossen, H., 2000, Extensional tectonics in the Caledonides: Synorogenic or postorogenic?: *Tectonics*, v. 19, no. 2, p. 213–224.
- Fossen, H., 2010, Extensional tectonics in the North Atlantic Caledonides: a regional view: Geological Society, London, Special Publications, v. 335, no. 1, p. 767–793.

- Fossen, H., and Dallmeyer, R., 1998,  $^{40}\text{Ar}/^{39}\text{Ar}$  muscovite dates from the nappe region of southwestern Norway: dating extensional deformation in the Scandinavian Caledonides: *Tectonophysics*, v. 285, no. 1, p. 119–133.
- Fossen, H., and Dunlap, W., 1998, Timing and kinematics of Caledonian thrusting and extensional collapse, southern Norway: evidence from  $^{40}\text{Ar}/^{39}\text{Ar}$  thermochronology: *Journal of Structural Geology*, v. 20, no. 6, p. 765–781.
- Fossen, H., and Dunlap, W., 1999, On the age and tectonic significance of Permo-Triassic dikes in the Bergen-Sunnhordland region, southwestern Norway: *Norsk Geologisk Tidsskrift*, v. 79, no. 3, p. 169–178.
- Fossen, H., and Holst, T., 1995, Northwest-verging folds and the northwestward movement of the Caledonian Jotun Nappe, Norway: *Journal of Structural Geology*, v. 17, no. 1, p. 3–15.
- Fossen, H., and Hurich, C., 2005, The Hardangerfjord Shear Zone in SW Norway and the North Sea: a large scale shear zone in the Baltic crust: *Journal of the Geological Society, London*, v. 162, p. 675–687.
- Fossen, H., Mangerud, G., Hesthammer, J., Bugge, T., and Gabrielsen, R., 1997, The Bjorøy Formation: a newly discovered occurrence of Jurassic sediments in the Bergen Arc System: *Norsk Geologisk Tidsskrift* 77, v. 77, p. 269–287.
- Fossen, H., and Rykkelid, E., 1992, Post-collisional extension of the Caledonide orogen in Scandinavia: structural expressions and tectonic significance: *Geology*, v. 20, p. 737–740.
- Gaal, G., and Gorbatshev, R., 1987, An outline of the Precambrian evolution of the Baltic Shield: *Precambrian Research*, v. 35, p. 15–52.
- Gabrielsen, R., Braathen, A., Dehls, J., and Roberts, D., 2002, Tectonic lineaments of Norway: *Norsk Geologisk Tidsskrift*, v. 82, no. 3, p. 153–174.
- Gabrielsen, R., Faleide, J., Pascal, C., Braathen, A., Nystuen, J., Etzelmuller, B., and O'Donnell, S., 2010a, Latest Caledonian to Present tectonomorphological development of southern Norway: *Marine and Petroleum Geology*, v. 27, no. 3, p. 709–723.
- Gabrielsen, R., Faleide, J., Pascal, C., Braathen, A., Nystuen, J., Etzelmuller, B., and O'Donnell, S., 2010b, Reply to discussion of Gabrielsen et al.(2010) by Nielsen et al.(this volume): Latest Caledonian to present tectonomorphological development of southern Norway: *Marine and Petroleum Geology*, v. 27, no. 6, p. 1290–1295.
- Galbraith, R.F., 2005, *Statistics for fission track analysis*: CRC Press.
- Galbraith, R., 1981, On statistical models for fission track counts: *Journal of the International Association for Mathematical Geology*, v. 13, no. 6, p. 471–478.
- Galbraith, R., 1988, Graphical display of estimates having differing standard errors: *Technometrics*, v. 30, no. 3, p. 271–281.
- Galbraith, R., 1990, The radial plot: Graphical assessment of spread in ages: *International Journal of Radiation Applications and Instrumentation. Part D. Nuclear Tracks and Radiation Measurements*, v. 17, no. 3, p. 207–214.
- Gallagher, K., and Brown, R., 1997, The onshore record of passive margin evolution: *Journal of the Geological Society*, v. 154, no. 3, p. 451–457.

- Gallagher, K., Brown, R., and Johnson, C., 1998, Fission track analysis and its applications to geological problems: *Annual Review of Earth and Planetary Sciences*, v. 26, p. 519–572.
- Gallagher, K., Stephenson, J., Brown, R., Holmes, C., and Fitzgerald, P., 2005, Low temperature thermochronology and modeling strategies for multiple samples 1: Vertical profiles: *Earth and Planetary Science Letters*, v. 237, no. 1, p. 193–208.
- Gee, D., 1975, A tectonic model for the central part of the Scandinavian Caledonides: *American Journal of Science*, v. 275, p. 468–515.
- Gee, D., Fossen, H., Henriksen, N., and Higgins, A., 2008, From the early Paleozoic platforms of Baltica and Laurentia to the Caledonide Orogen of Scandinavia and Greenland: *Episodes*, v. 31, no. 1, p. 44.
- Gilchrist, A., and Summerfield, M., 1990, Differential denudation and flexural isostasy in the formation of rifted margin upwarps: *Nature*, v. 346, p. 739–742.
- Gleadow, A., and Brown, R., 2000, *Fission-track thermochronology and the long-term denudational response to tectonics*: John Wiley & Sons, Chichester.
- Gleadow, A., 1981, Fission-track dating methods: what are the real alternatives?: *Nuclear Tracks*, v. 5, no. 1, p. 3–14.
- Gleadow, A., Belton, D., Kohn, B., and Brown, R., 2002, Fission track dating of phosphate minerals and the thermochronology of apatite: *Reviews in mineralogy and geochemistry*, v. 48, no. 1, p. 579–630.
- Gleadow, A., and Duddy, I., 1981, A natural long-term track annealing experiment for apatite: *Nuclear Tracks*, v. 5, p. 169–174.
- Gleadow, A., Duddy, I., Green, P., and Lovering, J., 1986, Confined fission track lengths in apatite: a diagnostic tool for thermal history analysis: *Contributions to Mineralogy and Petrology*, v. 94, no. 4, p. 405–415.
- Gleadow, A., and Lovering, J., 1977, Geometry factor for external detectors in fission track dating: *Nuclear Track Detection*, v. 1, no. 2, p. 99–106.
- Green, P., 1988, The relationship between track shortening and fission track age reduction in apatite: combined influences of inherent instability, annealing anisotropy, length bias and system calibration: *Earth and Planetary Science Letters*, v. 89, p. 335–352.
- Green, P., Duddy, I., Gleadow, A., Tingate, P., and Laslett, G., 1985, Fission-track annealing in apatite: track length measurements and the form of the Arrhenius plot: *Nuclear Tracks and Radiation Measurements*, v. 10, no. 3, p. 323–328.
- Green, P., Duddy, I., Gleadow, A., Tingate, P., and Laslett, G., 1986a, Thermal annealing of fission tracks in apatite: 1. A qualitative description: *Chemical Geology: Isotope Geoscience section*, v. 59, no. 0, p. 237–253, calibration of the Phanerozoic Time Scale.
- Green, P., Duddy, I., Gleadow, A., Tingate, P., and Laslett, G., 1986b, Thermal annealing of fission tracks in apatite: 1. A qualitative description: *Chemical Geology: Isotope Geoscience section*, v. 59, p. 237–253.
- Green, P., Duddy, I., Laslett, G., Jegarty, K., Gleadow, A., and Lovering, J., 1989, Thermal annealing of fission tracks in apatite: *Chemical Geology (Isotope Geoscience Section)*, v. 79, p. 155–182.

- Green, P., and Durrani, S., 1977, Annealing studies of tracks in crystals: *Nuclear Track Detection*, v. 1, no. 1, p. 33 – 39.
- Griffin, W., and Brueckner, H., 1980, Caledonian Sm-Nd ages and a crustal origin for Norwegian eclogites: *Nature*, v. 285, p. 319–321.
- Grønlie, A., Naeser, C., Naeser, N., Mitchell, J., Sturt, B., and Ineson, P., 1994, Fission-track and K-Ar dating of tectonic activity in a transect across the More-Trondelag Fault Zone, central Norway: *Norsk Geologisk Tidsskrift*, v. 74, no. 1, p. 24–34.
- Hallet, B., Hunter, L., and Bogen, J., 1996, Rates of erosion and sediment evacuation of glaciers: A review of field data and their implications: *Global and*, v. 12, p. 213–235.
- Hartz, E., and Torsvik, T., 2002, Baltica upside down: a new plate tectonic model for Rodinia and the Iapetus Ocean: *Geology*, v. 30, p. 255–258.
- Hendriks, B., Andriessen, P., Huigen, Y., Leighton, C., Redfield, T., Murrell, G., Gallagher, K., Nielsen, S., et al., 2007, A fission track data compilation for Fennoscandia: *Norsk Geologisk Tidsskrift*, v. 87, no. 1/2, p. 143.
- Hendriks, B., and Redfield, T., 2005, Apatite fission track and (U-Th)/He data from Fennoscandia: An example of underestimation of fission track annealing in apatite: *Earth and Planetary Science Letters*, v. 236, p. 443–458.
- Hendriks, B., and Redfield, T., 2006, Reply to: Comment on Apatite Fission Track and (U-Th)/He data from Fennoscandia: An example of underestimation of fission track annealing in apatite: *Earth and Planetary Science Letters*, v. 248, p. 569–577.
- Hoffman, P., 1991, Did the breakout of Laurentia turn Gondwanaland inside-out?: *Science*, v. 252, no. 5011, p. 1409–1412.
- Holtedahl, H., 1967, Notes on the formation of fjords and fjord-valleys: *Geografiska Annaler. Series A. Physical Geography*, p. 188–203.
- Huigen, Y., and Andriessen, P., 2004, Thermal effects of Caledonian foreland basin formation, based on fission track analyses applied on basement rocks in central Sweden: *Physics and Chemistry of the Earth, parts A/B/C*, v. 29, no. 10, p. 683–694.
- Hurfurd, A., 1990a, International Union of Geological Sciences Subcommittee on Geochronology recommendation for the standardization of fission track dating calibration and data reporting: *International Journal of Radiation Applications and Instrumentation. Part D. Nuclear Tracks and Radiation Measurements*, v. 17, no. 3, p. 233–236.
- Hurfurd, A., 1990b, Standardization of fission track dating calibration: Recommendation by the Fission Track Working Group of the I.U.G.S. Subcommittee on Geochronology: *Chemical Geology: Isotope Geoscience section*, v. 80, no. 2, p. 171–178.
- Hurfurd, A., and Carter, A., 1991, The role of fission track dating in discrimination of provenance: *Geological Society, London, Special Publications*, v. 57, no. 1, p. 67–78.
- Hurfurd, A., and Green, P., 1982, A users' guide to fission track dating calibration: *Earth and Planetary Science Letters*, v. 59, no. 2, p. 343–354.
- Hurfurd, A., and Green, P., 1983, The zeta age calibration of fission-track dating: *Chemical Geology*, v. 41, no. 0, p. 285–317.

- Hurford, A., and Hammerschmidt, K., 1985,  $^{40}\text{Ar}/^{39}\text{Ar}$  and K/Ar dating of the bishop and fish canyon tuffs: Calibration ages for fission-track dating standards: *Chemical Geology: Isotope Geoscience section*, v. 58, p. 23–32.
- Huuse, M., 2002, Cenozoic uplift and denudation of southern Norway: insights from the North Sea Basin: Exhumation of the North Atlantic Margin: Timing, Mechanisms and Implications for Petroleum Exploration, v. 5, no. 196, p. 209.
- Johannessen, K.C., Kohlmann, F., Ksienzyk, A.K., Dunkl, I., and Jacobs, J., 2013, Tectonic evolution of the sw norwegian passive margin based on low-temperature thermochronology from the innermost hardangerfjord area: *Norwegian Journal of Geology/Norsk Geologisk Forening*, v. 93.
- Jonckheere, R., Enkelmann, E., Min, M., Trautmann, C., and Ratschbacher, L., 2007, Confined fission tracks in ion-irradiated and step-etched prismatic sections of Durango apatite: *Chemical Geology*, v. 242, no. 1, p. 202–217.
- Jonckheere, R., and Wagner, G., 2000, On the occurrence of anomalous fission tracks in apatite and titanite: *American Mineralogist*, v. 85, no. 11-12, p. 1744–1753.
- Ketcham, R., Carter, A., Donelick, R.A., Barbarand, J., and Hurford, A.J., 2007a, Improved modeling of fission-track annealing in apatite: *American Mineralogist*, v. 92, no. 5-6, p. 799–810.
- Ketcham, R., and Donelick, R., 2013, Hefty manual version 1.8.0: .
- Ketcham, R., Donelick, R., Balestrieri, M., and Zattin, M., 2009, Reproducibility of apatite fission-track length data and thermal history reconstruction: *Earth and Planetary Science Letters*, v. 284, p. 504–515.
- Ketcham, R., Donelick, R.A., and Carlson, W.D., 1999, Variability of apatite fission-track annealing kinetics: III. Extrapolation to geological time scales: *American Mineralogist*, v. 84, p. 1235–1255.
- Ketcham, R., 2005a, Forward and inverse modeling of low-temperature thermochronometry data: *Reviews in Mineralogy and Geochemistry*, v. 58, no. 1, p. 275–314.
- Ketcham, R., 2005b, The role of crystallographic angle in characterizing and modeling apatite fission-track length data: *Radiation measurements*, v. 39, no. 6, p. 595–601.
- Ketcham, R., Carter, A., Donelick, R., Barbarand, J., and Hurford, A., 2007b, Improved measurement of fission-track annealing in apatite using c-axis projection: *American Mineralogist*, v. 92, no. 5-6, p. 789–798.
- Kohlmann, F., Ksienzyk, A.K., Fossen, H., and Jacobs, J., 2013, Exhumation along the hardangerfjord shear zone - new insights from combined (u-th)/he and fission track analysis: *Abstracts and Proceedings of the Geological Society of Norway*, 1-2013, 73.
- Kooi, H., and Beaumont, C., 1994, Escarpment evolution on high-elevation rifted margins: insights derived from a surface process model that combines diffusion, advection, and reaction: *Journal of Geophysical Research*, v. 99, p. 191–209.
- Ksienzyk, A.K., 2012, From mountains to basins: geochronological case studies from southwestern Norway, western Australia and east Antarctica [Ph.D. thesis]: Department of Earth Science, University of Bergen.



- Ksienzyk, A.K., Dunkl, I., Jacobs, J., Fossen, H., and Kohlmann, F., 2014, From orogen to passive margin: constraints from fission track and (U-Th)/He analyses on Mesozoic uplift and fault reactivation in SW Norway: Geological Society, London, Special Publications, v. 390, p. SP390–27.
- Lal, D., Rajan, R., and Tamhane, A., 1969, Chemical composition of nuclei of  $z > 22$  in cosmic rays using meteoric minerals as detectors: *Nature*, v. 221, p. 33–37.
- Larson, S., C., C.E., Tullborg, E.L., and Stiberg, J.P., 2006, Comment on "Apatite fission track and (U-Th)/He data from Fennoscandia: An example of underestimation of fission track annealing in apatite": *Earth and Planetary Science Letters*, v. 248, p. 561–568.
- Larson, S., Tullborg, E.L., Cederbom, C., and Stiberg, J.P., 1999, Sveconorwegian and Caledonian foreland basins in the Baltic Shield revealed by fission-track thermochronology: *Terra Nova-Oxford*, v. 11, no. 5, p. 210–215.
- Larson, W., and Redfield, T., 2006, Reply to: Comment on Apatite Fission Track and (U-Th)/He data from Fennoscandia: An example of underestimation of fission track annealing in apatite by BWH Hendriks and TF Redfield: *Earth and Planetary Science Letters*, v. 248, p. 569–577.
- Laslett, G., Galbraith, R., and Green, P., 1994, The analysis of projected fission track lengths: *Radiation measurements*, v. 23, no. 1, p. 103–123.
- Laslett, G., Gleadow, A., and Duddy, I., 1984, The relationship between fission track length and track density in apatite: *Nuclear Tracks and Radiation Measurements*, v. 9, no. 1, p. 29–38.
- Laslett, G., Green, P., Duddy, I., and Gleadow, A., 1987, Thermal annealing of fission tracks in apatite 2. A quantitative analysis: *Chemical Geology: Isotope Geoscience section*, v. 65, no. 1, p. 1–13.
- Laslett, G., Kendall, W., Gleadow, A., and Duddy, I., 1982, Bias in measurement of fission-track length distributions: *Nuclear Tracks and Radiation Measurements (1982)*, v. 6, no. 2, p. 79–85.
- Leighton, C., 2007, Post Caledonian reactivation of ancient structures in central southern Norway, constrained by apatite fission-track data, *in* *Geophysical research abstracts*, v. 9: p. 295.
- Lidmar-Bergström, K., Ollier, C., and Sulebak, J., 2000, Landforms and uplift history of southern Norway: *Global and Planetary Change*, v. 24, no. 3, p. 211–231.
- Lundin, E., and Dore, A., 1997, A tectonic model for the Norwegian passive margin with implications for the NE Atlantic: Early Cretaceous to breakup: *Journal of the Geological Society*, v. 154, p. 545–550.
- Mosar, J., 2003, Scandinavia's North Atlantic passive margin: *Journal of Geophysical Research: Solid Earth*, v. 108.
- Nadin, P., Kusznir, N., and Cheadle, M., 1997a, Early Tertiary plume uplift of the North Sea and Faeroe-Shetland basins: *Earth and Planetary Science Letters*, v. 148, no. 1, p. 109–127.

- Nadin, P., Kuszniir, N., and Cheadle, M., 1997b, Early Tertiary plume uplift of the North Sea and Faeroe-Shetland basins: *Earth and Planetary Science Letters*, v. 148, no. 1, p. 109–127.
- Naeser, C., 1979, Thermal history of sedimentary basins; fission-track dating of subsurface rocks: *Special Publication - Society of Economic Paleontologists and Mineralogists*, , no. 26, p. 109–112.
- Naeser, C., and Faul, H., 1969, Fission track annealing in apatite and sphene: *Journal of Geophysical Research*, v. 74, no. 2, p. 705–710.
- Nagpaul, K., Mehta, P., and Gupta, M., 1974, Annealing studies on radiation damages in biotite, apatite and sphene and corrections to fission track ages: *pure and applied geophysics*, v. 112, no. 1, p. 131–139.
- Nielsen, S., Clausen, O., Jacobsen, B., Thomsen, E., Huuse, M., Gallagher, K., Balling, N., and Egholm, D., 2010a, The ICE hypothesis stands: How the dogma of late Cenozoic tectonic uplift can no longer be sustained in the light of data and physical laws: *Journal of Geodynamics*, v. 50, no. 2, p. 102–111.
- Nielsen, S., Clausen, O., Pedersen, V., Leseman, J.E., Goleadowski, B., Huuse, M., Gallagher, K., and Summerfield, M., 2010b, Discussion of Gabrielsen et al. (2010): Latest Caledonian to Present tectonomorphological development of southern Norway: *Marine and Petroleum Geology*, v. 27, no. 6, p. 1285 – 1289.
- Nielsen, S., Gallagher, K., Leighton, C., Balling, N., Svenningsen, L., Jacobsen, B., Thomsen, E., Nielsen, O., Heilmann-Clausen, C., Egholm, D., et al., 2009, The evolution of western Scandinavian topography: a review of Neogene uplift versus the ICE (isostasy-climate-erosion) hypothesis: *Journal of Geodynamics*, v. 47, no. 2, p. 72–95.
- Norton, M., 1986, Late Caledonide extension in western Norway: A response to extreme crustal thickening: *Tectonics*, v. 5, no. 2, p. 195–204.
- Ollier, C., and Pain, C., 1997, Equating the basal unconformity with the palaeoplain: a model for passive margins: *Geomorphology*, v. 19, no. 1, p. 1–15.
- Osmundsen, P., Andersen, T., and Markussen, S., 1998, Tectonics and sedimentation in the hangingwall of a major extensional detachment: the Devonian Kvamshesten Basin, western Norway: *Basin Research*, v. 10, no. 2, p. 213–234.
- Osmundsen, P., and Redfield, T., 2011, Crustal taper and topography at passive continental margins: *Terra Nova*, v. 23, no. 6, p. 349–361.
- Paul, T., 1993, Transmission electron microscopy investigation of unetched fission tracks in fluorapatite - physical process of annealing: *Nuclear Tracks and Radiation Measurements*, v. 21, no. 4, p. 507–511.
- Paul, T., and Fitzgerald, P., 1992, Transmission electron microscopic investigation of fission tracks in fluorapatite: *American Mineralogist*, v. 77, no. 3-4, p. 336–344.
- Priem, H., Boelrijk, N., Hebeda, E., Verdurmen, E., and Verschure, R., 1976, Isotope geochronology of the Eidfjord Granite, Hardangervidda, West Norway: *Norges geologiske undersøkelse Bulletin*, v. 327, p. 35–39.

- Redfield, T., Braathen, A., Gabrielsen, R., Osmundsen, P., Torsvik, T., and Andriessen, P., 2005a, Late Mesozoic to Early Cenozoic components of vertical separation across the More–Trondelag fault complex, Norway: *Tectonophysics*, v. 395, no. 3, p. 233–249.
- Redfield, T., and Osmundsen, P., 2013, The long-term topographic response of a continent adjacent to a hyperextended margin: A case study from Scandinavia: *Geological Society of America Bulletin*, v. 125, no. 1-2, p. 184–200.
- Redfield, T., Osmundsen, P., and Hendriks, B., 2005b, The role of fault reactivation and growth in the uplift of western Fennoscandia: *Journal of the Geological Society*, v. 162, no. 6, p. 1013–1030.
- Redfield, T., Torsvik, T., Andriessen, P., and Gabrielsen, R., 2004, Mesozoic and Cenozoic tectonics of the More Trondelag Fault Complex, central Norway: constraints from new apatite fission track data: *Physics and Chemistry of the Earth, Parts A/B/C*, v. 29, no. 10, p. 673–682.
- Reusch, H., 1901, Nogle bidrag til forstaaelsen af hvorledes Norges dale og fjelde er blevne til: *Norges geologiske undersøkelse*, v. 32, p. 124–263.
- Roberts, A., Yielding, G., Kusznir, N., Walker, I., and Dorn-Lopez, D., 1995, Quantitative analysis of Triassic extension in the northern Viking Graben: *Journal of the Geological Society*, v. 152, no. 1, p. 15–26.
- Roberts, D., 2003, The Scandinavian Caledonides: event chronology, palaeogeographic settings and likely modern analogues: *Tectonophysics*, v. 365, p. 283–299.
- Roberts, D., Nordgulen, Ø., and Melezhik, V., 2007, The Uppermost Allochthon in the Scandinavian Caledonides: From a Laurentian ancestry through Taconian orogeny to Scandian crustal growth on Baltica: *Geological Society of America Memoirs*, v. 200, p. 357–377.
- Rohrman, M., Beek, P., Andriessen, P., and Cloetingh, S., 1995, Meso-Cenozoic morphotectonic evolution of southern Norway: Neogene domal uplift inferred from apatite fission track thermochronology: *Tectonics*, v. 14, no. 3, p. 704–718.
- Rohrman, M., and van der Beek, P., 1996, Cenozoic postrift domal uplift of North Atlantic margins: an asthenospheric diapirism model: *Geology*, v. 24, no. 10, p. 901–904.
- Ryan, P., and Dewey, J., 1997, Continental eclogites and the Wilson Cycle: *Journal of the Geological Society*, v. 154, no. 3, p. 437–442.
- Silk, E., and Barnes, R., 1959, Examination of fission fragment tracks with an electron microscope: *Philosophical Magazine*, v. 4, no. 44, p. 970–972.
- Steiger, R., and Jäger, E., 1977, Subcommittee on geochronology: convention on the use of decay constants in geo- and cosmochronology: *Earth and planetary science letters*, v. 36, no. 3, p. 359–362.
- Stephenson, J., Gallagher, K., and Holmes, C., 2006, Low temperature thermochronology and strategies for multiple samples: 2: Partition modelling for 2D/3D distributions with discontinuities: *Earth and Planetary Science Letters*, v. 241, no. 3, p. 557–570.
- Stillman, C., 1986, The Caledonide Orogen - Scandinavia and related areas: *NATURE*, v. 321, p. 482.

- Tagami, T., and O'Sullivan, P., 2005, Fundamentals of fission-track thermochronology: *Reviews in Mineralogy and Geochemistry*, v. 58, no. 1, p. 19–47.
- Torsvik, T., 2003, The Rodinia jigsaw puzzle: *Science*, v. 300, p. 1379–1381.
- Torsvik, T., and Cocks, L., 2004, Earth geography from 400 to 250 Ma: a palaeomagnetic, faunal and facies review: *Journal of the Geological Society*, v. 161, no. 4, p. 555–572.
- Torsvik, T., and Cocks, L., 2005, Norway in space and time: a centennial cavalcade: *Norwegian Journal of Geology*, v. 85, no. 1-2, p. 73–86.
- Torsvik, T., and Rehnström, E., 2001, Cambrian palaeomagnetic data from Baltica: implications for true polar wander and Cambrian palaeogeography: *Journal of the Geological Society*, v. 158, p. 321–329.
- Torsvik, T., and Rehnström, E., 2003, The Tornquist Sea and Baltica-Avalonia docking: *Tectonophysics*, v. 362, no. 1, p. 67–82.
- Torsvik, T., Smethurst, M., Meert, J., Van der Voo, R., McKerrow, W., Brasier, M., Sturt, B., and Walderhaug, H., 1996, Continental break-up and collision in the Neoproterozoic and Palaeozoic—a tale of Baltica and Laurentia: *Earth-Science Reviews*, v. 40, no. 3, p. 229–258.
- Vågnes, E., Gabrielsen, R., and Haremo, P., 1998, Late Cretaceous–Cenozoic intraplate contractional deformation at the Norwegian continental shelf: timing, magnitude and regional implications: *Tectonophysics*, v. 300, no. 1, p. 29–46.
- Van Den Haute, P., De Corte, F., Jonckheere, R., and Bellemans, F., 1998, The parameters that govern the accuracy of fission-track age determinations: A re-appraisal, *in* *Advances in fission-track geochronology*: Springer, p. 33–46.
- van der Beek, P., Cloetingh, S., and Andriessen, P., 1994, Mechanisms of extensional basin formation and vertical motions at rift flanks: Constraints from tectonic modelling and fission-track thermochronology: *Earth and Planetary Science Letters*, v. 121, no. 3, p. 417–433.
- van der Beek, P., 1995, Tectonic evolution of continental rifts. Inference from numerical modelling and fission track thermochronology [Ph.D. thesis]: Vrije Universiteit.
- Vineyard, G., 1976, Thermal spikes and activated processes: Radiation effects and effects in solids, v. 29, p. 245–248.
- Vrolijk, P., Donelick, R.A., Queng, J., and Cloos, M., 1992, Testing models of fission track annealing in apatite in a simple thermal setting: site 800, leg 129, *in* *Proceedings of the ocean drilling program, scientific results*, v. 129: p. 169–176.
- Wagner, G., and Van den Haute, P., 1992, *Fission track dating*, v. 6: Kluwer Academic Publishers.
- Wagner, G., 1968, Fission track dating of apatites: *Earth and Planetary Science Letters*, v. 4, no. 5, p. 411 – 415.
- Wagner, G., and Reimer, G., 1972, Fission track tectonics: The tectonic interpretation of fission track apatite ages: *Earth and Planetary Science Letters*, v. 14, no. 2, p. 263 – 268.
- Wagner, G., and Storzer, D., 1972, Fission track length reductions in minerals and the thermal history of rocks: v. 4.

- White, R., and McKenzie, D., 1989, Magmatism at rift zones: the generation of volcanic continental margins and flood basalts: *Journal of Geophysical Research: Solid Earth*, v. 94, p. 7685–7729.
- Woznitza, T., 2014, Exhumation history of the Caledonides in SW-Norway - (U-Th)/He ages on apatite and K/Ar age determinations [Master's thesis]: Georg-August-University of Göttingen.
- Young, E., Myers, A., Munson, E., and Conklin, N., 1969, Mineralogy and geochemistry of fluorapatite from Cerro de Mercado, Durango, Mexico: U.S. Geological Survey Professional Paper, p. D84–D93.
- Zeck, H., Andriessen, P., Hansen, K., Jensen, P., and Rasmussen, B., 1988, Paleozoic paleo-cover of the southern part of the Fennoscandian Shield-fission track constraints: *Tectonophysics*, v. 149, no. 1, p. 61–66.



## Appendix A: Container positions

---

### NoB-023

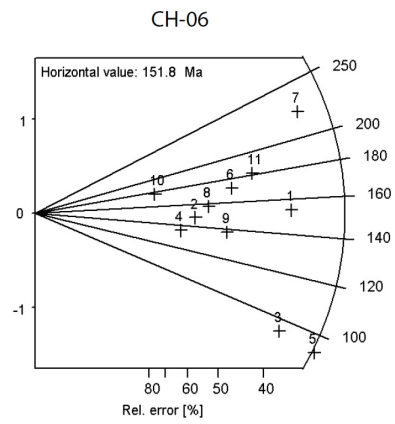
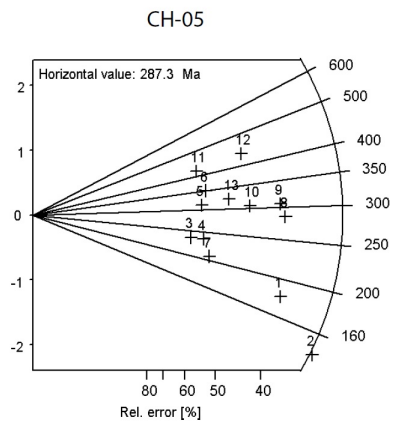
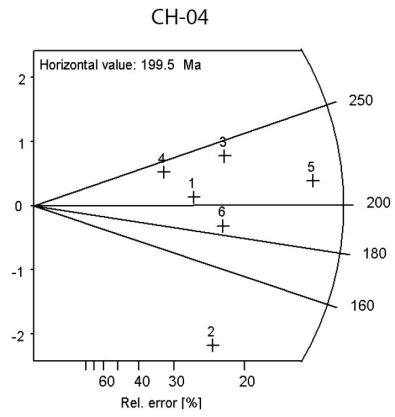
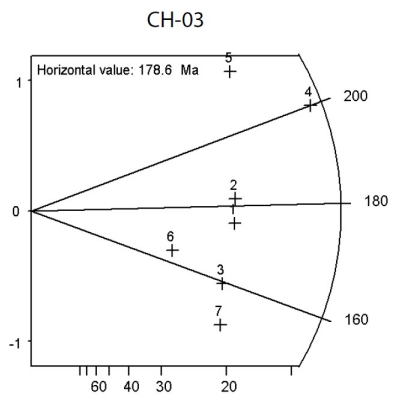
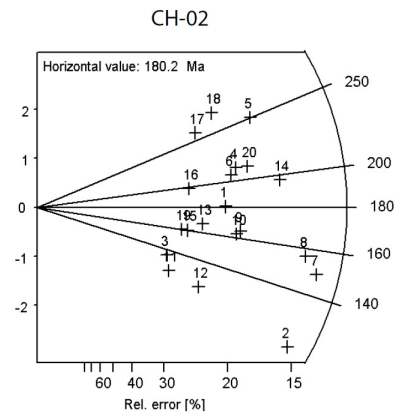
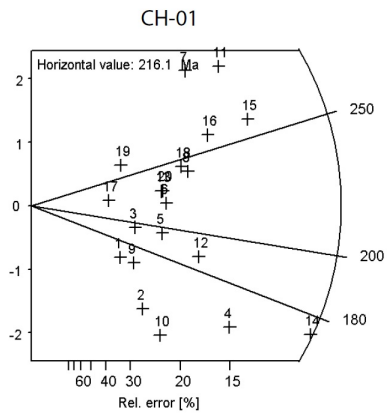
<b>Position</b>	<b>Sample ID</b>
1	<b>IRMM 1-1</b>
2	NTW-16-13
3	NTW-17-13
4	NTW-19-13
5	NTW-20-13
6	NTW-24-13
7	NTW-25-13
8	NTW-27-13
9	NTW-28-13
10	NTW-29-13
11	NTW-30-13
12	NTW-31-13
13	NTW-32-13
14	<b>IRMM 1-2</b>
15	BG-040
16	NTW-03-13
17	NTW-04-13
18	NTW-06-13
19	NTW-07-13
20	<b>DUR</b>
21	<b>FCT</b>
22	NTW-11-13
23	NTW-13-13
24	NTW-35-13
25	NTW-36-13
26	NTW-37-13
27	<b>IRMM 1-3</b>
28	NTW-38-13
29	NTW-39-13
30	NTW-47-13
31	NTW-49-13
32	NTW-50-13
33	NTW-51-13
34	NTW-53-13
35	NTW-54-13
36	NTW-55-13
37	<b>IRMM 1-4</b>

## NoB-025

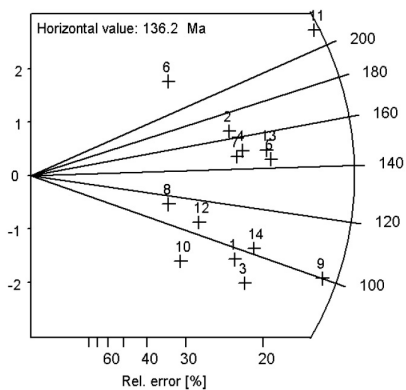
<b>Position</b>	<b>Sample ID</b>
1	<b>IRMM 2-2</b>
2	NTW-15-13
3	NTW-21-13
4	NTW-40-13
5	CH-01
6	CH-02
7	CH-03
8	CH-04
9	CH-05
10	CH-06
11	CH-07
12	CH-08
13	CH-09
14	CH-10
15	<b>DUR</b>
16	<b>FCT</b>
17	<b>IRMM 2-3</b>
18	BG-179
19	BG-180
20	BG-187
21	BG-189
22	EC-02
23	EC-03
24	EC-05
25	EC-06
26	EC-08
27	EC-09
28	EC-12
29	EC-12
30	EC-13
31	EC-14
32	EC-15
33	<b>IRMM 2-4</b>



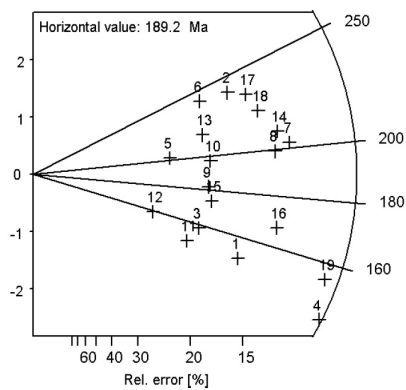
# Appendix B: Radial plots



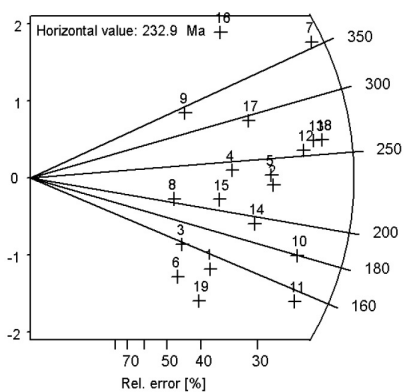
CH-07



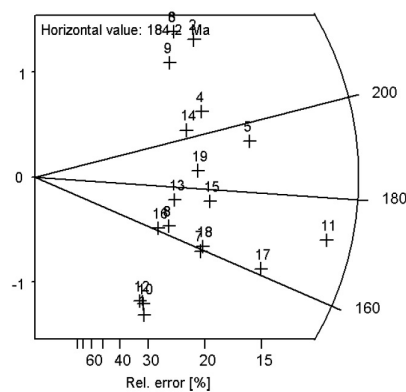
NTW-16-13



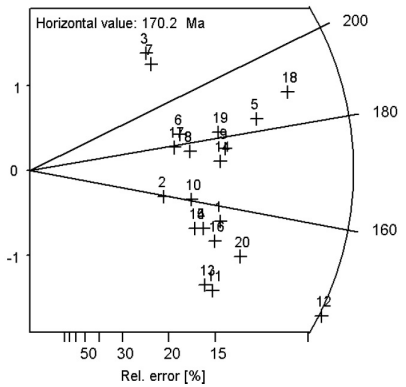
NTW-17-13



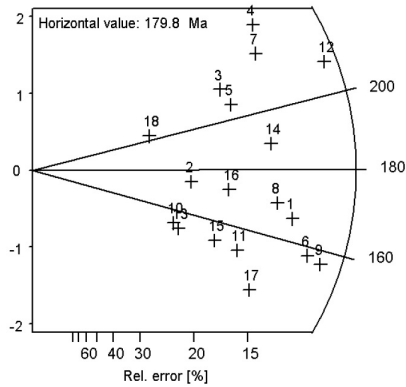
NTW-19-13



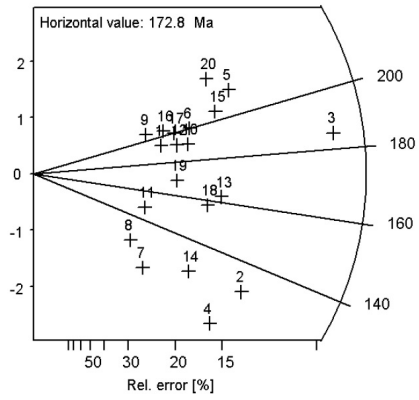
NTW-24-13



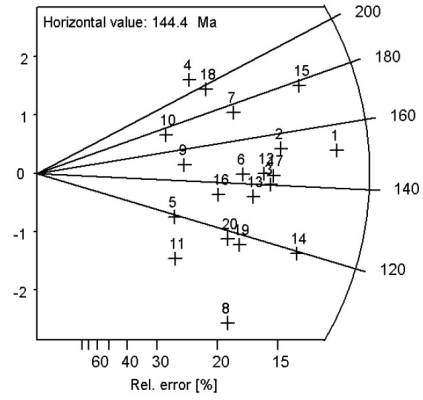
NTW-27-13



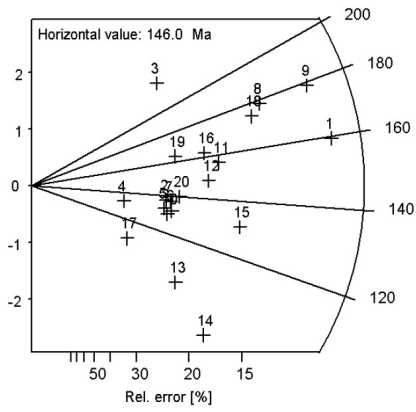
NTW-28-13



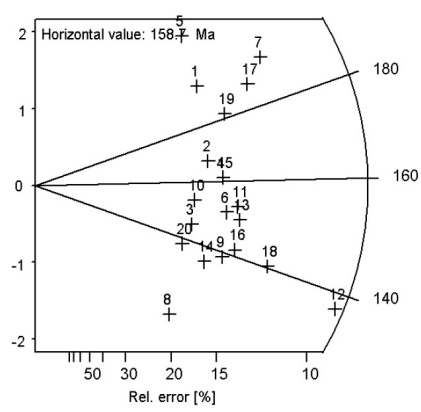
NTW-29-13



NTW-30-13



NTW-31-13



NTW-32-13

